DEPARTMENT OF BIOCHEMISTRY
UNIVERSITY OF OXFORD

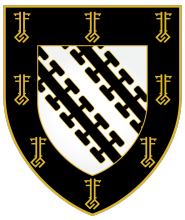

Investigating the Dynamics of KDEL Receptor Signalling

Fabian Spoendlin
Master of Science (by Research) in Biochemistry
Exeter College
Candidate Number: 1358380

Supervised by Prof. Jason Schnell

University of Oxford
Department of Biochemistry
South Parks Road, Oxford, OX1 3QU

Word Count: 20,000
Date: January 7, 2022

Acknowledgements

I would like to take this opportunity to thank Professor Jason Schnell for guiding me throughout the project and consistently providing valuable support and feedback. I am very grateful to have had the opportunity to conduct such an interesting project in his lab. Furthermore, I would like to thank Professor Simon Newstead for his insights into the field, especially during the later stages of the project.

I would also like to express my gratitude to the members of the Schnell and Newstead laboratories. I am especially thankful for the help of Dr. Feng Qu, Dr. Jelena Habjanič, and Ngai Lam Chung. Without their incredible efforts and guidance in the laboratory this project would not have been possible.

Finally, I would like to thank my family for their constant support during the completion of this dissertation in a year marked by the pandemic.

Abstract

The KDEL receptor (KDELR) is a trafficking receptor which is involved in the retrograde trafficking of ER resident proteins that escaped to the Golgi. For this function, the receptor cycles in COPI and COPII coated vesicles bet en Golgi, where cargo is bound, and the ER, where it is released. KDELR recognises its cargo by an ER retrieval sequence (ERS), the canonical signal consisting of a KDEL peptide motif. Cargo binding and dissociation is regulated by the pH difference between the two organelles. At low pH ERS binding is favoured whereas neutral pH triggers release. The crystal structures of the apo KDELR at pH 9.0 ('inactive' state) and the receptor bound to KDEL peptide at pH6.0 ('active' state) were solved recently. These revealed that the lysine-rich KDELR C-terminus forms the interface for COPI binding. A gain of structure transition of the C-terminus from 'inactive' to 'active' state is responsible for COPI recruitment to KDELR which initiates vesicle formation and retrograde trafficking. In this study, solution state NMR is used to investigate the molecular mechanism of KDELR2 signalling to COPI through its functionally important C-terminus. I aim to bridge the divide between the static crystal structures and the dynamic behaviour of the receptor in solution, which often holds the key to understand the function of a protein in the cell. Reductive methylation of lysine side chains with carbon-13 is used to introduce highly sensitive NMR active probes into the KDELR C-terminus. ^{1}H-^{13}C correlation spectra were recorded of the receptor with the two variables of pH and presence of KDEL peptide. The NMR data revealed that pH by itself does not initiate KDELR signalling and solely regulates affinity of the receptor to peptide. Furthermore, I show that the KDELR C-terminus is highly dynamic in solution, sampling multiple conformations on the microsecond-millisecond timescale. In the absence of peptide, the C-terminus rapidly switches between its 'active' and 'inactive' states. Upon peptide binding the conformational equilibrium is shifted towards the 'active' state. However, a low level of conformational exchange remains. Based on these findings a model of KDELR signalling is proposed. The low pH in the Golgi primes the receptor for cargo binding, but does not initiate receptor signalling directly. The event of cargo binding is signalled across the membrane by the stabilisation of the 'active' conformation of the C-terminus. This leads to rapid recruitment of COPI and efficient retrograde trafficking to the ER. In case the Golgi is depleted of cargo, apo receptor is retained in the Golgi. The conformational flexibility and transient adoption of the 'active' conformation of the C-terminus in this state may allow for some signalling and a low level of receptor retrieval. This could prevent the receptor from following the bulk flow to the lysosome where it would get degraded. This study supports the hypothesis that protein dynamics is critical for KDELR function in the cell.

Contents

Abbreviations

CHS	Cholesteryl hemisuccinate
COPI	Coat protein I
COPII	Coat protein II
CSP	Chemical shift perturbation
DDM	n-Dodecyl-β-D-Maltopyranoside
DMSO	Dimethyl sulfoxide
DTT	Dithiothreitol
EDTA	Ethylenediaminetetraacetic acid
ER	Endoplasmic reticulum
ERS	ER retrieval sequence
GFP	Green fluorescent protein
GPCR	G protein coupled receptor
His8	Octa histidine tag
HMQC	Heteronuclear multiple quantum coherence
HSQC	Heteronuclear single quantum coherence
His8	Octa histidine tag
IMAC	Immobilized metal affinity chromatography
KDELR	KDEL receptor
LB	Lysogeny broth
MWCO	Molecular weight cut-off
NMR	Nuclear magnetic resonance

OD	Optical density
PBS	Phosphate-buffered saline
PCR	Polymerase chain reaction
PEG	Polyethylene glycol
RT	Room temperature
SC	Synthetic complete
SEC	Size exclusion chromatography
Syb37	Sybody 37
SDS-PAGE	Sodium dodecyl sulphate-polyacrylamide gel electrophoresis
TEV	Tobacco Etch Virus
THB	Triple helix bundle
TM	Transmembrane helix
UV	Ultra violet

1 Introduction

1.1 Cellular function of KDELR

Compartmentalisation of the eukaryotic cell into organelles allows the presence of distinct biochemical environments. This, however, creates the demand for the cell to sort and transport proteins to the correct organelle. Inter-organelle transport occurs in cellular vesicles which are formed through the recruitment of vesicle coat proteins located in the cytoplasm. As transmembrane proteins span across the membrane, they can directly recruit coat proteins to their cytosolic side. By contrast, soluble proteins require a trafficking receptor for sorting. These receptors recognise soluble cargo by peptide signals and relay this information via conformational changes across the membrane to recruit coat proteins [1, 2].

Membrane and secretory proteins are synthesized and folded in the endoplasmic reticulum (ER). These proteins possess ER exit signals which trigger active transport to the Golgi in COPII-coated vesicle [3, 4], from where they are transported further to their appropriate location. The ER harbours a resident population of chaperones and other proteins assisting during the folding process [1, 2]. Despite the lack of ER exit signals, chaperones can escape to the Golgi by sticking to their substrates or simply following the bulk flow [5, 6]. For proper function of the cell it is essential that escaped chaperones are retrieved to the ER.

ER resident proteins possess a C-terminal ER retrieval sequence (ERS), the canonical signal consisting of a Lys-Asp-Glu-Leu (KDEL) peptide motif [7, 8]. KDEL receptors

(KDELRs), localised to the cis-Golgi, recognise escaped ER proteins and bind their ERS [9]. The receptor relays the signal across the membrane to initiate retrograde trafficking to the ER in coat protein I (COPI)-coated vesicles [1, 10, 11]. COPI-coated vesicles are vesicles trafficking proteins from Golgi to the ER. Their formation is driven by COPI, a cytosolic, seven subunit protein complex. COPI recognises and binds to the cargo-bound KDELR and is recruited to the Golgi membrane. COPI then forms additional interactions with the membrane, these interactions mechanically cause the membrane to curve which eventually leads to the budding of a membrane-bounded vesicle coated with COPI. The COPI-coated vesicle, containing both KDELR and cargo proteins, is transported to the ER where it fuses with the target membrane [12]. In the ER, KDELR releases its cargo and the apo receptor is cycled back to the Golgi in coat protein II (COPII)-coated vesicles. These vesicles function to transport proteins from ER to the Golgi. Their formation is driven by the binding of COPII to apo KDELR. Vesicles budding occurs by a similar mechanism as described above for COPI [13, 14]. A schematic of the cycling of KDELR between Golgi and ER is shown in figure 1.1. This cycle relies on the pH difference between cis-Golgi (pH6.6-6.7) [15] and ER (pH7.2-7.4) [16]. Cargo binding is favoured at low pH, whereas neutral pH favours release [17, 18].

In the Golgi of a mammalian cell KDELR is present at concentrations of 0.2-0.3 μM [18, 20, 21, 22]. Cargo concentration is approximately 100-fold higher, thus quick recycling of the receptor is required [21].

Several variants of the canonical KDEL signal exist. Mammalian KDELR also bind HDEL, which is primarily used by low abundance proteins, and RDEL motifs. The affinity of KDELR for HDEL is approximately 10-times stronger than for KDEL and RDEL [18, 20, 21]. The difference in affinity is required by the system to transport both high and low abundance cargo efficiently [21]. Despite a high degree of sequence similarity [19], yeast KDELRs also recognise DDEL and ADEL signal sequences [23, 24].

The mammalian cell has three different KDELRs (KDELR1, KDELR2, KDELR3), however, it is unknown how these three differ in function. Under normal conditions,

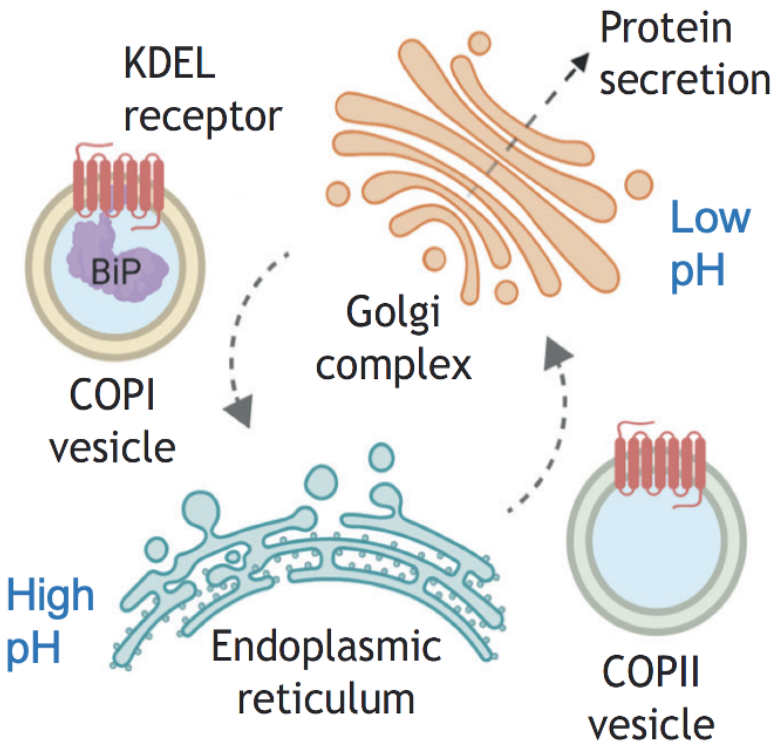

Figure 1.1: Schematic of KDELR cycling between ER and Golgi to capture escaped ER proteins (e.g. BiP). Figure adapted from [19].

KDELR1 and KDELR2 are more abundant in the cell than KDELR3. KDLER3 is upregulated during stress and was suggested to bind HDEL signals more selectively [25, 26].

1.2 Structural basis of KDELR function

KDELRs are 26 kDa proteins encoded by *ERD2* genes [10] and belong to the PQ (Proline, Glutamine)-loop superfamily of integral membrane proteins. This functionally diverse family is characterised by a Pro-Gln motif [27] and, besides KDELR, consists of various amino acid and nutrient transporters [28, 29, 30].

The crystal structures of the *Gallus gallus* KDELR2 in complex with KDEL [17], HDEL and RDEL peptides [21] were solved recently and provide structural insights into the receptor function (fig. 1.2). KDELR2 consists of 7 transmembrane helices (TM). Helices 1-3 and 5-7 form two triple helix bundles (THBs) in 1-3-2 order. These are

arranged inverted towards each other by a rotation axis in the plane of the membrane. The two THBs are connected by the linker helix TM4.

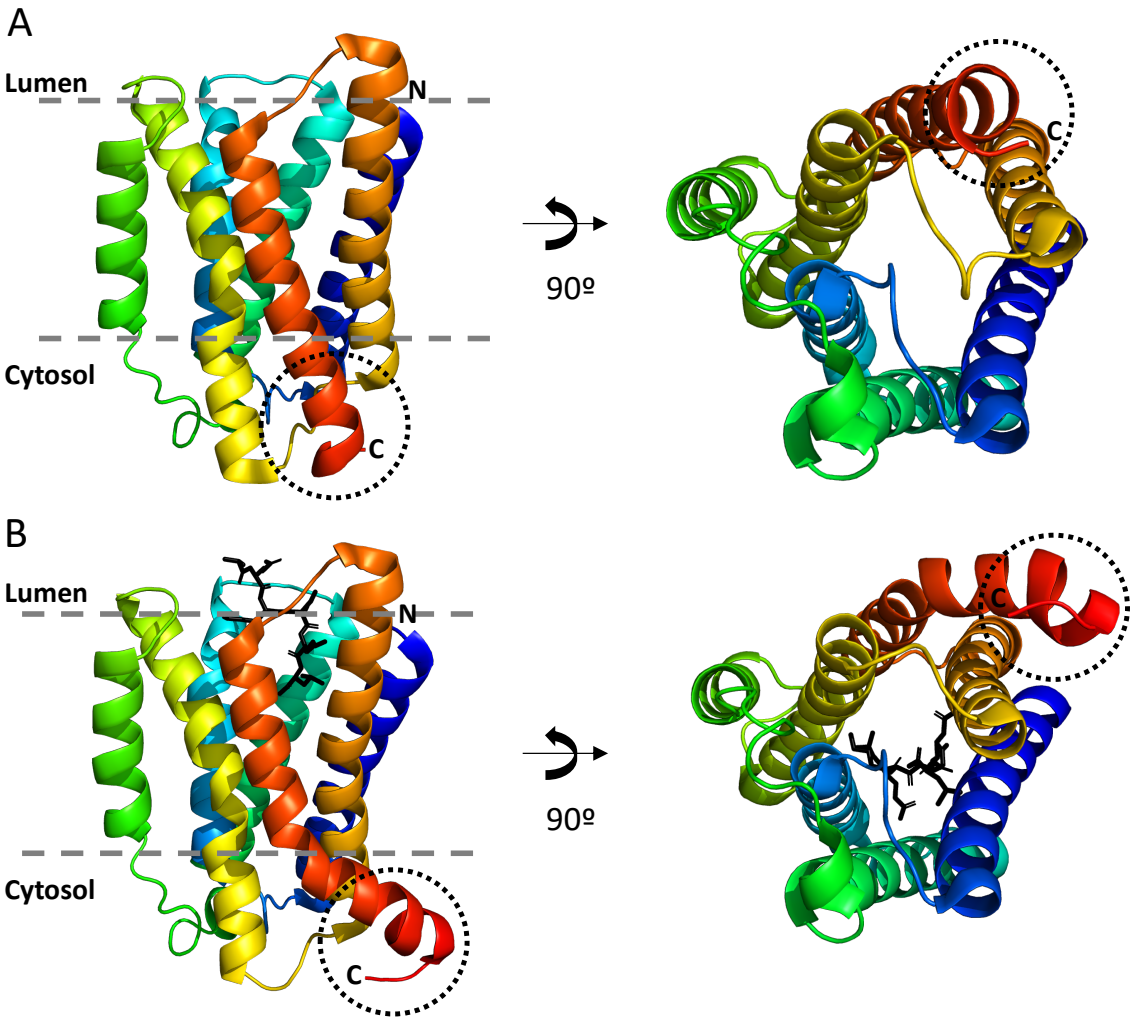

Figure 1.2: KDELR2 crystal structures in 'active' and 'inactive' state. (A) KDELR2 in apo state at pH 9.0 (PDB: 6I6B). (B) Peptide-bound KDELR2 at pH 6.0 (PDB: 6I6H). The black dotted circle highlights the position of the functionally important C-terminal lysine motif. The peptide is shown in black stick representation. The C- and N-termini are labelled.

In the apo state at high pH, the cytosolic face of the receptor forms a negatively charged band (fig. 1.3). Charge is contributed by the strictly conserved residues D87, E143 and E145. These are reminiscent of the di-acidic COPII recognition motifs [31]. As mutation of the three residues leads to retention of the receptor in the ER [32], they are expected to form the binding interface with COPII.

The luminal side of the receptor contains a large polar cavity with dipolar character

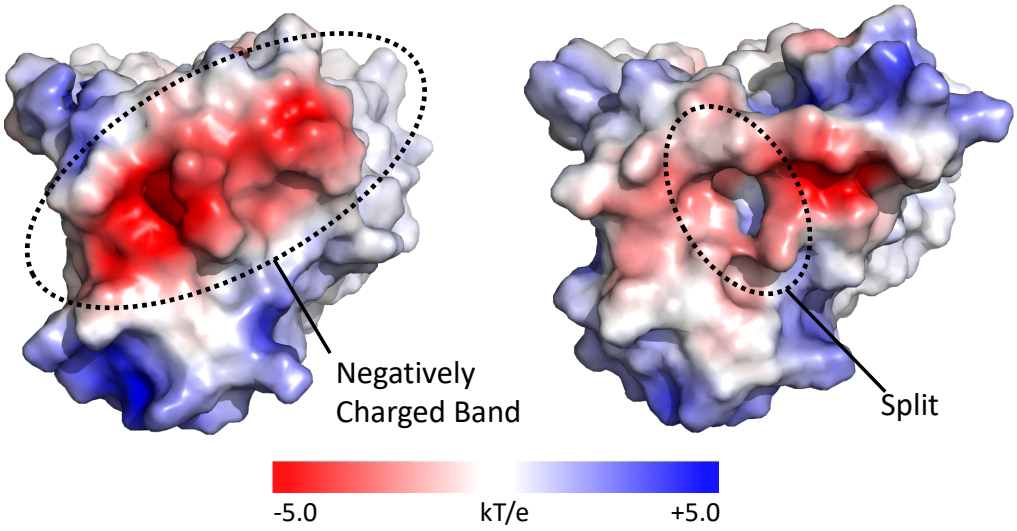

Figure 1.3: Electrostatic surface representation of the cytoplasmic face of the KDELR2. Left: KDELR is shown in the apo state to highlight the negatively charged band. Right: peptide-bound KDELR is shown indicating the split of the negatively charged band.

(complementary in charge to the KDEL peptide) which forms the peptide-binding pocket. Peptide binding was shown to occur by the following mechanism. The -1 to -3 residues of the KDEL sequence (residues D, E and L), common to all variants of the motif, consist of three carboxyl groups (2 side chains and the C-terminus). First, the C-terminal carboxyl makes contact with R169 on the receptor (fig. 1.4). The peptide is then passed down an arginine ladder further consisting of R5 and R47 until the three carboxyls interact with the three arginines. This step is believed to be pH independent and occurs in both ER and Golgi. In the mammalian KDELR, E117 acts as a gate keeper residue and interacts with the residue at the -4 position of the peptide. This residue selects for the HDEL, KDEL and RDEL variants of the ERS based on their charge. The higher affinity of the receptor for HDEL as compared to KDEL and RDEL is explained by additional interactions of the residue at -4 position with W120. Besides cation-π, present in all peptides, the histidine of HDEL is able to form π-π interaction [21].

As a final step in the peptide binding mechanism a rotation of TM6 occurs. This causes the receptor to close around the peptide and lock it in position. This step is pH dependent [21] and regulated by the protonation state of residue histidine 12. Molecular dynamics simulations showed that peptide binding leads to the formation of

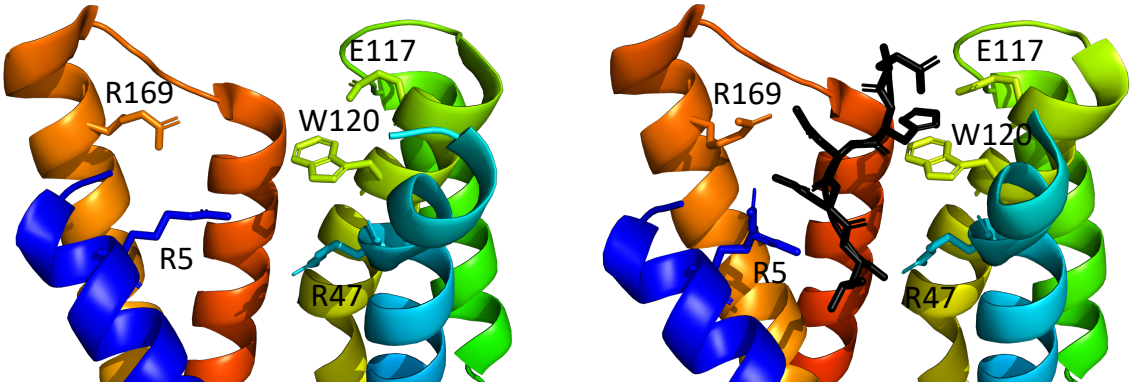

Figure 1.4: KDELR2 peptide binding pocket. The peptide (black) and residues R5, R47, E117, W120 and R169 important for peptide binding are highlighted in stick representation. Left: KDELR2 in the apo state at high pH (PDB: 6I6B). Right: peptide-bound KDELR2 at low pH (PDB: 6Y7V).

two constricted water pockets within the binding site. The 'pH sensor' H12 sits in between these two pockets (fig. 1.5) and upon protonation of this residue a continuous water network forms which stabilises a hydrogen bond formed between E127 in TM5 and Y158 in TM6. This hydrogen bond is, in turn, required to hold TM6 in its rotated conformation. By this mechanism pH controls peptide binding [16]. The importance of H12, E127 and Y158 was also shown in cells. Their mutation leads to receptor retention in the Golgi [17].

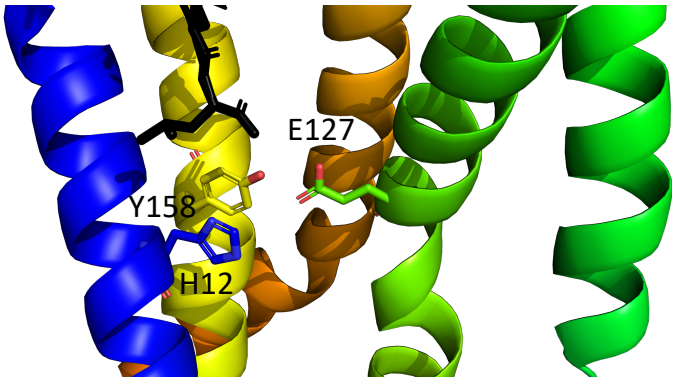

Figure 1.5: Role of H12 in stabilising the E127-Y158 salt bridge. Structure of the peptide-bound KDELR is shown. The peptide (black) and residues H12, E127 and Y158 are highlighted in stick representation. PDB: 6I6H.

Furthermore, peptide binding together with low pH trigger the cytosolic half of TM7 to kink outward which leads to the rearrangement of the lysine-rich KDELR C-terminus

(including residues K201, K204, K206 & K207). In the crystal structures of the apo receptor at high pH, only residues to 203 are observed suggesting they are structured. The kink in TM7 with peptide binding and low pH allows the C-terminus to fold back against the receptor which leads to the structuring of residues 204-210 (fig. 1.2). The C-terminal lysine-rich sequence resembles known COPI binding motifs (KxKxx & KKxx) [33, 34] and mutation of the lysines leads to KDELR localisation in the Golgi [17]. Based on these two findings it is highly likely that this C-terminal lysine motif forms the binding interface with COPI. The transition of the C-terminus from its disordered ('inactive') to its structured ('active') conformation, hence, is believed to be responsible for KDELR signalling to COPI. The rearrangement of the cytosolic face of the receptor upon peptide binding also splits the above described negatively charge band, thus, COPII and COPI binding motifs occur mutually exclusively (fig. 1.3).

The 'active' conformation of the C-terminus appears to be stabilised by a salt bridge between E143 and K207 (fig. 1.6). As E143 forms part of the COPII recognition motif, this salt bridge may act as a 'switch' between the adoption of COPI and COPII binding motifs.

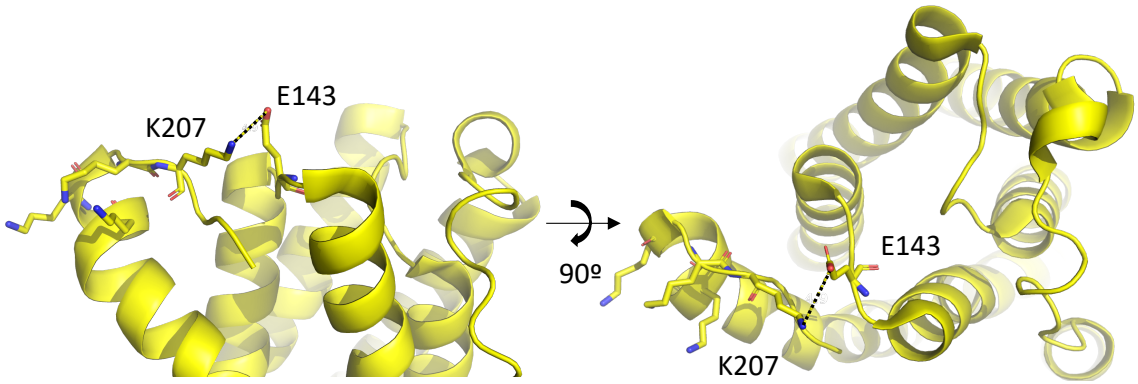

Figure 1.6: KDELR2 crystal structures highlighting the E143-K207 salt bridge. The 4.9 Å long salt bridge, indicated with a dashed black line, appears to stabilise the 'active' conformation of the C-terminus. PDB: 6Y7V.

Furthermore, it was discovered that a synthetic nanobody, sybody37 (Syb37), which binds to the luminal side of KDELR, leads to the redistribution of the receptor to the lysosome along with the bulk flow. The crystal structure of the Syb37-KDELR2 complex

was solved (fig. 1.7). This showed that Syb37 binds with its CDR3 loop inside the KDELR2 binding cavity and that the receptor is highly similar in conformation as in the apo state (RMSD = 1.4 Å). As the apo receptor does not travel to the lysosome, the crystal structures are not able to explain the difference in behaviour [17].

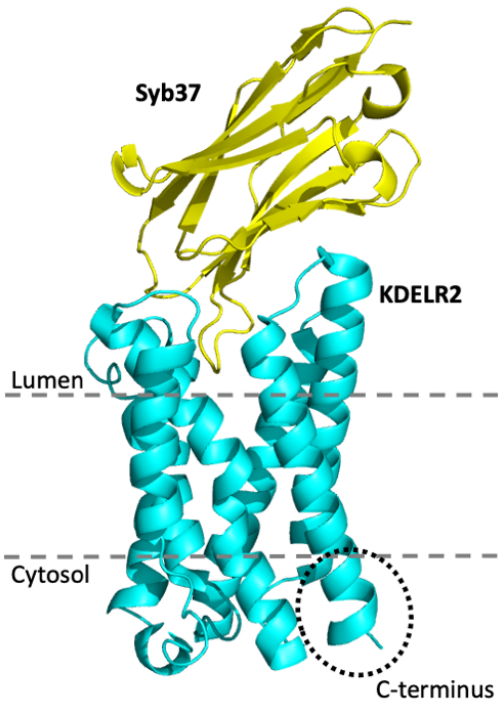

Figure 1.7: Crystal structure of KDELR2 in complex with sybody 37. KDELR2 is shown in cyan, Syb37 in yellow. The conformation of the functionally important C-terminus is highlighted by the black dotted circle. PDB: 6I6J.

1.3 NMR and protein dynamics

Proteins are highly dynamic macromolecules. X-ray crystallography and cryogenic electron microscopy provide a high resolution 'snapshot' of a single conformation occupied by a protein and limited information on ordering within the crystalline environment. However, in solution proteins can spontaneously sample transiently stable conformational states. This dynamic behaviour is central to the function of protein and its study holds the key to understand many aspects of their molecular mechanisms [35, 36, 37].

Solution NMR is a powerful tool to study protein dynamics. It is sensitive to NMR

active nuclei switching between two or more chemical environments over a range of timescales. Depending on the rate of this chemical exchange a distinct behaviour of NMR peaks is detectable. An overview of this behaviour in one dimensional NMR spectra is shown in figure 1.8. Conformational exchange occurring in the microsecond to millisecond timescale [38] falls into the 'intermediate exchange' regime. As movements on this timescale lead to peak broadening [39, 40, 41], information on conformational exchange can be extracted from NMR spectra by measuring the width of a peak at half of its height, i.e. line shape analysis.

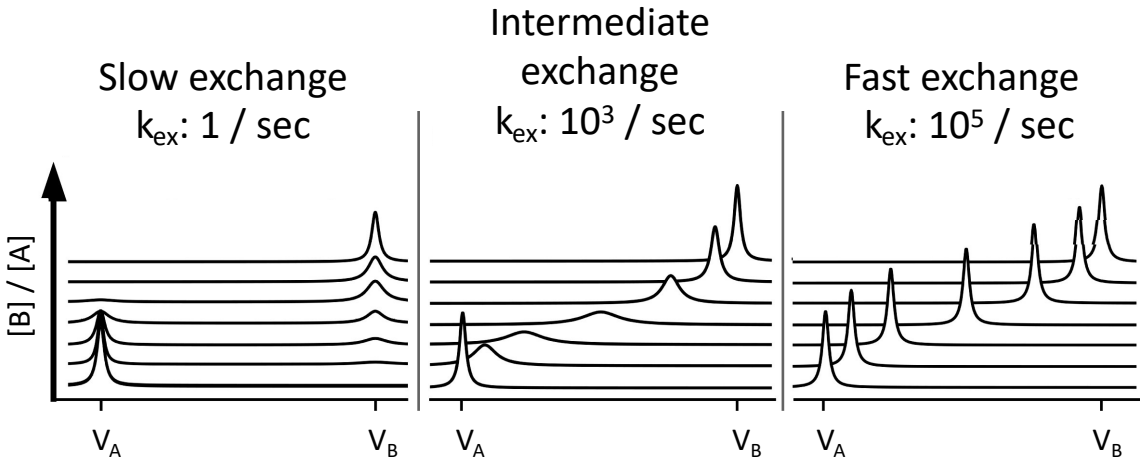

Figure 1.8: The impact of chemical exchange on NMR peaks in 1D experiments. Depending on the timescale of the exchange three distinct behaviours are observable. Slow exchange leads to the occurrence of two NMR peaks, the intensity of the two peak correlates with the relative concentration of the two states. Intermediate exchange is characterised by a broadening of peaks. The broadening is most severe when the concentrations of both states are equal. Fast exchange leads to the occurrence of a single sharp peak. The chemical shift of the peak depends of the relative concentration of the two states [39, 40]. A: Protein in state A, v_A: resonance frequency of state A. B: Protein in state B. v_B: resonance frequency of state B. Figure adapted from [40].

The importance of protein dynamics is highlighted by recent studies investigating GPCRs. These have resulted in novel insights into their function [42, 43]. NMR [44, 45] and molecular dynamics simulation [46, 47] studies of the β_2-adrenergic receptor showed a new model of GPCR activation. Coupling between the extracellular ligand binding pocket and the intracellular G-protein binding interface appears to be much looser than expected. Ligand binding, either agonist or antagonist, triggers a conformational

change of the extracellular receptor domain. This event has to be signalled across the membrane by a change in the intracellular domain. However, it was observed that the intracellular domain is conformationally heterogeneous and can sample several states relatively independent of the conformation of the binding pocket. Thus, ligand binding does not dictate which conformation the intracellular domain adopts. However, it merely influences the time the G-protein binding interface spends in each of its states. Hence, ligand binding is signalled across the membrane by shifting the conformational equilibrium of the intracellular receptor domain and not by a straight switch from an inactive to an active state. This mechanism allows for additional regulation. Several distinct ligands can activate the receptor to a different degree depending on how much they shift the conformational equilibrium.

This mechanism of GPCR activation, whereby extracellular ligand binding is associated with conformational flexibility of the opposite side of the receptor, is referred to as the conformational equilibrium model. A similar mechanisms was observed for several GPCRs such as the β_1-adrenergic receptor [48], the μ-opioid receptor [49] and the adenosine A_{2A} receptor [50]. However, it remains to be investigated if it is generalisable to other classes of receptors.

In contrast, the GPCR rhodopsin shows much tighter coupling between ligand binding and intracellular domains. Here, ligand binding strictly dictates the conformation of the G-protein coupling interface and no conformational equilibrium of the intracellular domain is observed [51, 52, 53, 54]. This can be described as an on-off model of receptor activation.

Studies of GPCR dynamics have revealed molecular mechanisms of their functions that static protein structures could not explain directly. For example, the poorly understood phenomenon of biased signalling, which harbours enormous potential in the drug industry, is believed to depend on transiently adopted conformational state [55]. These findings highlight the importance of studying the dynamic behaviour of other types of receptors.

1.4 Aims

Using NMR spectroscopy this project aims to investigate the dynamic behaviour of KDELR in solution with the goal of complementing information from static crystal structures. This marks the first dynamic study of a trafficking receptor and, as shown in the example GPCRs, promises to reveal further details about the molecular basis of KDELR function.

Recent structural studies have revealed details of the molecular events leading to peptide binding on the luminal side of the receptor. In contrast, little is known about how this information is relayed across the membrane. Thus, this project focusses on the molecular behaviour of the functionally important KDELR C-terminus and, especially, how the COPI binding surface changes with pH and peptide binding.

Specifically, this project aims to address four issues:

1. The crystal structures of KDELR in its 'active' and 'inactive' states differ in two variables, pH and presence of peptide. I investigate the individual role of pH and peptide binding in KDELR signalling.

2. Studies of GPCRs have revealed two mechanisms of receptor activation. Are these generalisable to trafficking receptors and does the KDELR C-terminus signal by the on-off or conformational equilibrium model?

3. Does the E143-K207 salt bridge stabilise the 'active' conformation of the KDELR C-terminus?

4. Can the redistribution of KDELR upon sybody binding be explained by a dynamic study of the receptor?

1.5 Introduction of NMR methods

To address these four question a method previously described in protein NMR was used [49, 56, 57, 58, 59]. The method is based on the post-translational introduction of NMR active nuclei into the protein. Specifically, amide groups are reductively methylated with carbon-13 (fig. 1.9).

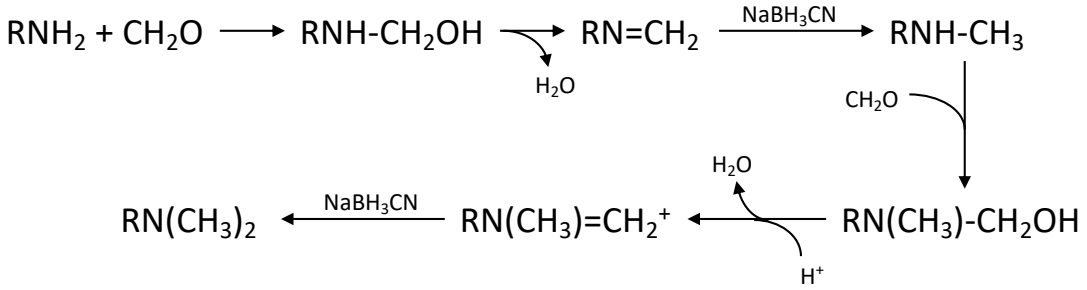

Figure 1.9: Reductive methylation of amide groups

This reaction is specific to the ζ-amide of lysine side chains and the α-amide of the protein N-terminus [60, 61, 62, 63]. KDELR2 contains 11 lysine residues, 4 of which are located in the C-terminal COPI binding motif. Thus, this method is optimally suited to investigate the functionally important C-terminus.

The methylation only marginally effects the pKa of lysine side chains and owing to the small size of methyls, structural perturbations are minimal [60, 56, 64]. Additionally, lysine methyl probes are well suited for NMR studies of large membrane proteins, such as KDELR, owing to their high sensitivity [65].

A downside to this method is the time-consuming way of resonance assignment. Conventional methods using triple resonance experiments do not work as the NMR active nuclei are not covalently bound to each other. NOEs have previously been used for assignments in methyl NMR experiments [66, 67]. However, the distance between lysines tend to be too big to observe NOEs. Peaks are usually assigned by the laborious systematic mutagenesis of lysines residues [56, 49, 68], which is also the method used for this project. Alternative methods of peak assignments using mass spectrometry have been described, however, these are less straight forward [69].

2 Materials and Methods

Unless specified otherwise, all experiments were conducted at room temperature and all chemicals purchased from Sigma-Aldrich. Unless specified otherwise H_2O refers to MilliQ water from Millipore Milli-Q system.

2.1 Microbiology

This study used *Escherichia coli* for the molecular biology steps and *Saccharomyces cerevisiae* for protein expression. Table 2.1 provides details about the cells used. Unless specified otherwise, plated *E. coli* cells were grown at 37°C and liquid cultures in a shaking incubator at 37°C and 200 rpm. Unless specified otherwise, plated *S. cerevisiae* cells were grown at 30°C and liquid cultures in a shaking incubator at 30°C and 250 rpm.

Table 2.1: List of bacterial and yeast strains used in this study

Organism	Strain	Genotype	Source
Escherichia coli	DH5α-T1^R	F- ϕ80lacZΔM15 Δ(lacZYA-argF) U169 deoR recA1 endA1 hsdR17 (r -, m +) phoA supE44 δ- thi-1 gyrA96 relA1 tonA	ThermoFisher
Saccharomyces cerevisiae	BJ5460	MATa ura3-52 trp1 lys2-801 leu2Δ1 his3Δ200 pep4::HIS3 prb1Δ1.6R can1 GAL	ATCC

2.2 Molecular Biology

2.2.1 The protein construct

The protein construct expressed in this study is shown in figure 2.1. The construct is a fusion protein consisting of the *Gallus gallus* KDELR2, encoded by the *ERD22_CHICK* gene (Uniprot: Q5ZKX9), that contains an S54C mutation. This mutation allows for the covalent binding of TACHDEL peptide to the receptor, which holds the peptide in the binding pocket and prevents dissociation during experiments. Furthermore, green fluorescent protein (GFP) is attached to the C-terminus of KDELR2, owing to its characteristic fluorescent properties GFP allows to monitor the protein concentration during expression and purification. KDELR2 and GFP are separated by a Tobacco Etch Virus (TEV) protease recognition sequence (ENLYFQG). After protease cleavage is carried out during protein purification, the non-native residues ENLYFQ remain attached to KDELR2. Additionally, the construct contains a C-terminal octo histidine-tag which allows for protein purification with immobilised metal affinity chromatography (IMAC).

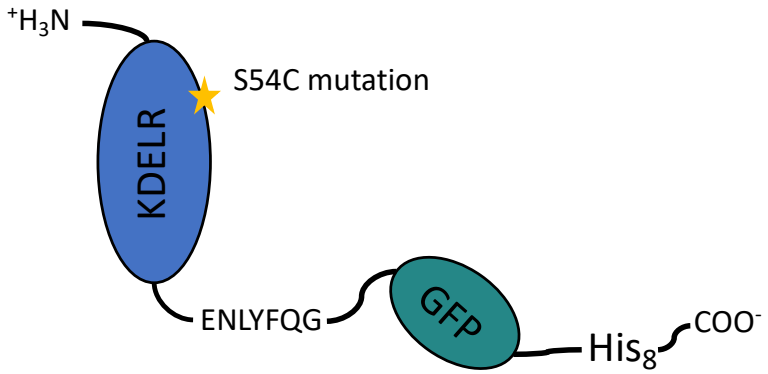

Figure 2.1: Schematic of protein construct expressed in this study. The construct is a fusion of KDELR2 with a S54C mutation and GFP, seperated by a TEV protease recognition sequence (ENLYFQG). The construct also contains a C-terminal octo histidine-tag to allow for purification with IMAC.

2.2.2 Plasmids

Table 2.2 provides a list of all plasmids used in this study. The pDDGFP-LEU2D *ERD22_CHICK* S54C plasmid, provided by the Newstead lab in the Department of Biochemistry at the University of Oxford, was used as the starting material for mutagenesis. This plasmid consists of the *ERD22_CHICK* gene (Uniprot: Q5ZKX9), which encodes the *Gallus gallus* KDELR2, with a S54C mutation contained in a pDDGFP-LEU2D backbone. Properties of the backbone are listed in table 2.3 [70].

Table 2.2: List of plasmids used in this study

Plasmid	Plasmid backbone	Gene	Mutations
pDDGFP-LEU2D ERD22_CHICK S54C	pDDGFP-LEU2D	ERD22_CHICK	S54C
pDDGFP-LEU2D ERD22_CHICK S54C K81R	pDDGFP-LEU2D	ERD22_CHICK	S54C, K81R
pDDGFP-LEU2D ERD22_CHICK S54C K83R	pDDGFP-LEU2D	ERD22_CHICK	S54C, K83R
pDDGFP-LEU2D ERD22_CHICK S54C K201R	pDDGFP-LEU2D	ERD22_CHICK	S54C, K201R
pDDGFP-LEU2D ERD22_CHICK S54C K204R	pDDGFP-LEU2D	ERD22_CHICK	S54C, K204R
pDDGFP-LEU2D ERD22_CHICK S54C K206R	pDDGFP-LEU2D	ERD22_CHICK	S54C, K206R
pDDGFP-LEU2D ERD22_CHICK S54C K207R	pDDGFP-LEU2D	ERD22_CHICK	S54C, K207R
pDDGFP-LEU2D ERD22_CHICK S54C E143A	pDDGFP-LEU2D	ERD22_CHICK	S54C, E143A

Table 2.3: Properties of the plasmid backbone

Plasmid backbone	Addgene ID	Host organisms	Selection Markers	Tags	Induction
pDDGFP-LEU2D	#58352	Escherichia coli, Saccharomyces cerevisiae	Ampicillin (E. coli), minus Uracil and minus Leucine (S. cerevisiae)	GFP, His8	Galactose

2.2.3 Site-directed mutagenesis

The pDDGFP-LEU2D *ERD22_CHICK* S54C plasmid was mutated using the Invitrogen GENEART site-directed mutagenesis system (#A13282). Mutagenesis was performed following the manufacturers manual to produce seven plasmids carrying an additional point mutation (table 2.2).

For the methylation of the original plasmid and the mutagenesis reaction, the mixture described in table 2.4 with the corresponding primer pairs given in table 2.5 was prepared. Suitable primers to introduce the point mutations were produced using the default settings of the online tool PrimerX. The PCR reaction was run with parameters defined in table 2.6.

Table 2.4: List of reagents used for the methylation and mutagenesis reaction

Reagents	Volume (μL)
10x AccuPrime Pfx Reaction mix	5
10x Enhancer	5
10 μM forward Primer	1.5
10 μM reverse Primer	1.5
35 ng/μL pDDGFP-LEU2D *ERD22_CHICK* S54C Plasmid	1
4 U/μL DNA Methylase	1
25x S-adenosyl-methionine	2
2.5 U /μL AccuPrime Pfx DNA Polymerase	0.4
Water	32.6

The recombination reaction to circularise the PCR product was set up with the reagents outlined in table 2.7. The mixture was incubated at room temperature for 10 minutes, then the reaction was stopped by addition of 1 μL 0.5 M EDTA and placed on ice.

Competent *E. coli* cells (table 2.1) were transformed with the recombination product. 2 μL of the recombination reaction was added to 50 μL of cells and incubated on ice

Table 2.5: List of site-directed mutagenesis primers. Upper case bases denote annealing bases, lower case bases highlight mutations.

Template	Primer	Sequence	Tm (°C)
pDDGFP-LEU2D ERD22_CHICK S54C	KDELR2_K81R_F	5'-ACCTGATCTATATGAgaTT CAAGGCTACCTAC-3'	71
	KDELR2_K81R_R	5'-GTAGGTAGCCTTGAAtcTC ATATAGATCAGGT-3'	71
	KDELR2_K83R_F	5'-TCTATATGAAGTTCAgaGC TACCTACGATGGT-3'	71
	KDELR2_K83R_R	5'-ACCATCGTAGGTAGCtcTG AACTTCATATAGA-3'	71
	KDELR2_K201R_F	5'-ACTTGTACGTTACCAgaGT CTTGAAGGGTAAG-3'	72
	KDELR2_K201R_R	5'-CTTACCCTTCAAGACtcTG GTAACGTACAAGT-3'	72
	KDELR2_K204R_F	5'-CGTTACCAAGGTCTTGAgaG GTAAGAAATTGTCTTTG-3'	75
	KDELR2_K204R_R	5'-CAAAGACAATTTCTTACCtcT CAAGACCTTGGTAACG-3'	75
	KDELR2_K206R_F	5'-AGGTCTTGAAGGGTAgaAAA TTGTCTTTGCCA-3'	71
	KDELR2_K206R_R	5'-TGGCAAAGACAATTTtcTACC CTTCAAGACCT-3'	71
	KDELR2_K207R_F	5'-TCTTGAAGGGTAAGAgaTTGT CTTTGCCAGCT-3'	72
	KDELR2_K207R_R	5'-AGCTGGCAAAGACAAtcTCTT ACCCTTCAAGA-3'	72
	KDELR2_E143A_F	5'-CATGATTTCTAAGACCGGTGc tGCTGAAACCATTACTACTC-3'	78
	KDELR2_E143A_R	5'-GAGTAGTAATGGTTTCAGCa gCACCGGTCTTAGAAATCATG-3'	78

Table 2.6: Thermocycling conditions for the methylation and mutagenesis reaction

Temperature (°C)	Duration	Cycles
37	20 min	1
94	2 min	
94	20 sec	3
57	30 sec	
68	4.5 min	
68	5 min	1
4	hold	

Table 2.7: Reagents for the recombination reaction

Reagent	Volume (μL)
5x Reaction Buffer	4
Water	10
PCR Product	4
10x Enzyme mix	2

for 12 minutes. Then the cells were heat shocked for 30 seconds in a 42°C water bath and placed on ice for at least 2 minutes. The transformed cells were plated on Lysogeny broth (LB) agar containing ampicillin and grown overnight at 37°C. A single colony was collected from the plates and grown overnight in high salt LB in a shaking incubator at 37°C and 200 rpm.

The plasmids were subsequently isolated using the QIAprep spin miniprep kit and analysed by sequencing. Additionally, analytical digestion of the plasmids was performed. The mixture detailed in table 2.8 was incubated for 1 h at 37°C and the product analysed on a 1% agarose gel.

Table 2.8: Reagents for the analytical plasmid digestion

Reagents	Volume (μL)
300 ng/μL Plasmid DNA	1
10x NEB rCutSmart Buffer	1
20 U/μL BamHI-HF	0.5
20 U/μL HindIII-HF	0.5
Water	7

2.3 Protein expression

KDELR2 with a S54C mutation was provided by the Newstead lab, University of Oxford Department of Biochemistry. The KDELR2 constructs carrying additional mutations were expressed as described below.

2.3.1 Yeast transformation

Plasmids were transformed into *S. cerevisiae* strain BJ5460 (table 2.1) using a PEG/LiT transformation method. Specifically, 600 μL of a fresh overnight culture were harvested by centrifugation at 16,000 x*g* and resuspended in LiT (table 2.9). Approximately, 1 μg of the plasmid to transform, 5 μg of ssDNA and 400 μL PEG/LiT were added to the cell suspension, vortexed and incubated on a rotating wheel at RT for 30 min. Next, DMSO was added to the cells to a final concentration of 10% (v/v) and the cells were placed in a 42°C heat block for 15 min. The cells were pelleted by centrifugation at 500 x*g* and resuspended in 75 μL water. Successfully transformed cells were selected using the minus uracil and minus leucine selection markers. Hence, the cells were plated on synthetic complete (SC) agar minus uracil with 2% glucose (w/v) for 3 days at 37°C. Approximately, 20 colonies were collected, restreaked on a plate with SC agar minus leucine with 2% glucose (w/v) and grown for another 3 days.

Table 2.9: Reagents used for the yeast transformation

Reagent name	Ingredients
LiT	100 mM lithium acetate, 10 mM Tris-HCl, pH 7.4, in water
PEG/LiT	100 g polyethylene glycol 3350 dissolved in 100 mL LiT

2.3.2 Mutant expression trials

Expression trials were carried out to analyse if the KDELR2 mutants express well. A few transformed *S. cerevisiae* colonies were collected from the plate, suspended in 15 mL

growth medium (table 2.10) and grown overnight in a shaking incubator at 30°C and 250 rpm. This culture was diluted 1:3 into expression medium (table 2.10) and grown until the optical density (OD) measured at 600 nm (OD600) exceeded 2. Then expression was induced by addition of 1.5% galactose (w/v). After a further 20 h, the yeast were harvested by centrifugation at 6000 x*g* for 15 minutes and the cell pellet resuspended in 1.5 mL PBS. Cells were lysed mechanically by addition of 250 μl glass beads and vigorous vortexing for 15 min. The lysate was centrifuge at 17,000 x*g* for 10 seconds to remove debris and unbroken cells. The supernatant was collected and centrifuged at 30,000 x*g* for 1 h to pellet the membranes. Membranes were resuspended in 450 μl PBS with 1% n-Dodecyl-β-D-maltoside (DDM) and 0.05% Cholesteryl hemisuccinate (CHS) and incubated for 1 h to solubilise membrane proteins. The solubilised proteins were isolated from the membrane remains by centrifugation at 30,000 x*g* for 45 minutes. The supernatant was collected and analysed by size exclusion chromatography using a Superose 6 Increase column. GFP-fluorescence emission was measured at 512 nm by excitation at 488 nm.

Table 2.10: Media used for KDELR2 expression in *S. cerevisiae*

Media	Ingredients
Growth medium	Yeast nitrogen base (YNB), Drop-out mix minus leucine, 2% glucose (w/v)
Expression medium	Yeast nitrogen base (YNB), Drop-out mix minus leucine, 2% lactate (v/v)

2.3.3 Large scale expression

The large scale expression of KDELR2 was carried out as described previously [17]. Specifically, all *S. cerevisiae* colonies from a transformed plate were collected, suspended in 100 mL growth medium (table 2.10) and grown for 24 h in a shaking incubator at

30°C and 250 rpm. This culture was diluted 1:5 into 400 mL of fresh growth medium and grown for another 24 h. Subsequently, the culture was diluted 1:10 into 4 L expression medium (table 2.10) and grown in flasks in 0.8 L of media. Once the OD600 exceeded 2 (after approximately 15h) expression was induced by addition of 1.5% galactose (w/v). After a further 20 h, the yeast was harvested by centrifugation for 15 min at 6000 x*g* and the cell pellet stored at -80°C.

2.4 Protein purification

Membranes were prepared as described in [71] and the remaining steps in the KDELR2 purifications are described in [72].

2.4.1 Buffers

Table 2.11: List of buffers used during the KDELR2 purification

Buffer	Ingredients
1x PBS	137 mM NaCl, 2.7 mM KCl, 10 mM Na2HpO4, 1.8 mM KH2PO4, pH 7.4
Membrane wash buffer	20 mM HEPES (pH 7.5), 10% potassium acetate (w/v)
Solubilisation buffer	1x PBS, 150 mM NaCl, 10% glycerol (v/v), 1% DDM (w/v), 0.05% CHS (w/v)
IMAC wash 1 buffer	25 mM imidazole, 1x PBS, 150 mM NaCl, 10% glycerol (v/v), 0.1% DDM (w/v), 0.005% CHS (w/v)
IMAC wash 2 buffer	37.5 mM imidazole, 1x PBS, 150 mM NaCl, 10% glycerol (v/v), 0.1% DDM (w/v), 0.005% CHS (w/v)
IMAC elution buffer	250 mM imidazole, 1x PBS, 150 mM NaCl, 10% glycerol (v/v), 0.1% DDM (w/v), 0.005% CHS (w/v)
SEC buffer	20 mM Tris (pH 7.5), 150 mM NaCl, 0.02% DDM, 0.001% CHS

* All buffers were prepared in H_2O. DDM: n-Dodecyl-β-D-Maltoside, CHS: Cholesteryl hemisuccinate

2.4.2 Membrane preparation

The cell pellets from the large scale expression protocol were thawed at RT and PBS (table 2.11) was added to at least 5-times the weight of the pellet. The suspended cells were lysed mechanically by two passes at 38 kPSI with a high pressure cell disruptor (model CF1 manufactured by Constant Systems Ltd.). The lysate was centrifuged for 30 min at 30,000 xg to remove debris and unbroken cells. The supernatant was collected and centrifuged for 1.5 h at 45,000 rpm to pellet the membranes. The membrane pellet was resuspended in membrane wash buffer (table 2.11) using a Dounce homogeniser. The resuspended membranes were pelleted again by centrifugation for 1.5 h at 45,000 rpm. The membrane pellets were resuspended in 5 ml PBS per gram of membrane using a Dounce homogeniser and stored at -80°C.

2.4.3 Membrane solubilisation

The membrane pellets were thawed at RT. 3x concentrated solubilisation buffer was added to the membranes and the mixture diluted to 1x concentration of solubilisation buffer (table 2.11). The mixture was incubated for 1.5 h at 4°C to solubilise membrane proteins. The solubilised proteins were isolated from the membrane remains by centrifugation for 1 h at 45,000 rpm and the supernatant was collected.

2.4.4 IMAC

In a first step, KDELR2 was purified using standard immobilised metal-affinity chromatography (IMAC). 25 mM imidazole and Ni-NTA resin (0.07 mL resin per mL of supernatant) were added to the supernatant. KDELR2 was allowed to bind to the resin for 5 h before running the IMAC. The column was washed twice and eluted with buffers described in table 2.11.

2.4.5 Reverse IMAC

Tobacco Etch Virus (TEV) protease was added to the eluate (0.2 mg protease per mL of elution). The mixture was dialysed overnight against SEC buffer (table 2.11) using a 3.5 kDa molecular weight cut-off (MWCO) dialysis tube. The dialysed protein was filtered with a 0.22 μm syringe filter. A reverse IMAC without imidazole was performed to remove the His-tagged TEV protease and cleaved GFP. The flow-through containing KDELR2 was collected.

2.4.6 SEC

The flow through of the reverse IMAC was concentrated in a 50 kDa molecular weight cut off (MWCO) spin concentrator to below 0.5 μL. Size exclusion chromatography (SEC) was run to further purify the protein. The concentrated KDELR2 was applied to a Superdex 200 Increase column and 0.5 mL fractions collected. Fractions were run on a 13.5% polyacrylamide gel to assess their purity. Pure fractions were pooled and further concentrated to above 12 mg/mL with a 50 kDa MWCO spin concentrator. The pure and concentrated protein was snap frozen in liquid nitrogen and stored at -80°C.

2.5 Post-translational protein modifications

2.5.1 KDELR2 peptide binding and dissociation

For peptide-binding, purified KDELR2 at a concentration of 12 mg/mL was diluted to 0.4 mg/mL with NMR buffer at pH 5.5 (table 2.12). TACHDEL peptide or biotin-CHDEL was added to KDELR2, now at pH 5.5, at a molar ratio of 10:1. Peptide was allowed to bind for 1 h at 4°C. After one hour, excess peptide was eliminated by dialysis (3.5 MWCO) for 1 h against fresh pH 5.5 NMR buffer. Owing to the cysteine residue in the peptide and the S54C mutation of KDELR2 a disulphide bond forms between peptide and receptor. Thus, the peptide is covalently attached to the protein and does

not dissociate on its own.

Dissociation of the peptide is only possible at pH 7.2 and above, as the peptide rebinds the receptor at lower pH values. The disulphide bond between peptide and KDELR2 was broken by the addition of 10 mM of the reducing agent Dithiothreitol (DTT). The peptide was then eliminated by dialysis (3.5 MWCO) for 1 h against NMR buffer at the correct pH containing 10 mM DTT.

2.5.2 Labelling by lysine methylation

KDELR2 was labelled for NMR studies by ^{13}C methylation of the ζ-amide of lysine side chains and the α-amide of the protein N-terminus with a method described previously [60]. The apo or peptide-bound KDELR2 were prepared in NMR buffer pH 5.5 (table 2.12) at a concentration of 0.25 or 0.4 mg/mL. The labelling reaction was initiated by the addition of 10 mM ^{13}C-formaldehyde and 10 mM $NaBH_3CN$ to the protein at 4°C. After 4h an extra 5 mM ^{13}C-formaldehyde was added and the reaction was allowed to proceed overnight. The labelled protein was dialysed (3.5 MWCO) for 2-24 h against NMR buffer of the right pH to eliminate excess reagent and change the pH of the samples for NMR experiments. The pH of the sample was measured and if required adjusted to $\pm$0.01 pH units of the desired pH by addition of HCl or NaOH.

2.5.3 Lysine methylation tests

Thermal unfolding and SEC were carried out to test the methylated KDELR2. Thermal unfolding was performed on samples of 0.25 mg/mL methylated KDELR2 using the Prometheus system (manufactured by NanoTemper). Melting scans were run with a starting temperature of 20°C, followed by an increase of 0.5°C per minute until the final temperature of 90°C was reached. Analytical SEC was performed on samples of 0.25 mg/mL methylated KDELR2 using a Superdex 200 Increase column.

2.5.4 Sybody binding

0.11 mg sybody 37 and 0.15 mg methylated KDELR2, both in NMR buffer pH 6.6 (table 2.12), were mixed and fresh buffer added to a total volume of 500 μL. Syb37 and KDELR2, now at a molar ratio of 1.2:1, were incubated at 4°C for 1 h to allow binding. An analytical SEC was run to assess the complex formation. The mixture was injected into a Sepax SRT-10C column and fractions of 0.5 mL collected. The SEC profile was analysed and fractions of interest run on a 15% polyacrylamide gel. Fractions containing the Syb37-KDELR2 complex were pooled and concentrated to 500 μl with a 50 kDa MWCO spin concentrator. The concentrated complex was then used for NMR experiments.

2.6 NMR

2.6.1 Buffers

Table 2.12: List of buffers for NMR experiments

Used pH range	Buffer components
5.5 - 7.0	20 mM MES (at correct pH), 150 mM NaCl, 0.02% DDM, 0.001% CHS
7.2 - 8.5	20 mM Tris (at correct pH), 150 mM NaCl, 0.02% DDM, 0.001% CHS

2.6.2 NMR experiments

500 μL of ^{13}C-methylated KDELR2 at a concentration of 0.4 mg/mL at the desired pH and in the correct NMR buffer (table 2.12) were used for each sample. 5% D_2O and 0.04 mM sodium trimethylsilylpropanesulfonate (DSS) were added and the samples transferred into standard round-bottom NMR tubes. NMR spectra were collected on a

950 MHz or a 750 MHz (^{1}H) Bruker NMR spectrometer. ^{1}H-^{13}C correlation spectra were recorded using the SOFAST-heteronuclear multiple quantum coherence (SOFAST-HMQC) [73] or heteronuclear single quantum coherence (HSQC) pulse sequences. The acquisition parameters for each experiment are listed in table 2.13. Experiments with 112 scan per FID were recorded and the acquisition time varied between 3-4 hours per sample for SOFAST-HMQC and 8 h for HSQC experiments.

Table 2.13: Acquisition parameters for NMR experiments

Experiment	^{1}H Frequency (MHz)	Spectral width (Hz)		Orig. number of points		Reference chemical shift (ppm)	
		^{1}H	^{13}C	^{1}H	^{13}C	^{1}H	^{13}C
^{13}C SOFAST HMQC	949.664	12285.013	9551.879	1220	384	4.700	40.000
^{13}C SOFAST HMQC	749.914	9689.923	7542.902	2048	384	4.700	40.000
^{13}C HSQC	749.914	12019.230	7542.895	1276	384	4.730	40.000

2.6.3 Processing of NMR spectra

NMR spectra were processed with the NMRPipe/NMRDraw pipeline [74]. The functions and parameters used for processing of ^{13}C SOFAST-HMQC and ^{13}C HSQC spectra are detailed in table 2.14. Visualisation and overlays of the processed spectra were produced in CARA [75]. To calculate peak intensities, volumes and linewidths spectra were simulated using the autoFit script part of the NMRPipe package. The quality of the simulated spectra was examined visually.

Table 2.14: Functions and parameters used for the processing of NMR spectra

		Parameters	
Dimension	Function	^{13}C-SOFAST HMQC	^{13}C-HSQC
^{1}H	Adjustable sin window	Sine start: 0.25, sine end: 1.0, sine exponent: 1, number of points: 585	Sine start: 0.4, sine end: 1.0, sine exponent: 1
	Zero fill	Final size: 4000	
	Complex fourier transform	Default parameters	
	Phase correction	Zero order: specific for spectrum, first order: 0	
	2D Transpose		
^{13}C	Adjustable sin window	Sine start: 0.45, sine end: 1.0, sine exponent: 3	Sine start: 0.55, sine end: 1.0, sine exponent: 1
	Zero fill	Final size: 750	
	Complex fourier transform	Sign alternation mode	
	Phase correction	Zero order: -90, first order: 180	Zero order: -90, first order: 0
	Base line correction via local median	Default parameters	
	2D Transpose		

3 Results

Unless otherwise specified all instances of KDELR2 in this study refer to KDELR2 with an S54C mutation. This mutation leads to the covalent binding of the TACHDEL peptide to the receptor and prevents dissociation during the experiments.

3.1 Lysine methylation tests

The dimethylation of lysine side chains chemically alters functionally important residues in KDELR2. It was previously reported that methylation does not effect the charge of lysine residues and generally only causes minimal structural perturbation of proteins [49, 56, 60]. Nevertheless, we first carried out several tests to assess the impact of the labelling method on KDELR2.

3.1.1 Analytical SEC

Analytical size exclusion chromatography (SEC) was used to assess whether methylation effects the fold of the receptor. SEC was performed on methylated KDELR2 in both apo and peptide-bound states. These results were compared to data obtained from the un-methylated control (fig. 3.1). The elution profile of all samples is highly similar with a large peak appearing at 13 ml of elution volume. The position of this peak is characteristic for KDELR2 under the experimental setting used. Notably, this peak is not perfectly monodisperse, however, this is typical for KDELR. Furthermore, a smaller peak appears at 8 ml. This secondary peak is most pronounced for the methylated

receptor in the apo state and less so in the other samples. As 8 ml corresponds exactly to the void volume of the column this peak most likely contains some form of oligomeric KDELR states or potentially aggregates. Formation of such higher molecular weight structures are occasionally observed for KDELR and, thus, are not of concern. The high similarity of the elution profiles of methylated receptor and control indicate that the labelling procedure does not effect the fold of KDELR2.

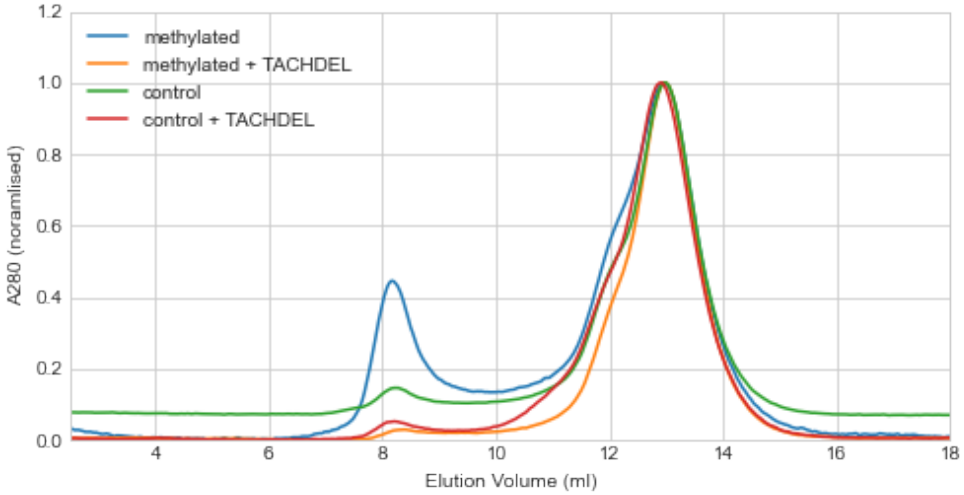

Figure 3.1: Analytical size exclusion chromatography of methylated KDELR2 and not methylated control. The absorbance of UV light at 280 nm (A280) as a fraction of its maximal value is plotted against the elution volume. Experiments were carried out in NMR buffer with pH 7.5 (table 2.12). The column void volume is 8 ml.

3.1.2 Thermal unfolding

To assess if methylation effects the stability of KDELR2 thermal unfolding was used. The melting temperature (Tm) of the labelled receptor was measured under various conditions and is compared to unlabelled control (table 3.1). Comparing measurement of methylated and control samples shows a general trend that methylation slightly decreases the Tm of the receptor. This effect is largest in the apo sample at pH 7.5 where the difference is approximately 6°C. Overall, however, the reduction in Tm upon methylation is minimal and the receptor remains highly stable.

Table 3.1: Melting temperature of the peptide-bound and apo KDELR2 at pH 5.5 and pH 7.2. Note, the peptide was bound to the receptor before labelling. Values with an error are derived from multiple measurements and the ones without from a single measurement.

Sample		apo	+TACHDEL
pH 7.5	methylated	$45 \pm 4°C$	$72.1 \pm 0.3°C$
	control	$51 \pm 1°C$	$73.5 \pm 0.7°C$
pH 5.5	methylated	$46 \pm 1°C$	$69.2°C$
	control	$49 \pm 4°C$	$73.4 \pm 0.1°C$

As a lysine residue (K64) is located inside the peptide binding pocket, it was assessed if labelling effects peptide binding and dissociation. Table 3.1 shows that there is a significant difference in stability of the peptide-bound and apo KDELR2. The Tms of bound and apo receptor are approximately 70°C and 50°C respectively. Thus, thermal unfolding can be used to monitor peptide binding.

Firstly, I looked at dissociation of peptide from the receptor. As the peptide is covalently bound to KDELR2 with a S54C point mutation dissociation requires the addition of the reducing agent Dithiothreitol (DTT) to the protein. Melting scans of peptide-bound KDELR2 with 1 mM and 10 mM DTT were recorded (table 3.2). After addition of 1 mM DTT the Tm of all samples remains high at approximately 70°C and only if the concentration of DTT is increased to 10 mM the Tm is reduced. Hence, both labelled KDELR2 and control behave identically with 10 mM DTT required for efficient removal of the peptide. I conclude that labelling does not affect peptide dissociation.

Secondly, the effect of labelling on peptide binding was investigated. Table 3.1 shows that the Tm of KDELR2 bound to peptide before methylation is similar to control. Thus, if peptide is bound to the receptor before labelling it is not affected by the reaction. Furthermore, it was assessed if peptide binding is still possible after the receptor has been methylated. Melting scans were recorded of KDELR2 that was incubated with peptide after labelling (table 3.3). This shows that, unlike in the control sample, the Tm of the methylated receptor remains low after attempted peptide binding. These results suggest

that peptide binding is no longer possible after KDELR2 has been methylated.

Table 3.2: Melting temperature of the peptide-bound KDELR2 treated with DTT. Values with an error are derived from multiple measurements and the ones without from a single measurement.

Sample		+TACHDEL +1 mM DTT	+TACHDEL +10 mM DTT
pH 7.5	methylated	$71.6 \pm 0.4°C$	$55.3°C$
	control	$73.4 \pm 0.3°C$	$57 \pm 1°C$
pH 5.5	methylated	$69.6°C$	$56.5°C$
	control	$73.3°C$	$57 \pm 1°C$

Table 3.3: Melting temperature of KDELR2 if peptide binding is attempted after labelling. In this set of experiments a modified peptide was used where a CHDEL motif is attached to biotin. This construct behaves highly similar to the TACHDEL peptide.

Sample		+bio-CHDEL	+bio-CHDEL +1 mM DTT
pH 5.5	methylated	$48°C$	$49°C$
	control	$72°C$	$52°C$

In conclusion, analytical SEC and thermal unfolding show that labelling does not affect the fold of KDELR2 and has a minor effect on stability only. Furthermore, peptide binding, if done before labelling, and peptide dissociation are not impacted by the reaction.

3.2 Preliminary NMR experiments

Once confirmed that the methylation reaction does not impact the fold, stability and function of KDELR2 preliminary NMR spectra were recorded. These were aimed at finding the lysine methyls peaks and determining a suitable temperature to record further NMR experiments.

In order to find the lysine methyl peaks in the ^{1}H-^{13}C correlation spectra, I recorded ^{13}C SOFAST-HMQC spectra of methylated KDELR2 in pH5.5 and pH8.5 NMR buffer

(table 2.12). Additional spectra were collected of protein-free control samples, these consisted of buffer labelled identically as the protein samples. Overlays of control and KDLER2 spectra are shown in figure 3.2. Peaks unique to the protein spectra were identified to distinguish protein from buffer peaks. Independent of pH, a distinct group of protein peaks is visible between 3.2 and 2.2 ppm in the ^{1}H dimension and 43 and 47 ppm in the ^{13}C (highlighted by green box). Previous studies detected lysine methyl peaks at similar chemical shifts [49, 56]. As methyls exhibit highly specific chemical shifts depending on their chemical connectivity, I conclude that the highlighted peaks correspond to the lysine methyls.

A cluster of low intensity protein peaks is visible between 2.0 and 3.0 ppm in the ^{1}H and 33 and 39 ppm in the ^{13}C dimension (highlighted with the dark blue box). The labelling reaction under the here used condition leads to efficient di-methylation of lysine side chains. However, small amounts of monomethyl-lysines are expected to be formed as a by-product [60]. As monomethyl-lysines have been observed previously at similar chemical shifts as the here highlighted peaks [76], it is highly likely that these resonances correspond to mono-methylated lysine residues. Furthermore, several other groups of protein peaks are visible in the spectra which most likely originate from naturally occurring ^{13}C in other methyl groups in the protein.

Owing to their large size transmembrane proteins exhibit slow molecular tumbling rates which leads to a short T_2 relaxation and, consequently, a low signal-to-noise ratio in NMR spectra. The quality of spectra can be improved by increasing the temperature of the sample which leads to faster tumbling [77]. However, high temperature also accelerates protein precipitation which might impact long NMR experiments. Thus, experiments were carried out to find a suitable temperature to record further NMR experiments of KDELR2. I recorded SOFAST-HMQC spectra of the receptor over a range of temperatures from 15°C to 45 °C (figure 3.3). At 15°C, the signal-to-noise ratio is low and protein peaks cannot be distinguished from background noise. When the temperature was raised to 25°C the resolution of protein peaks significantly increased.

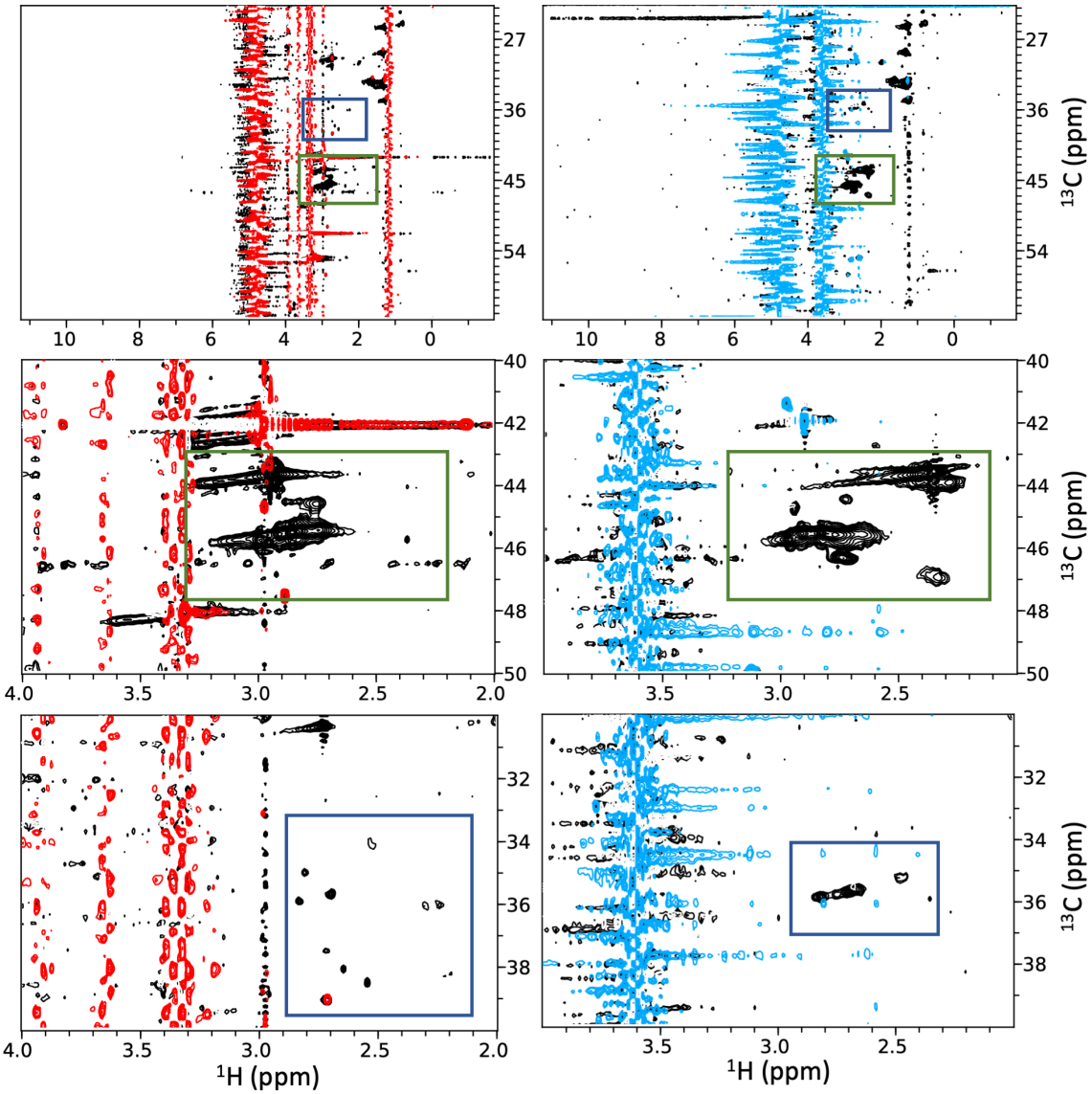

Figure 3.2: SOFAST-HMQC spectra of KDELR2 overlaid with protein-free controls. Left: Spectrum of KDELR2 (black) overlaid with pH 5.5 NMR buffer (red). Right: KDELR2 (black) overlaid with pH 8.5 NMR buffer (blue). The top, middle and bottom overlays show identical spectra with different axis limits. The green box highlights the identified lysine dimethyl peaks. The blue box indicates peaks likely corresponding to monomethyl-lysines. pH 5.5 NMR buffer: 20 mM MES (pH 5.5), 150 mM NaCl, 0.02% DDM, 0.001% CHS. pH 8.5 NMR buffer: 20 mM Tris (pH 8.5), 150 mM NaCl, 0.02% DDM, 0.001% CHS. Data collected on a 750 MHz spectrometer.

A further increase in temperature to 35°C and 45°C did not lead to big improvements of the resolution. Thus, all further NMR experiments are recorded at 25°C as this offers a good compromise between resolution and limiting the denaturation of the protein.

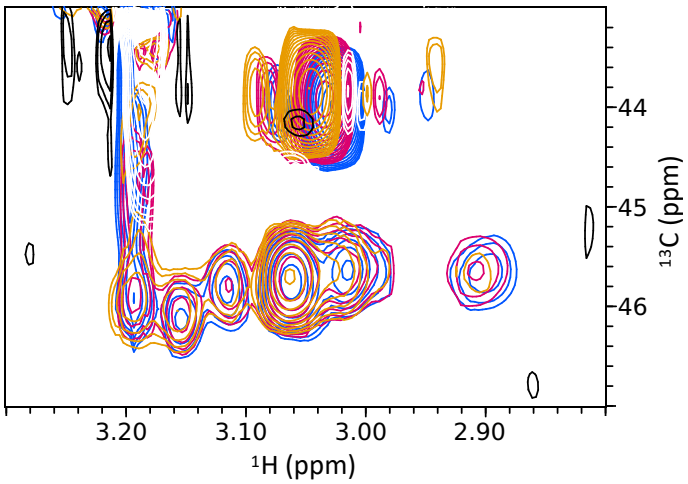

Figure 3.3: Temperature dependence of resolution of protein peaks. SOFAST-HMQC experiments of KDELR2 at pH 5.5 were recorded with 8 scans per FID at the following temperatures: 15°C (black), 25°C (orange), 35°C (red), 45°C (blue). Data collected on a 750 MHz spectrometer.

3.3 HMQC spectra of methylated KDELR2

The preliminary experiments confirmed that the lysine methylation method is suitable to investigate KDELR2 and helped to choose appropriate parameters for the NMR experiments. Next, I moved on to record experiments addressing the main aims of this project, to analyse the behaviour of the functionally important KDELR2 C-terminus during receptor activation and in solution. For this purpose, ^{13}C SOFAST-HMQC spectra were recorded of KDELR2 under conditions of interest. In particular, spectra under different pH conditions were recorded of the receptor in both the apo state and with the peptide covalently bound. pH 5.5 and pH 8.5 were chosen as these are close to the conditions the crystal structures were solved at (pH 6.0 and pH 9.0) and should facilitate comparison of findings [17, 21]. Furthermore, pH 6.6 and pH 7.2 were used to mimic conditions in the Golgi and ER, respectively [15, 16].

An overview panel of the eight recorded spectra is shown in figure 3.4. It is important to point out that in the spectra recorded at pH 6.6 there is interference of buffer signals with the lysine methyl peaks. This overlap complicates spectral analysis. Comparison of these spectra to the ones recorded at pH 5.5 reveals that the chemical shifts of protein peaks are highly similar. Thus, I assume that the receptor adopts an identical conformation at pH 5.5 and pH 6.6. For most parts of this study spectra recorded at pH 5.5 are used to characterise the behaviour of KDELR2 in the Golgi.

In depth analysis of the recorded spectra is not yet possible and requires resonance assignment which follows in the next section.

3.4 Production of mutants for peak assignments

3.4.1 Identification of mutants

Peak assignments were made using systematic mutagenesis of lysine residues. This approach is based on the principle that the methylation method is specific for lysine side chains. Thus, mutation of lysines to arginines will lead to the peak of the mutated lysine disappearing. This allows for assignment of the missing peak.

Assignment of all 11 lysines in the KDELR2 spectra would require the production of 11 individual lysine mutants. As this is very time consuming I decided to assign a total of six peaks. As I am most interested in the behaviour of the KDELR2 C-terminus it was decided to assign all four C-terminal lysines (K201, K204, K206, K207). Additionally, two residues outside the C-terminus were chosen to use as negative controls and to provide an internal standard for normalising spectral intensities (see section 3.5.2 below). Therefore, lysines had to be chosen which are not impacted by conformational changes of peptide binding and receptor activation. Based on the crystal structures K81 and K83 were selected (fig. 3.5). These are located on the opposite site of the cytoplasmic face of the receptor as the C-terminus. Furthermore, they appear to occupy identical conformations in the active and inactive state of KDELR2. Thus, I assume that

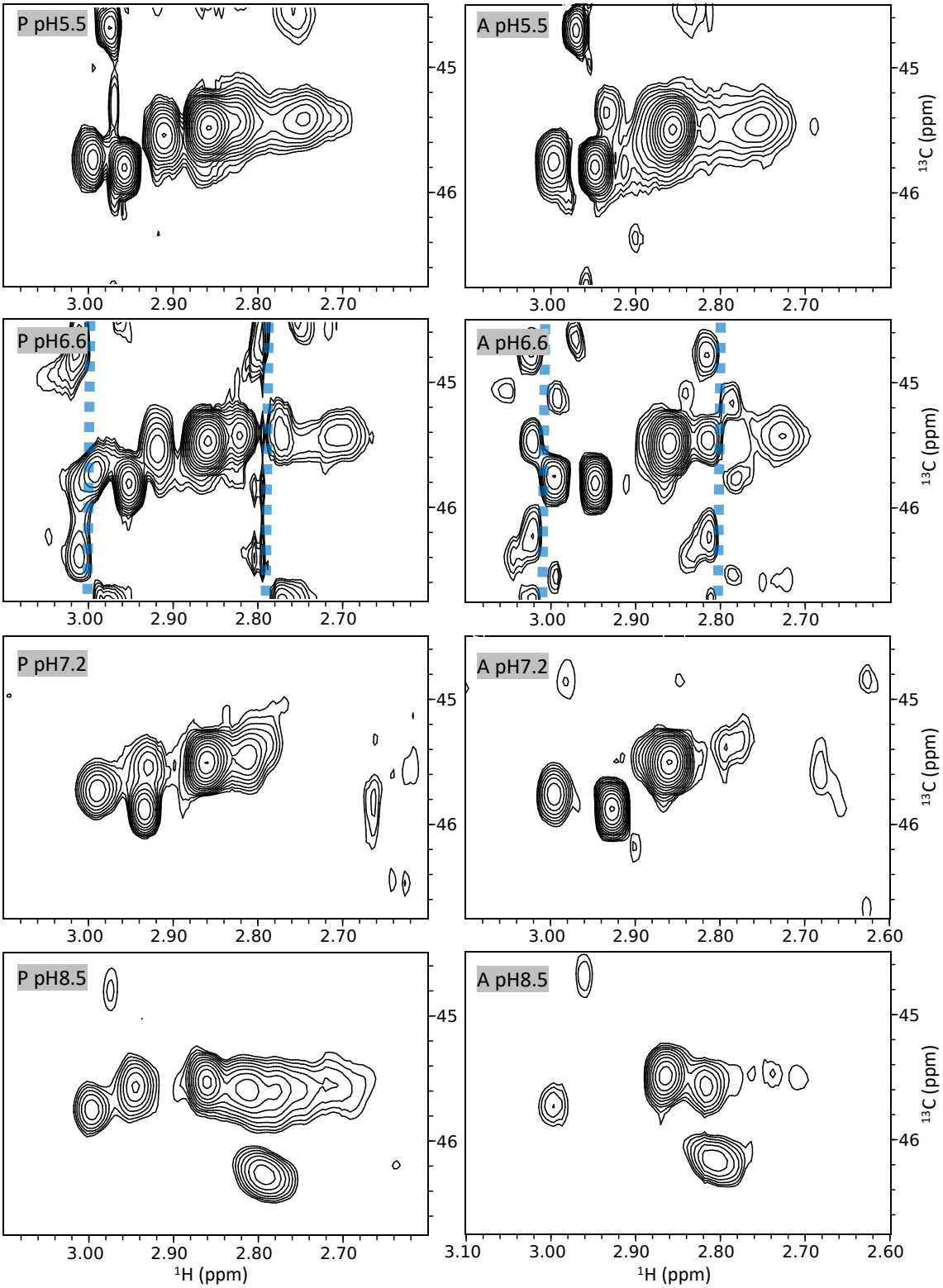

Figure 3.4: SOFAST-HMQC spectra of the methylated KDELR2. The region of the spectra containing previously identified lysine methyl peaks is shown. The blue vertical lines mark buffer interference. P: peptide-bound KDELR2, A: KDELR2 apo state. Data collected on a 950 MHz spectrometer.

the NMR signals originating from these two residues are constant in the experimental setup.

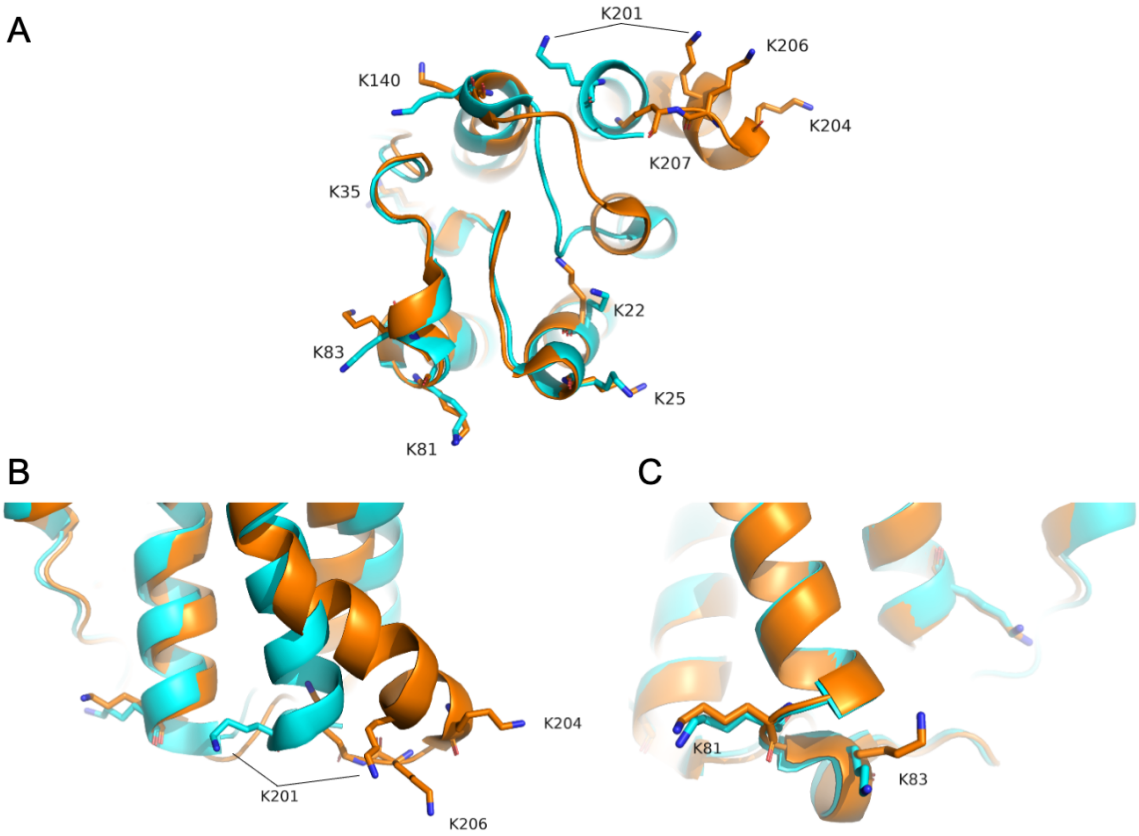

Figure 3.5: Arrangement of lysine residues in KDELR2. (A) View of the cytoplasmic face of the receptor. (B) Close-up view of the C-terminal lysine residues. Note that K204, K206 and K207 are not visible in the structure of the apo receptor at high pH. (C) Close-up view of residues K81 and K83 used as negative controls. The active receptor (peptide-bound, pH 6.0) is shown in orange (PDB: 6i6h). The inactive receptor (apo state, pH 9.0) shown in cyan (PDB: 6i6b). Lysine side chains are represented as sticks.

3.4.2 Mutant expression trials

To assign the peaks of the identified lysines, I set out to produce the six required lysine mutants. Plasmids carrying the KDELR2 S54C constructs were mutated using site-directed mutagenesis and transformed into *S. cerevisiae*. Initially, four mutants were expressed on a small scale to investigate whether the mutants are stable. The solubilised but not purified KDELR2 was run on SEC. The elution profile of KDELR2 was monitored by fluorescence detection of the GFP-tag.

The elution profile of the four constructs is shown in figure 3.6. All construct show a similar profile with a large peak between 35 and 40 minutes of elution time. Elution at this time is characteristic for KDELR2 under the conditions used. The peak is nicely monodisperse indicating that the constructs are folded and stable. An additional but much smaller smaller peak is visible between 20 and 25 minutes. With a void volume elution time of 20 minutes this peak indicates the formation of aggregates. However, the large difference in volume of the two peaks suggests that aggregation is minimal and the protein is overall stable. Taken together, the constructs express well and expression can be scaled up to produce sufficient material for the NMR experiments.

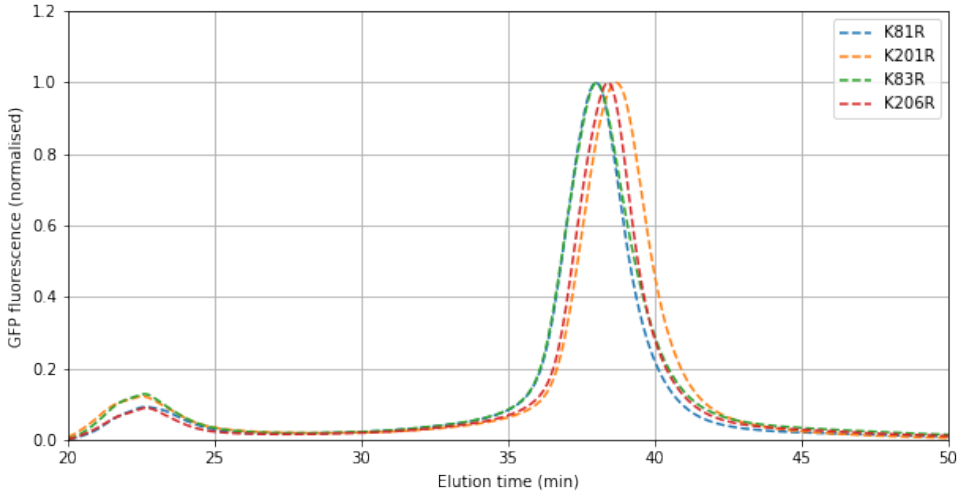

Figure 3.6: Fluorescence-detection size-exclusion chromatography of KDELR2 lysine mutants. The fluorescence emission of GFP at 512 nm excited at 488 nm is plotted as a fraction of its maximal value against the elution time. The void volume elution time of the column under the experimental settings used is 20 minutes.

3.4.3 Large scale expression and purification

After successful trials the expression was scaled up. Each mutant was expressed in 5 L of culture. The cells were harvested and membranes prepared. KDELR2 was then purified by IMAC, reverse IMAC and SEC. Figure 3.7 show an example of purification gels and the SEC elution profile of the representative KDELR2 S54C K206R mutant.

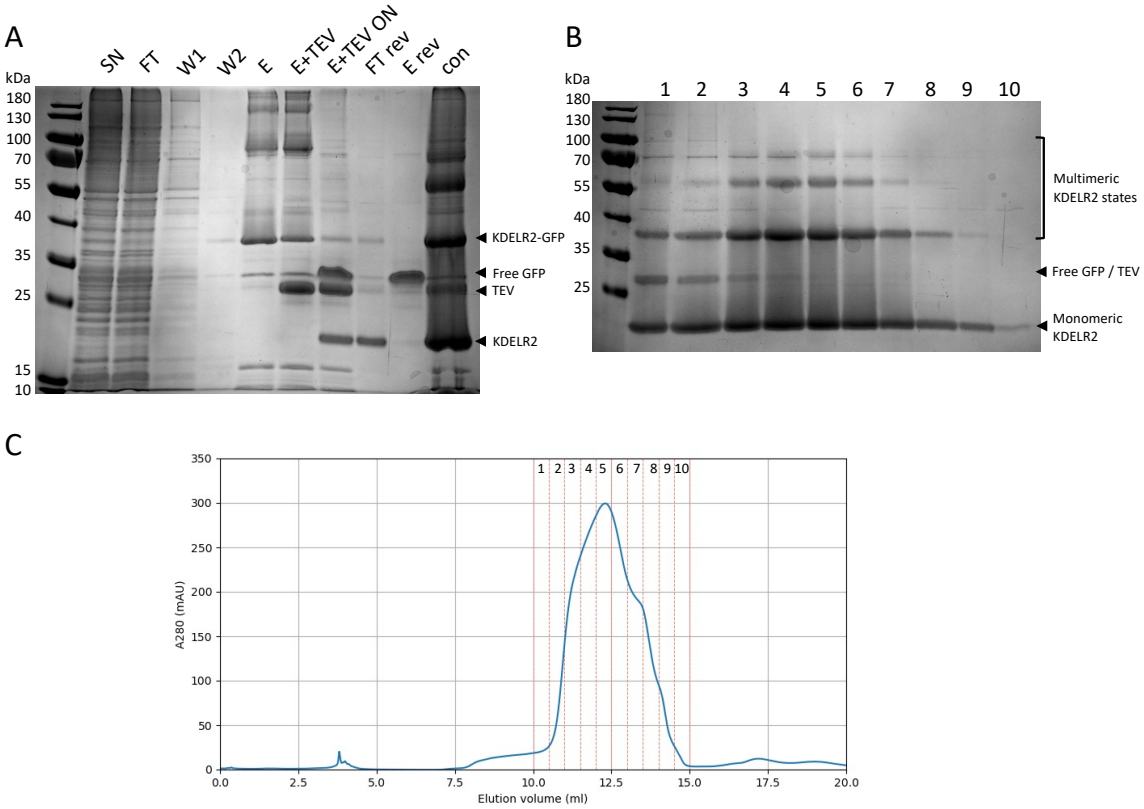

Figure 3.7: KDELR2 S54C K206R mutant purification. (A) Polyacrylamide gel of purification steps. The solubilised KDELR2 (SN) was purified using IMAC. After collection of the flow-through (FT), the column was washed with 15 mM (W1) and 37.5 mM (W2) imidazole, before elution with 250 mM imidazole (E). TEV protease was added to the elution to cleave the GFP and histidine tags (E+TEV) and incubated overnight (E+TEV ON). To separate TEV and GFP from KDELR a reverse IMAC was run. Flow-through (FT rev) and elution with 500 mM imidazole (E rev) were collected. The flow-through was concentrated to 500 μL (conc) and run on SEC. (B) Polyacrylamide gel with SEC fraction. The pure fractions, in this case 4-10, were pooled and used for NMR experiments. (C) Elution profile of SEC. Owing to several polymer states KDELR2 typically does not show a perfectly monodisperse peak. SEC fractions are indicated with vertical red lines.

3.5 Peak assignment

In order to assign the selected lysine peaks, ^{13}C SOFAST-HMQC spectra were recorded of the six mutants. Mutant spectra were overlaid with previously recorded WT spectra and missing peaks identified. The missing peaks were then assigned to the lysine residue which had been mutated. It is important to point out the WT in this section refers to the KDELR2 S54C construct with the covalently bound peptide and the term mutant is only used for KDELR2 lysine mutants. This method of peak assignment is based on the assumption that the efficiency of lysine methylation in mutant and WT spectra is identical. Thus, the disappearance of peaks is due to its mutation and not caused by a decreased labelling efficiency. As the mutations are conservative and not expected to cause structural perturbation this assumption is reasonable.

3.5.1 N-terminus

The peak corresponding to the methylated N-terminus was assigned without mutagenesis. In previous studies, the NMR signal of the N-terminus was observed as a resonance with high intensity and specific chemical shifts of approximately 43.5 ppm in the ^{13}C dimension [56, 49]. An intense peak with identical chemical shifts is also observed in the HMQC spectra of KDELR2 (fig. 3.8) and was assigned as the N-terminus. The peak is highly pH sensitive and titrates upfield with increasing pH. As the N-terminus does not provide information about the conformation of the KDELR2 C-terminus, this peak is not shown in most spectra in the following sections.

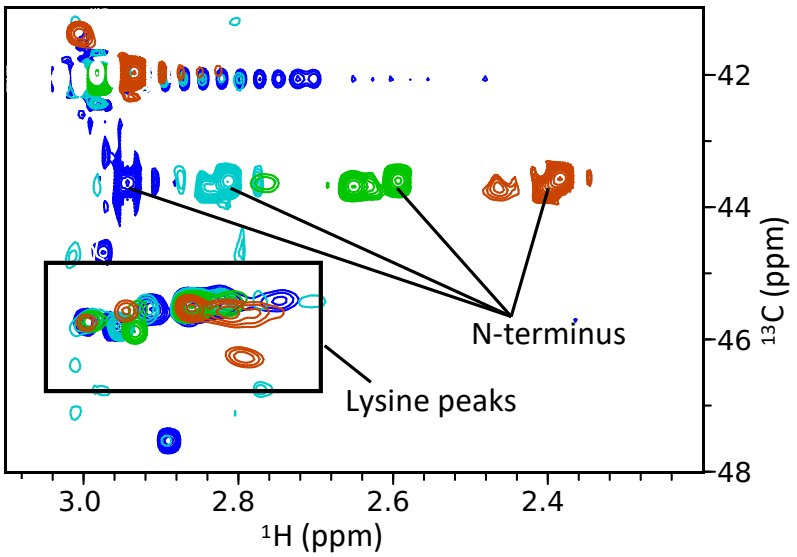

Figure 3.8: Assignment of the methylated N-terminus. Overlay of ^{13}C SOFAST-HMQC spectra of peptide-bound WT KDELR at pH 5.5 (blue), pH 6.6 (cyan), pH 7.2 (green), pH 8.5 (orange). The N-terminus is labelled and titrates upfield in the ^{13}C dimension with increasing pH. All data recorded on a 950 MHz spectrometer.

3.5.2 K83

Two dimensional spectra of the K83R mutant are overlaid with KDELR2 WT and shown in figure 3.9. The most prominent difference in all mutant spectra is that the peak at 3.00 ppm ^{1}H and 45.7 ppm ^{13}C is missing. Thus, this peak was assigned as K83.

Despite the assumption that the mutant and WT spectra should only differ in exactly one resonance, there are a few other peaks that appear to change in the overlays. Most noticeable is a slight shift of the peak at 2.7 - 2.8 ppm and 46 - 47 ppm in overlays at pH 8.5. The chemical shifts of this unassigned protein peak were observed to be highly pH sensitive across several spectra. Thus, the observed shift of this peak is very likely explained by minor differences in pH ($\pm$0.05 pH units) of the two samples and is consistent with a slightly higher pH of the mutant sample. Furthermore, the peak at 2.95 ppm and 44.5 - 45 ppm is more intense in mutant compare to WT (most prominent at pH 8.5). This peak was determined to originate from a buffer component and is present in all spectra, however, owing to its low intensity it is not visible at the contour levels chosen for some of the overlays. Again changes in intensity of this highly sensitive peak

are likely explained by minor differences in pH or buffer composition between samples. Similar changes in these two peaks are observed in several overlays in the following sections.

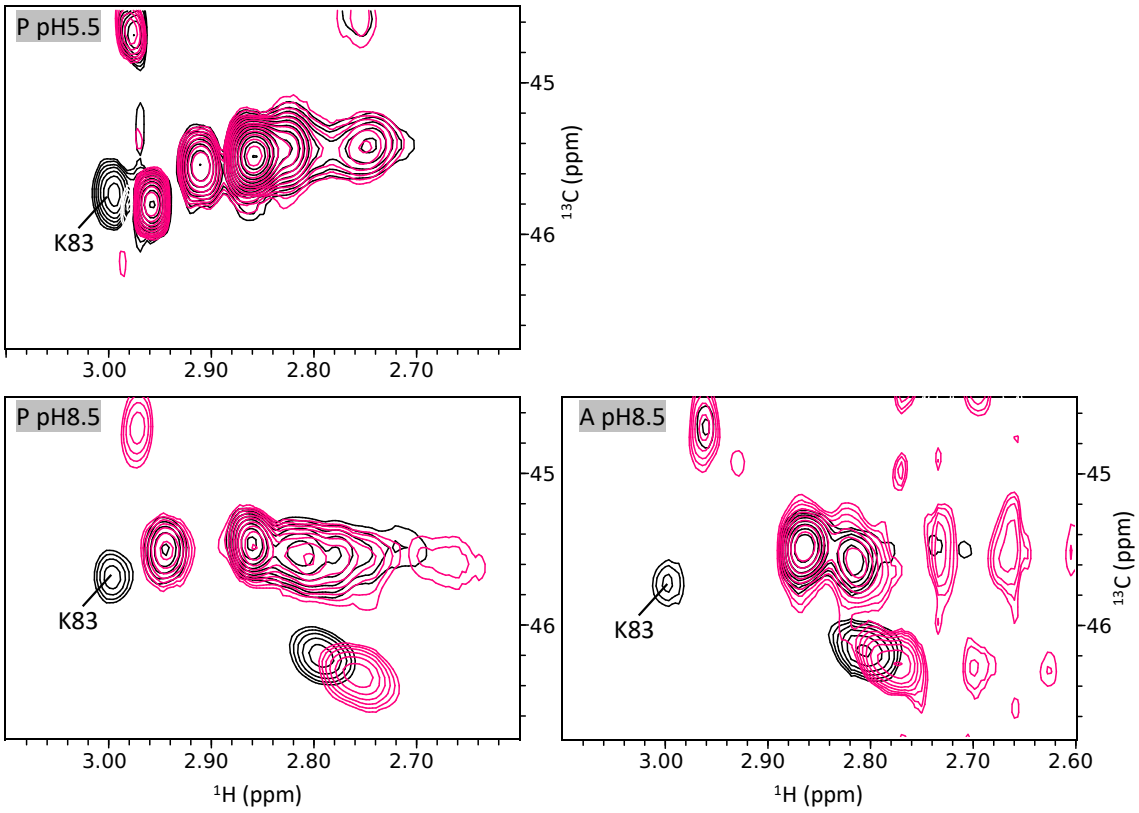

Figure 3.9: K83 assignment. Overlay of ^{13}C SOFAST-HMQC spectra recorded of WT (black) and the K83R mutant (red). P: peptide-bound KDELR2, A: apo KDELR2. All data recorded on a 950 MHz spectrometer.

Unambiguous assignment of the five remaining peaks requires the use of 1D projections from the 2D spectra. As there are slight variations in concentrations between samples these have to be appropriately scaled. As discussed in the previous section we do not expect the resonance of K83 to be effected by changing the experimental conditions. Thus, matching of the K83 peak was used to scaled the overlays of 1D projections in the following sections. There are a few exceptions to this in some of the low quality spectra due to high levels of noise.

3.5.3 K81

Figure 3.10 shows overlays of WT spectra with the K81R mutant. As the 2D overlays are not sufficient to identify a missing peak, 1D projections are shown in addition.

In the 1D projection at pH 5.5 intensity is missing in the peak at 2.86 ppm ^{1}H and 45.5 ppm ^{13}C. This peak does not disappear completely in the mutant spectra suggesting it consists of resonances originating from several lysine residues. The decreased intensity in the mutant, however, indicates that the resonance of K81 contributes to this peak. Further differences between mutant and WT spectra can be observed. Firstly, the peak at 2.95 ppm and 44.5 - 45 ppm appears to be missing in the mutant spectrum. However, when decreasing the contour level it becomes apparent that the peak is present in the mutant spectrum though with significantly reduced intensity. For a possible explanation of this change in intensity see section 3.5.2. Secondly, the peak at 2.95 ppm and 45.8 ppm exhibits a substantial increase in intensity in the mutant spectrum. This difference in intensity is observed in overlays of nearly all lysine mutants with WT at pH 5.5 and pH 7.2. This peak originates from the same protein residue as the peak at 2.7 - 2.8 ppm and 46 - 47 ppm in spectra at pH 8.5 (see fig. 3.16 for a pH titration of this peak). As discussed in the previous section this peak is highly sensitive to pH. Thus, differences in intensity may again be explained by slight differences in pH between the mutant and WT samples.

At pH 8.5, intensity is missing in the peak at 2.86 ppm ^{1}H and 45.5 ppm ^{13}C. Thus, K81 was assigned as a resonance contributing to this peak. In the peptide-bound overlay additional intensity is missing in the group of peaks between 2.75 and 2.85 ppm ^{1}H. Thus, it could be argued that K81 is overlapping with these peaks. However, if we observe the group more closely we can see that it consists of 3 individual peaks (a-c) with (a) in the WT only showing up as a slight shoulder. In the K81R spectrum these three peaks are matched, suggesting that there is no peak missing in this area despite the lower intensity.

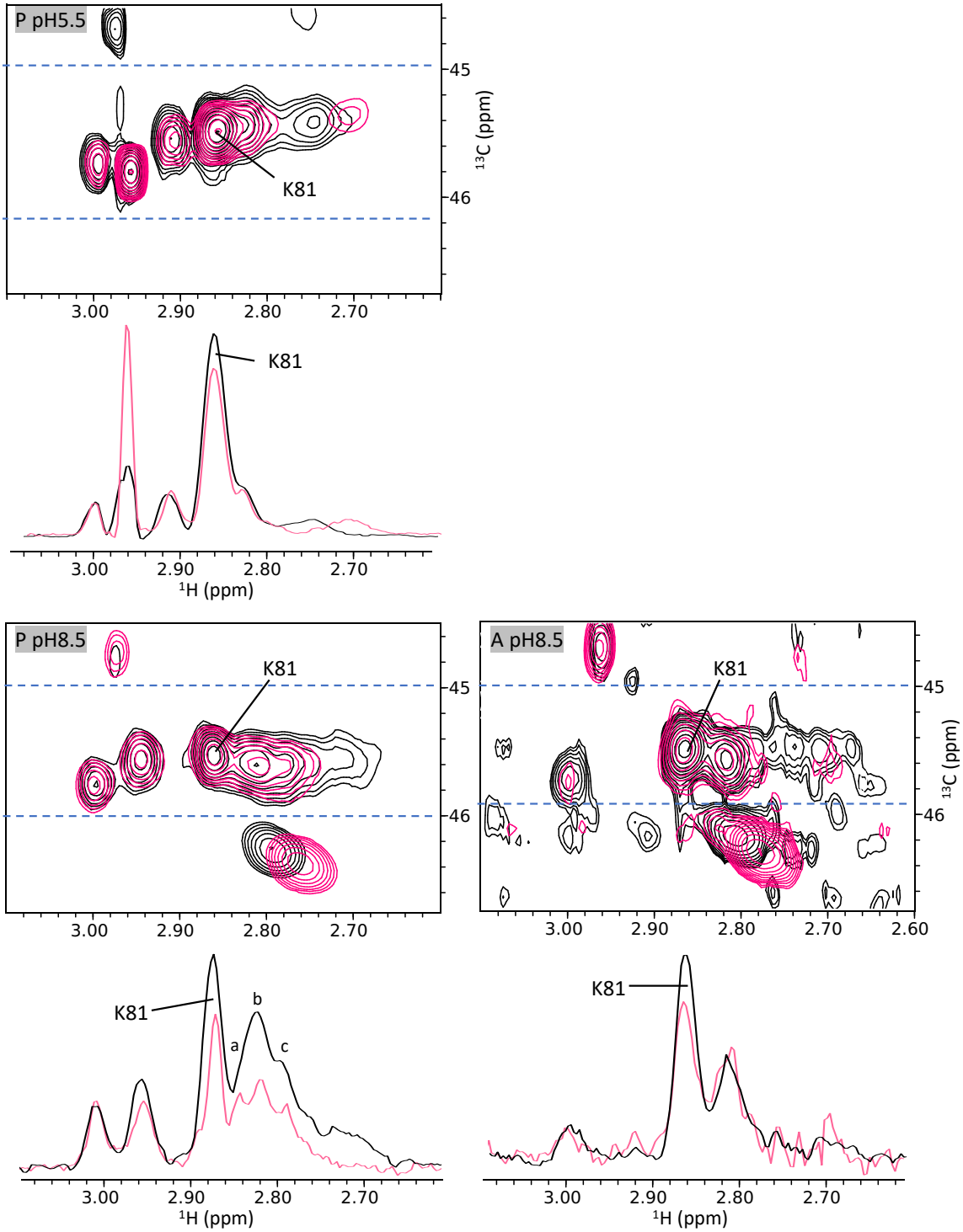

Figure 3.10: K81 assignment. Overlay of ^{13}C SOFAST-HMQC spectra recorded of WT (black) and the K81R mutant (red). The blue dotted lines indicate the area of which the 1D projections were produced. Intensities of K83 were matched to scale the 1D projections. P: peptide-bound KDELR2, A: apo KDELR2. WT spectra were collected on a 950 MHz spectrometer and K81R mutant spectra on a 750 MHz spectrometer.

3.5.4 K201

Overlays for the assignment of K201 are shown in figure 3.11. In the peptide-bound spectra at pH 5.5 and pH 7.2 a peak is missing at 2.81 and 2.80 ppm ^{1}H, respectively, and 45.4 ppm ^{13}C. At pH 8.5 the missing peak moved upfield and is now located at 2.77 ppm ^{1}H and 45.6 ppm ^{13}C. In the spectra of the apo state, across all pH values, no missing intensity can be identified. I conclude that K201 is not visible in the apo state. Absence of a signal for a specific residue can be explained by line broadening beyond the detection limit owing to dynamics in the microsecond to millisecond timescale resulting from conformational exchange [41]. In the overlays at pH 5.5 and 7.2 differences in intensity of the peak at 2.95 ppm and 44.5 - 45 ppm as well as the peak at 2.95 ppm and 45.8 ppm are observed between mutant and WT. Furthermore, there is a shift of the peak at 2.7 - 2.8 ppm and 46 - 47 ppm. These changes are very similar to the ones observed in overlays of K81R and K83R with WT and possible causes were discussed in more detail in the previous sections.

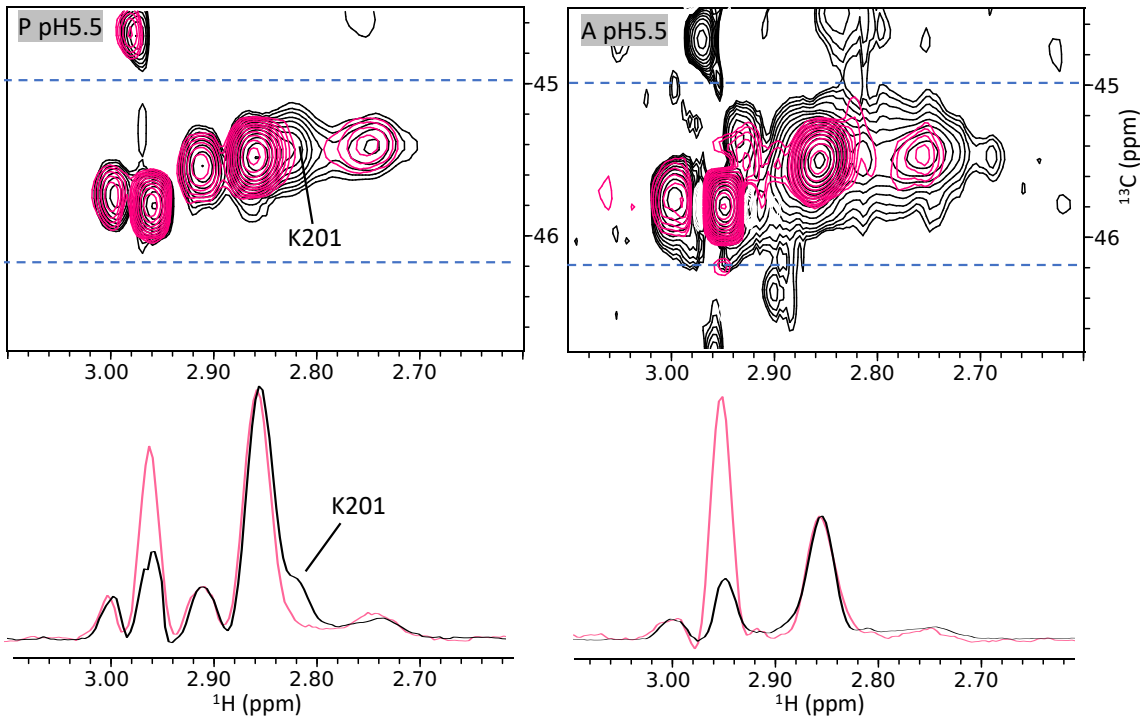

Figure 3.11: K201 assignment.

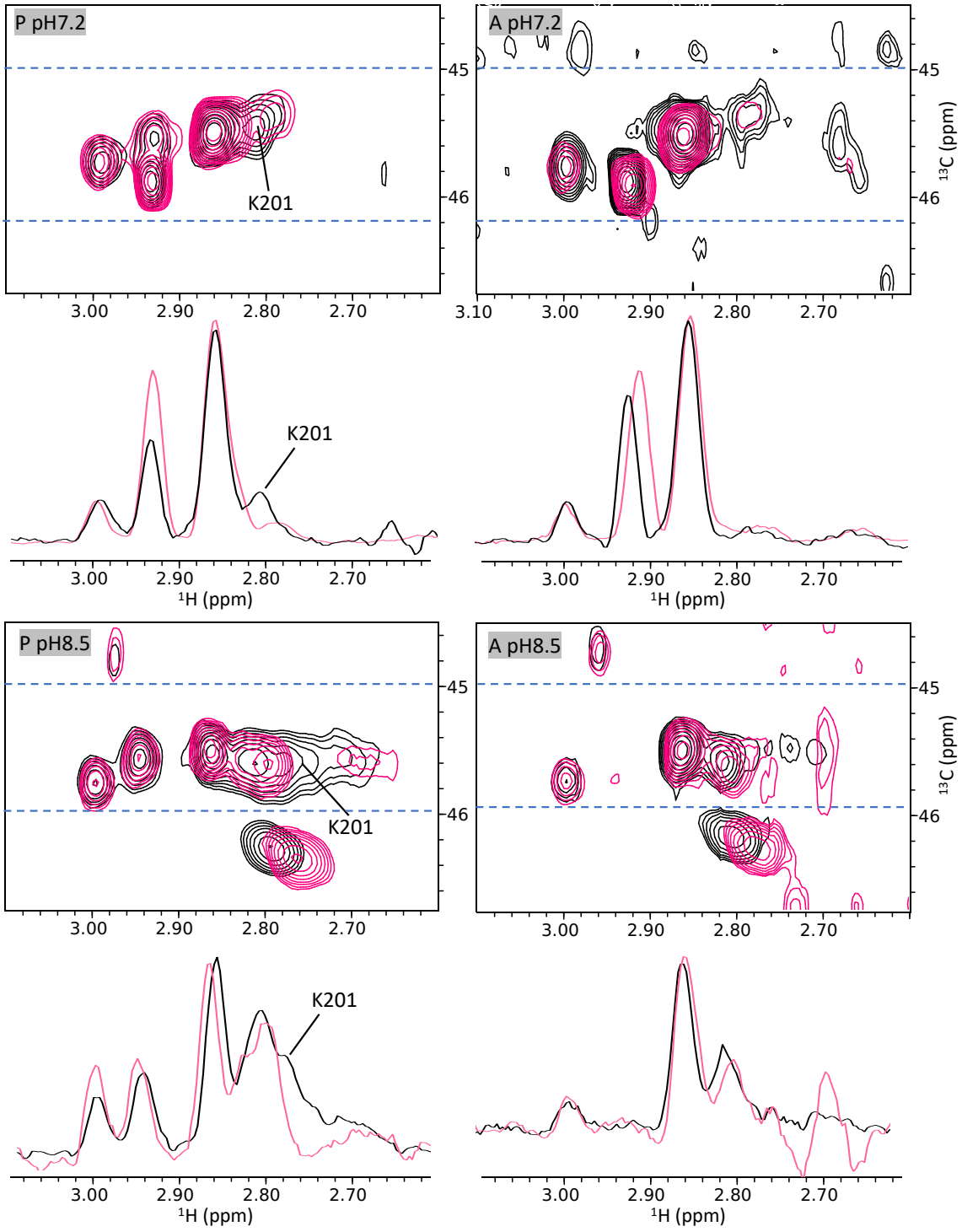

Figure 3.11: K201 assignment (cont.). Overlay of ^{13}C SOFAST-HMQC spectra recorded of WT (black) and the K201R mutant (red). The blue dotted lines indicate the area of which the 1D projections were produced. Intensities of K83 were matched to scale the 1D projections. P: peptide-bound KDELR2, A: apo KDELR2. All data recorded on a 950 MHz spectrometer.

3.5.5 K204

Overlays of K204R and WT are shown in figure 3.12. In the spectra of the peptide-bound receptor at pH 5.5 and pH 7.2 intensity is missing in the peak at 2.86 ppm ^{1}H and 45.5 ppm ^{13}C. This indicates that K204 is one of the overlapping resonances in this peak. While a large amount of intensity is missing in the spectra of the peptide-bound K204 mutant, very little intensity is missing in the apo state. This suggests that in the apo state K204 is significantly exchange broadened.

The mutant spectra collected at pH 8.5 are of low quality due to instability of the sample. Thus, assignment is less obvious. As mentioned previously, in the peptide-bound WT spectrum we see three overlapping peaks between 2.75 ppm and 2.85 ppm (a-c). In the mutant spectrum, a peak (a) at 2.81 ppm ^{1}H and 45.6 ppm ^{13}C is missing. In the apo spectrum, intensity is missing in the peak located at the same chemical shifts.

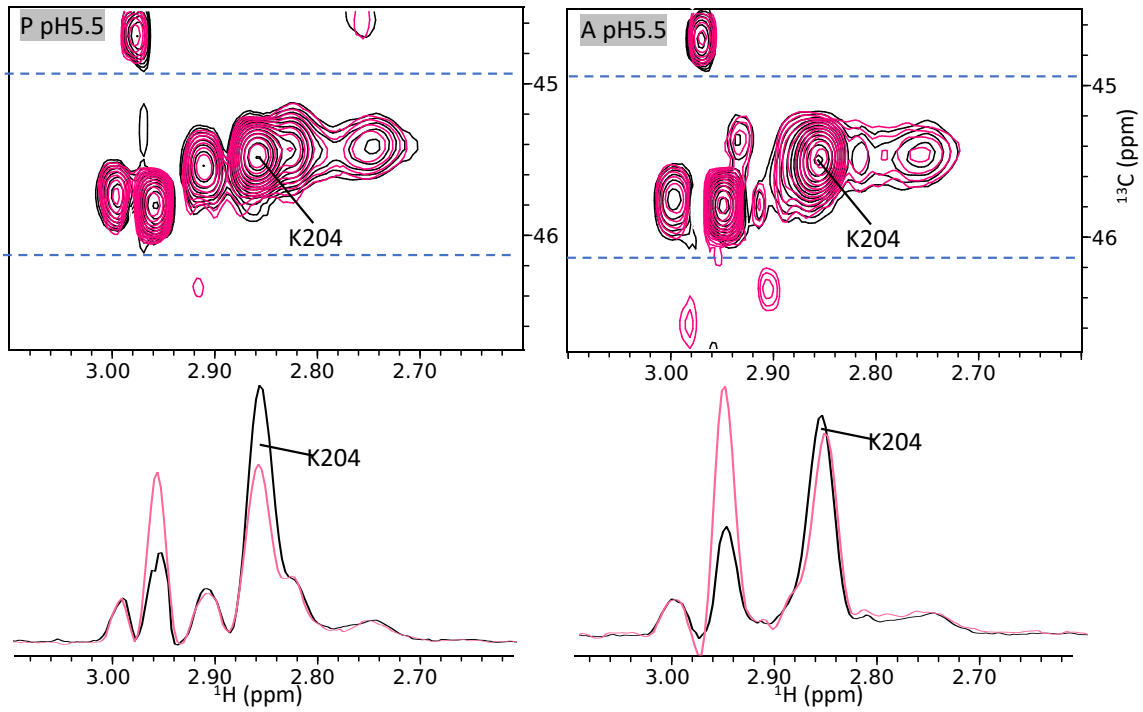

Figure 3.12: K204 assignment.

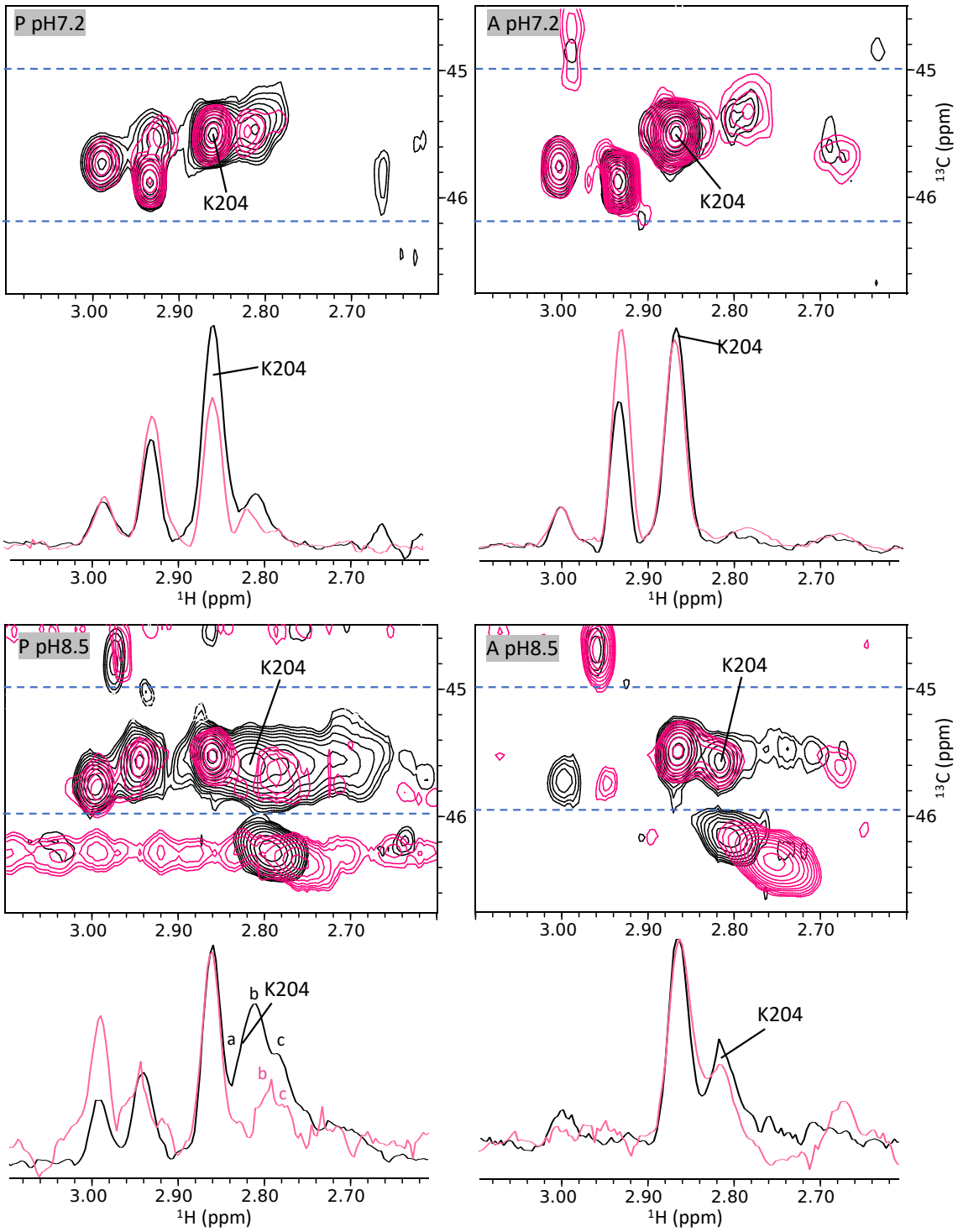

Figure 3.12: K204 assignment (cont.). Overlay of ^{13}C SOFAST-HMQC spectra recorded of WT (black) and the K204R mutant (red). The blue dotted lines indicate the area of which the 1D projections were produced. Intensities of K83 were matched to scale the 1D projections. P: peptide-bound KDELR2, A: apo KDELR2. All data recorded on a 950 MHz spectrometer.

3.5.6 K206

Overlays of K206R and WT spectra are shown in figure 3.13. In the spectrum of the peptide-bound receptor at pH 5.5 intensity is missing in the peak located at 2.86 ppm ^{1}H and 45.5 ppm ^{13}C. K206 is assigned as another overlapping resonance contributing to this peak. In the peptide-bound state at pH 8.5 the middle peak (b) is missing in the group of peaks between 2.75 and 2.85 ppm ^{1}H (a-c). In the apo state at high pH, no missing peak is observed. This again indicates peak broadening beyond the limit of detection.

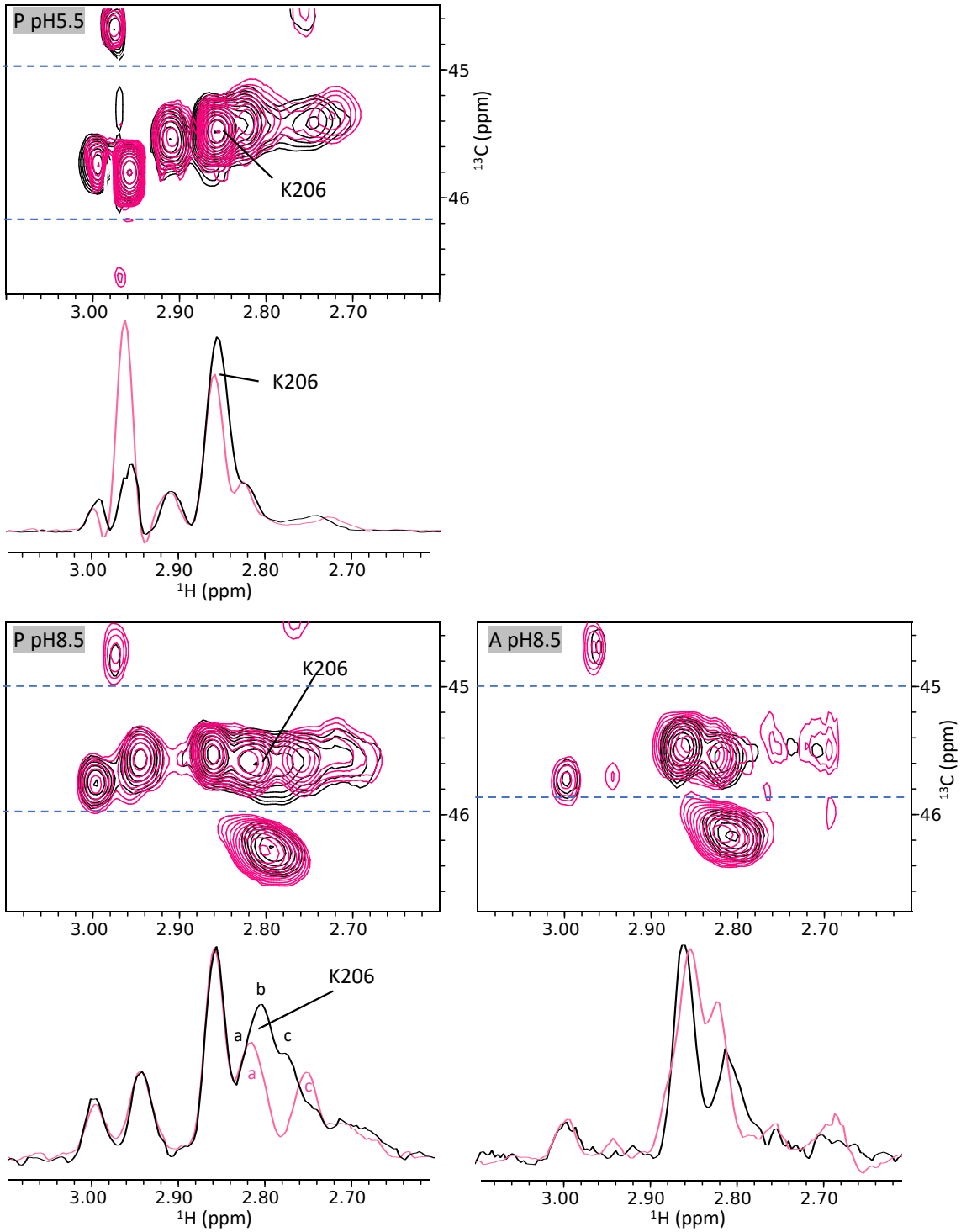

Figure 3.13: K206 assignment. Overlay of ^{13}C SOFAST-HMQC spectra recorded of WT (black) and the K206R mutant (red). The blue dotted lines indicate the area where of which the 1D projections were produced. Intensities of K83 were matched to scale the 1D projections. P: peptide-bound KDELR2, A: apo KDELR2. All data recorded on a 950 MHz spectrometer.

3.5.7 K207

Overlays of the K207R mutant and WT are shown in figure 3.14. In all overlays intensity is missing in the peak at 2.86 ppm ^{1}H and 45.5 ppm ^{13}C. Thus, K207 is assigned as another resonance contributing to this peak. As for K204 the difference in intensity between mutant and WT is significantly smaller in the apo compared to the peptide-bound state.

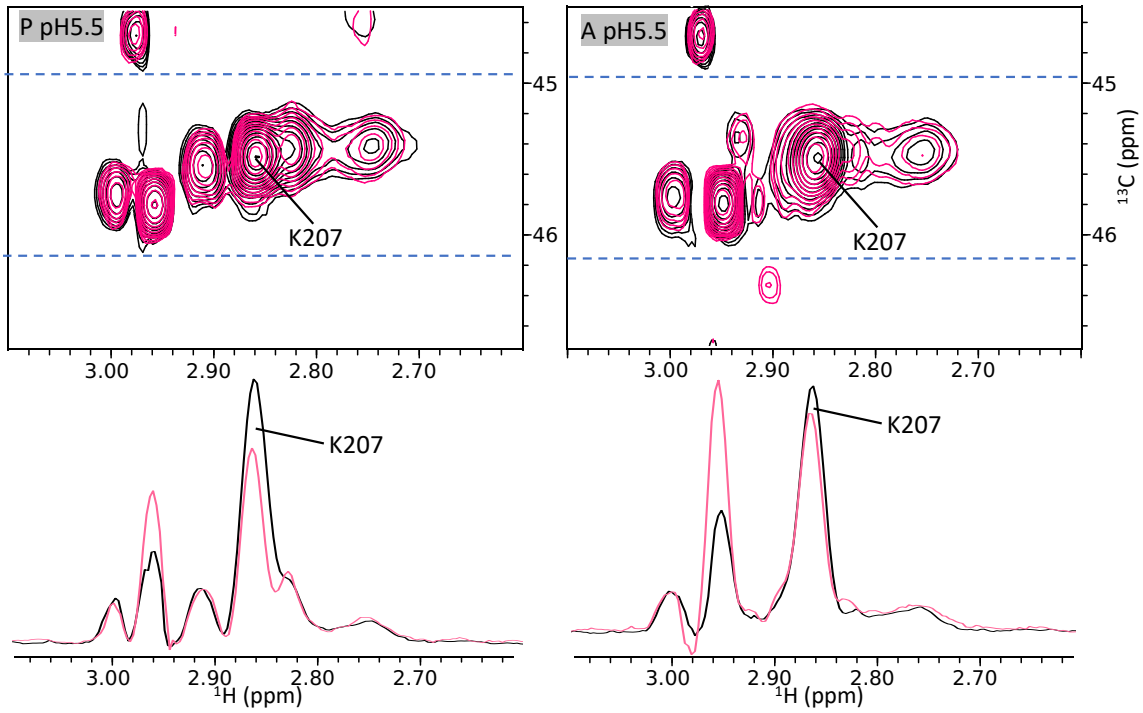

Figure 3.14: K207 assignment.

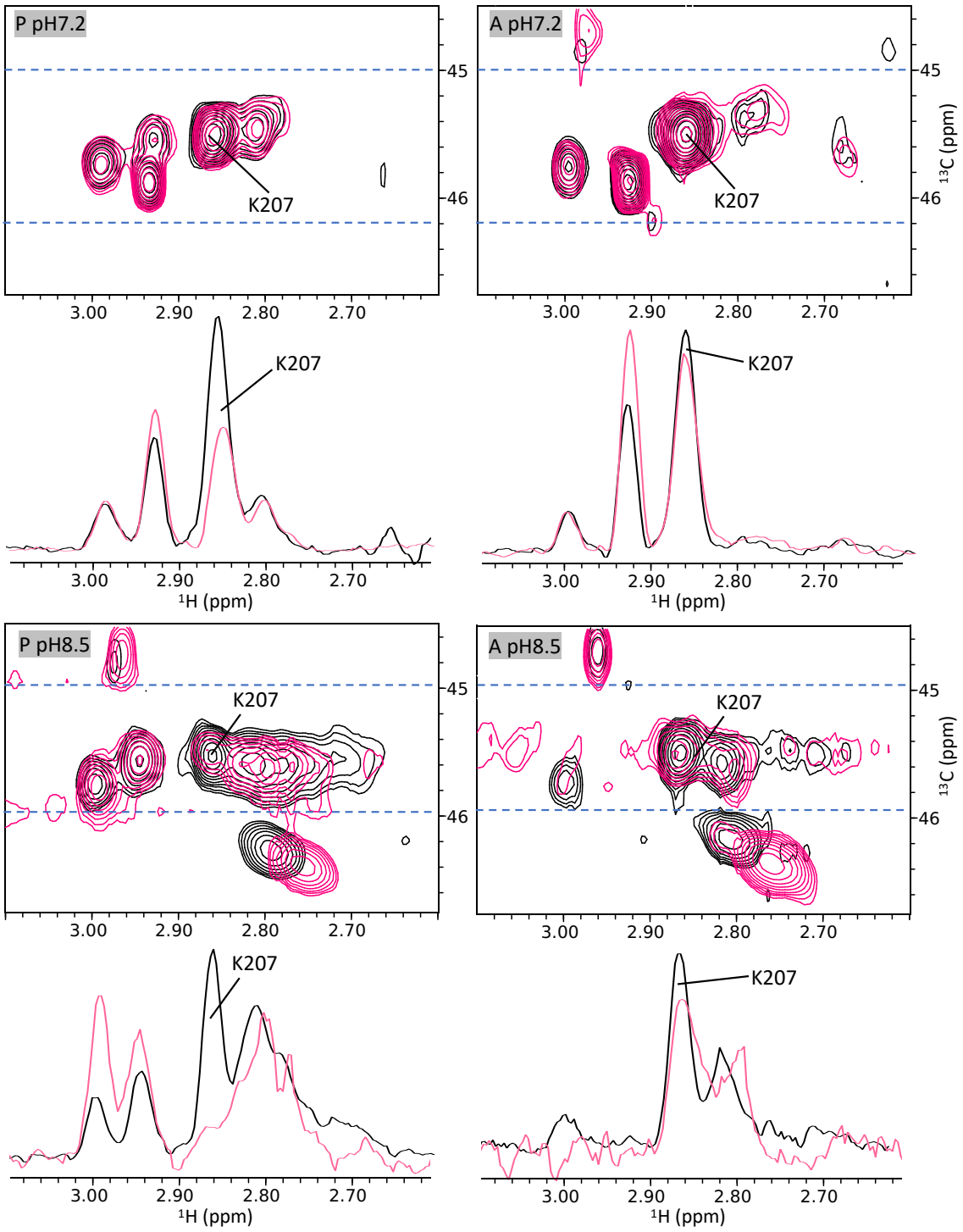

Figure 3.14: K207 assignment (cont.). Overlay of ^{13}C SOFAST-HMQC spectra recorded of WT (black) and the K206R mutant (red). The blue dotted lines indicate the area where of which the 1D projections were produced. Intensities of K83 were matched to scale the 1D projections. P: peptide-bound KDELR2, A: apo KDELR2. All data recorded on a 950 MHz spectrometer.

3.5.8 Overview of assignments

A spectra panel with all peaks assigned is show in figure 3.15. Peaks assigned based on the above described mutant spectra are labelled in black. As this does not cover all peaks in the 8 spectra the assignment of the remaining peaks was inferred (labelled in red).

The K81 and K83 peaks have identical chemical shifts in all assigned spectra. Thus, no changes in chemical shifts of these two residues are expected in the other spectra. Peaks with the same chemical shift were assigned with high confidence in the remaining spectra. Chemical shifts of the C-terminal lysine peaks (K201, K204, K206, K207) are unaffected when pH 5.5 and pH 7.2 are compared. Hence, it seems highly likely that at the intermediate pH value (pH 6.6) they are located at the same position.

Assignment of K201 and K206 in all spectra of KDELR2 in its apo state was not possible. These peaks are most likely broadened beyond the detection limit.

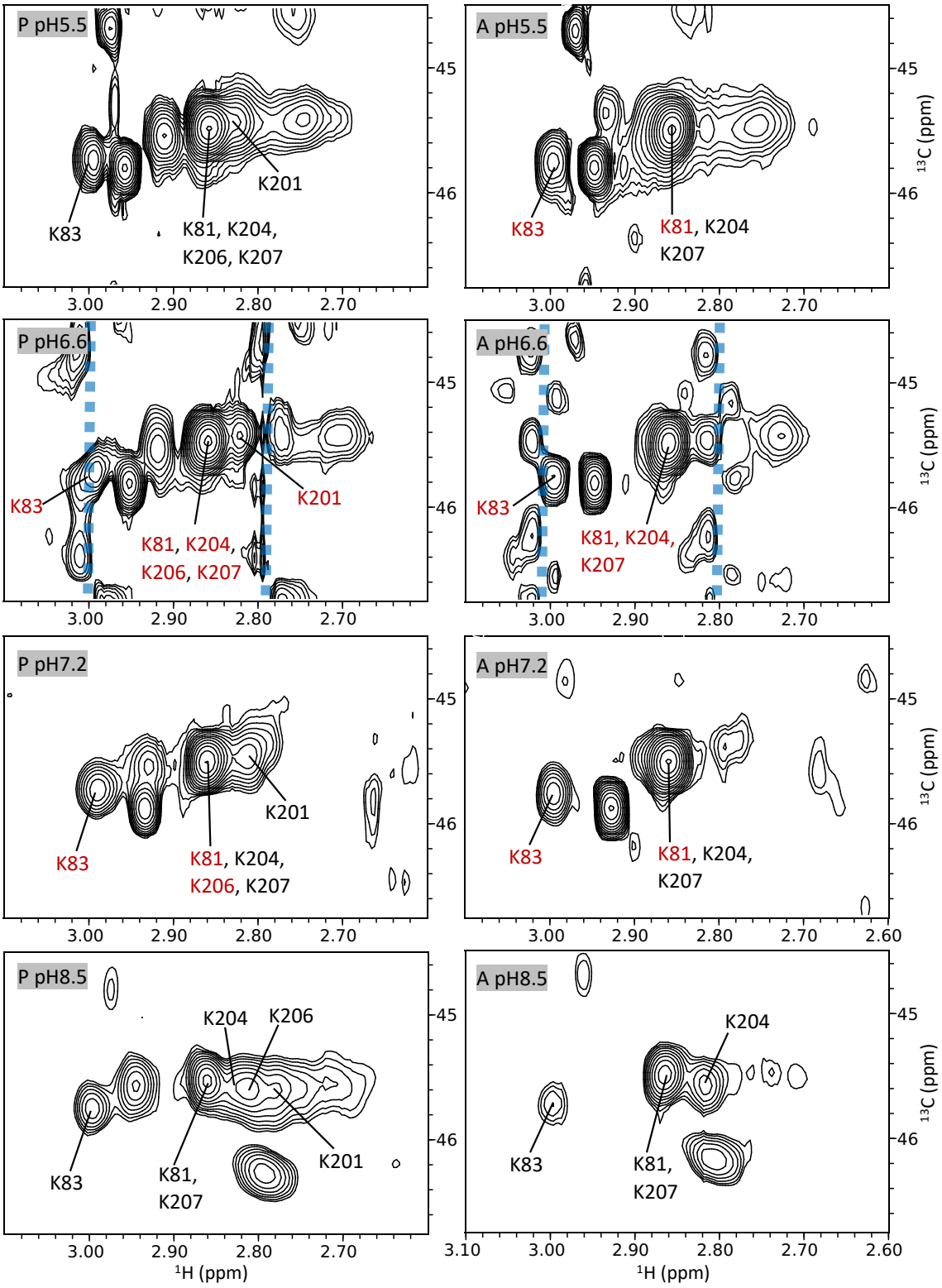

Figure 3.15: Spectra panel with peaks assigned. Peaks assigned with the help of mutant spectra are labelled in black. Inferred assignments are shown in red. The vertical blue lines indicate regions of buffer interference. P: peptide-bound KDELR2, A: KDELR apo state. All data recorded on a 950 MHz spectrometer.

3.6 Analysis of chemical shifts

With the peak assignment completed, I moved on to the analysis of the KDELR2 spectra. In the spectra there are two observables reporting on conformational exchange, chemical shift and linewidth. This section is focussed on the analysis of chemical shifts which report on the chemical environment of the lysine methyls. Thus, changes in chemical environment owing to a change in conformation would perturb the chemical shifts.

The chemical shifts in the ^{1}H dimension of all assigned lysine residues are summarised in table 3.4. Looking at the chemical shifts of K81 and K83, we can see that these are not effected by experimental conditions. This was expected for these two residues and confirms their suitability as negative controls.

Table 3.4: Chemical shifts in the ^{1}H dimension of assigned lysine residues. All values given in ppm.

	pH 5.5		pH 6.6		pH 7.2		pH 8.5	
Residue	peptide-bound	apo	peptide-bound	apo	peptide-bound	apo	peptide-bound	apo
K81	2.86	2.86	2.86	2.86	2.86	2.86	2.86	2.86
K83	3.00	3.00	2.99	3.00	2.99	3.00	2.99	2.99
K201	2.82	-	2.82	-	2.81	-	2.78	-
K204	2.86	2.86	2.86	2.86	2.86	2.86	2.83	2.82
K206	2.86	-	2.86	-	2.86	-	2.80	-
K207	2.86	2.86	2.86	2.86	2.86	2.86	2.86	2.86

In the peak assignment section we saw that in spectra collected between pH 5.5 and pH 7.2 resonances of K204, K206 and K207 are all overlapping. This is reflected in identical chemical shifts of these residues when compared within a column in table 3.4 (this is not true for pH 8.5). This finding indicates that at pH 7.2 and below K204, K206, and K207 occupy a highly similar chemical environment. Based on knowledge from crystal structures it is most likely that these exact chemical shifts reflect a completely solvent exposed lysine methyl. In comparison, K201 is shifted upfield in the ^{1}H dimension.

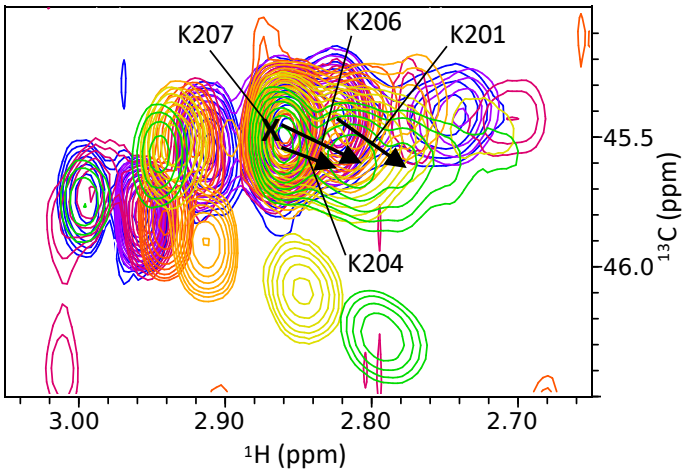

Figure 3.16: pH titration of peptide-bound KDELR2. The black arrows indicate the movement of C-terminal lysine peaks with increasing pH from left to right. blue: pH5.5, purple: pH6.0, red: pH6.6, dark orange: pH7.0, bright orange: pH7.5, yellow: pH8.0, green: pH8.5. ^{13}C SOFAST-HMQC spectra recorded on a 950 MHz spectrometer.

In the crystal structures K201 is located on the C-terminal side of TM7. The helix dipole causing a partial negative charge of this end of the helix would result in the K201 methyls being slightly more shielded. Thus, despite being solvent exposed K201 is shifted upfield.

Next, the effect of pH on the chemical shifts of the C-terminal lysines was investigated. To enable a more detailed analysis, NMR spectra at additional pH values were recorded of the peptide-bound KDELR2. An overlay of the complete pH titration is shown in figure 3.16. It was not possible to reproduce the titration with additional pH points for the receptor in the apo state due to its lower stability. The movement of C-terminal lysine peaks is highlighted with arrows in figure 3.16. An upfield shift in the ^{1}H dimension is observed for K201, K204 and K206 with increasing pH. The chemical shifts of K207 are not effected by pH.

Chemical shift perturbations in the ^{1}H dimension with pH were plotted in figure 3.17. In both apo and peptide-bound state there appears to be relatively little change in chemical shifts between pH 5.5 and pH 7.2. Large perturbations only occur above pH 7.2. This indicates that the C-terminal lysines titrate with a pKa significantly above pH 7.2. As described previously [17, 16] histidine 12 acts as the pH sensor residue of KDELR2 and regulates cargo binding in the Golgi and release in the ER. For this function H12

requires a pKa in between or very close to pH 6.6 and pH 7.2. As the C-terminal lysine residues titrate with a considerably higher pKa, this data suggest that protonation of the pH sensor residue H12, and more generally pH changes over the physiologically relevant range, do not result in the conformational remodelling of the KDELR2 C-terminus.

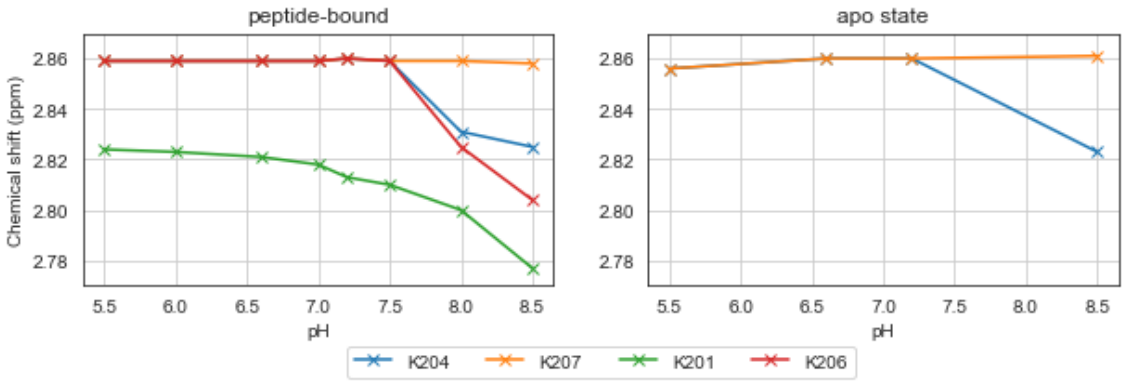

Figure 3.17: Chemical shift perturbations of the four C-terminal lysine residues with pH. The plot on the left shows a pH titration of peptide-bound KDELR2 and the one on the right of the apo state. Chemical shifts of the ^{1}H dimension are plotted against pH.

The large changes of chemical shifts above pH 7.2 are likely caused by the titration of a nearby imidazole with higher pKa. Histidine 150 is located in close proximity to the C-terminus (fig. 3.18). The rearrangement of the crystal structures between pH 6 and 9 is consistent with residue H150 going from its protonated to its deprotonated state. This change in charge affects the local chemical environment and could explain the perturbations of chemical shifts. Furthermore, some local structural details observed in the crystal structure at pH 9 may be due to this protonation event.

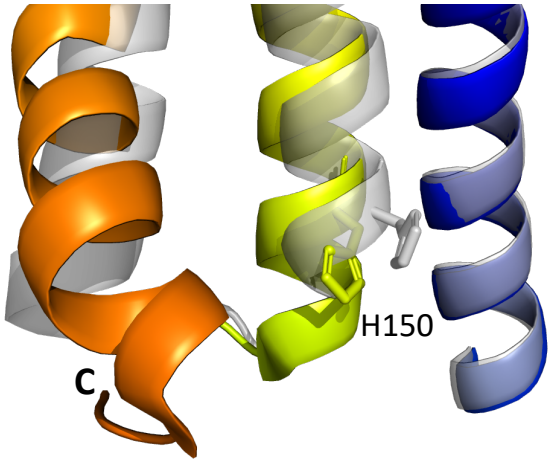

Figure 3.18: Local environment of residue H150. Overlay of the crystal structure of peptide-bound KDELR2 at pH 6.0 (coloured, PDB: 6I6H) and apo KDELR2 at pH 9.0 (grey, PDB: 6I6B). TM7 is coloured in orange and the C-terminus containing residues K201, K204, K206 and K207 is labelled. Residue H150 is shown in stick representation.

3.7 Linewidth analysis

In a next step, I moved on to analyse the line shapes in the recorded NMR spectra. Linewidth is measured as the full-width of a peak at half-height and provides information on conformational exchange. Peaks of residues that exhibit conformational exchange are broadened compared to residues adopting a single stable conformation. Broadening indicates a shorter T_2 relaxation which is caused directly by movements on the microsecond to millisecond time scale. Linewidth relates to T_2 relaxation of the magnetisation by the following relation [78]:

$$T_2\ (s) = \frac{1}{\pi * linewidth\ (Hz)}$$

As linewidth analysis in HSQC spectra is more straightforward compared to HMQCs [79], additional HSQC spectra of KDELR were collected. Spectra of the peptide-bound and apo KDELR2 at pH 5.5 and pH 7.2 are shown in figure 3.19 and the extracted linewidths are indicated. Owing to the significant overlap of K81, K204, K206 and K207 peaks their individual linewidth could not be determined. Furthermore, the K201 peak

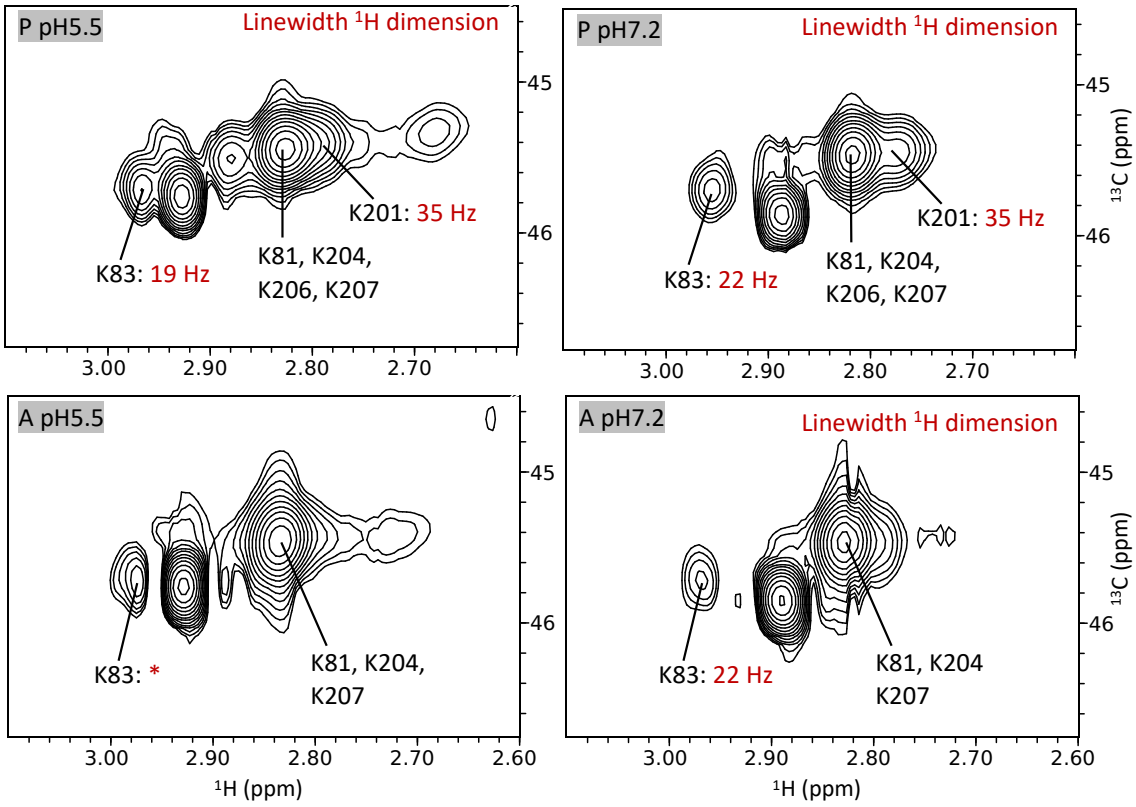

Figure 3.19: HSQCs spectra of KDELR2. The linewidth in the ^{1}H dimension of the K83 and K201 peaks is shown in red. (*) This peak appears narrower than expected due to truncations artefacts ('sinc wiggles') of the neighbouring peak, a good estimate of its linewidth could not be obtained. P: peptide-bound KDELR2, A: apo KDELR2. Spectra recorded on a 750 MHz spectrometer.

is not visible in the spectra of the apo state and no linewidth was obtained.

Firstly, I analysed if pH affects the dynamics of the KDELR2 C-terminus. For this purpose I compared linewidth of K201 at pH 5.5 and pH 7.2. The K201 peak has an identical linewidth of 35 Hz in both spectra. This indicates that K201 is equally dynamic on the microsecond-millisecond time scale at pH 5.5 and pH 7.2. This suggests, that changes in pH, over the physiologically relevant range, do not significantly affect the amount of conformational exchange the KDELR2 C-terminus exhibits.

Next, it was assessed if peptide binding impacts the amount of conformational exchange observed at the C-terminus. Comparing HSQC spectra of the two states (fig. 3.19), we observe overall fewer peaks and less dispersion of peaks in the apo compared to the peptide-bound state. The same trend is observed in the HMQC spectra in figure

3.15. At a first glance this is a clear indication that KDELR2 in the apo state is more dynamic on the microsecond-millisecond timescale, which indicates more conformational exchange, than in the peptide-bound state.

I used the linewidth of K201 to get information on the conformational exchange of the C-terminus in the peptide-bound state. Once again K83 acts as a control because it is found in the same conformation and environment in all crystallographic structures and is not expected to undergo conformational exchange. This peak has a consistent linewidth of 20 ± 2 Hz across all spectra, suggesting a T_2 of 15 ms. In the peptide-bound state K201 has a linewidth of 35 Hz which translates to a T_2 of 9 ms. In comparison to K83, the K201 peak is broadened by an extra 15 Hz and its T_2 reduced by 6 ms, indicating that K201 undergoes conformational exchange on the microsecond-millisecond time scale in the peptide-bound state.

K201 is not visible in the apo state, thus, it is not possible to use its linewidth to analysis the dynamics of the C-terminus in this state. However, as line broadening causes a decrease in peak intensity, we can use the intensity of K201 to indirectly report on its dynamics. This approach comes with an important caveat. In this experimental set up, a change in peak intensity may, besides line broadening, also be caused by differences in the lysine methylation efficiency between samples. As some samples were labelled in the apo state and others in the peptide-bound state, we need to consider if there could have been differences in the methylation efficiency. Based on the crystal structures, the C-terminal lysine residues adopt one of two possible conformations but both are expected to be solvent exposed. As they are easily accessible for the reagents, I expect efficient labelling of all four C-terminal lysines in both states. Furthermore, NMR experiments provide more direct evidence that the state in which the receptor was labelled does not influence the efficiency. This is discussed in detail in figure (fig. 3.20). Thus, for the rest of this study I assume that the labelling efficiency of all samples is identical. By extension decreased peak intensity is used as evidence of line broadening.

The disappearance of the K201 peak can alternatively be described as a decrease

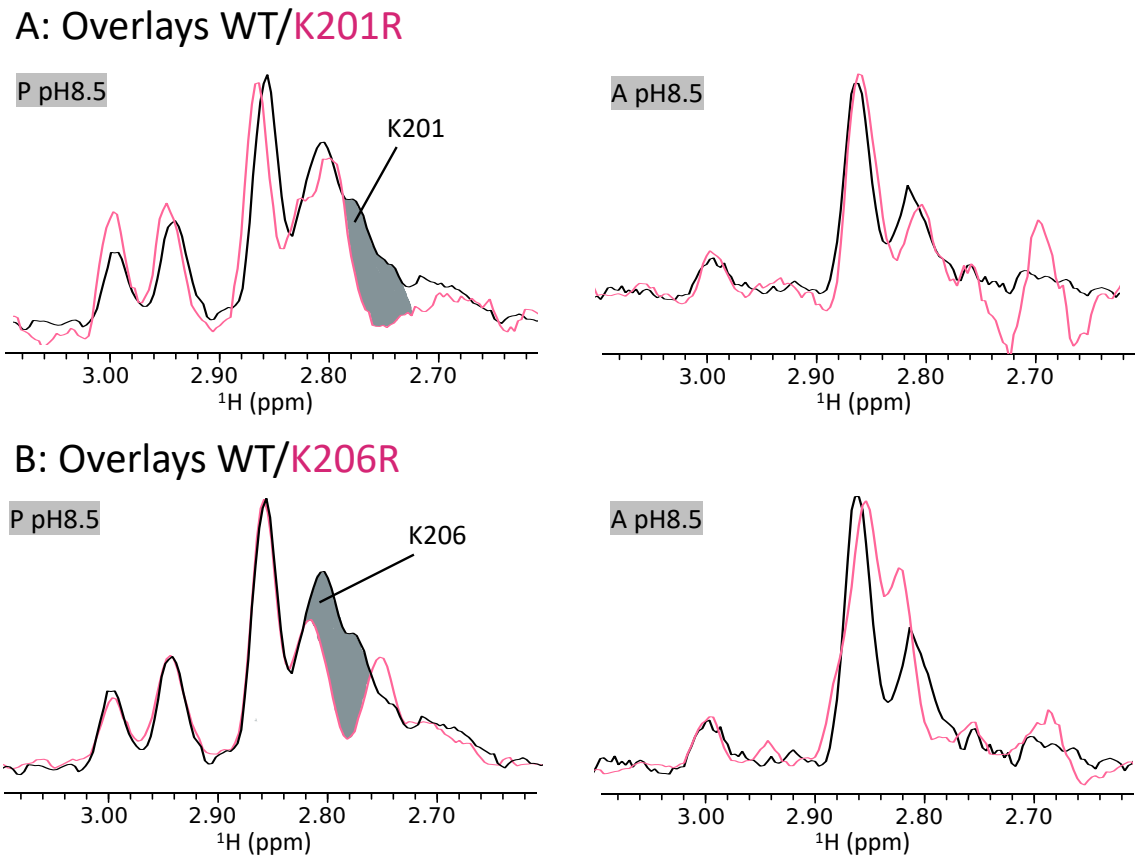

Figure 3.20: Assessment of labelling efficiency. This figure shows 1D projections from ^{1}H SOFAST-HMQC spectra collected of KDELR2 WT and the K201R and K206R constructs at pH 8.5. The samples used to record these spectra were treated differently to most other samples in this study. The samples were labelled in the peptide-bound state and an initial NMR spectrum recorded. Afterwards the peptide was dissociated and spectra collected in the apo state. Thus, the spectra in the peptide-bound and apo state were collected of the exact same sample, which guarantees identical labelling efficiency. In (A) an overlay of WT with the K201R mutant is shown. The difference in these spectra (grey shading) thus represents the intensity of K201. Looking at the peptide-bound state, we can see that the K201 peak has substantial intensity and is clearly visible. In the apo state there is essentially no difference in the two spectra, suggesting the intensity of K201 is below the detection limit. The same is true for the K206 peak in (B). This observation provides evidence that the reduction in peak intensity in the apo state observed for K201 and K206 at pH 8.5 is not caused by differences in labelling efficiency, but indeed by peak broadening. This finding can be generalised to spectra recorded at all pH values, as all samples were labelled at pH 5.5. The pH was adjusted for the NMR experiments only after labelling. P: peptide-bound KDELR2. A: KDELR2 apo state. All data collected on a 950 MHz spectrometer.

in peak intensity from peptide-bound to apo state. Figure 3.21 showing 1D overlays of the two states visualises this phenomenon. Whereas we see a clear peak of K201 in the peptide-bound state, there is no significant intensity for K201 visible in the apo state. The decrease in intensity of K201 below the detection limit in the apo state indicates a significant increase in line broadening as compared to the peptide-bound state. The additional line broadening suggests more conformational exchange and increased dynamics on the microsecond-millisecond timescale in the apo state.

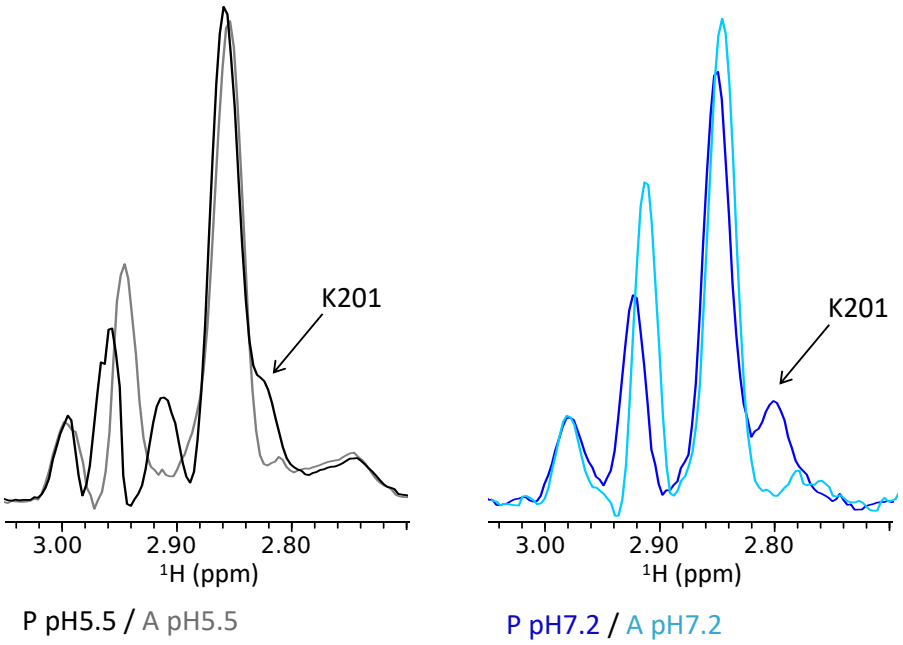

Figure 3.21: Comparison of K201 intensity in apo and peptide-bound states. Overlays of 1D projection from HMQC spectra recorded on a 950 MHz spectrometer. Intensities of K83 were matched to scale the 1D projections. P: peptide-bound KDELR2, A: apo KDELR2.

Taken together, analysis of linewidth and intensity of the K201 peak shows that the C-terminus of KDELR2 is highly dynamic on the microsecond-millisecond timescale. In the peptide-bound state, a slight broadening of K201 indicates some level of conformational exchange. However, it is generally true that the spectra of peptide-bound KDELR2 are both more dispersed and have narrower linewidths. This is consistent with a more defined conformation for the peptide-bound state. In the apo state, further broadening of the K201 peak indicates more conformational exchange and a less well

defined conformational state.

To support this conclusion I investigate the peak intensities of the other C-terminal lysines. Similar to K201, the K206 peak is only visible in the peptide-bound state and disappears in the apo state (fig. 3.15). This again suggests additional line broadening in the apo state.

In contrast, K204 and K207 were assigned in both states. Owing to significant overlap determination of their intensities is more complicated. Here I use a strategy to indirectly estimate their intensities. In this approach, overlays of the K204R and K207R mutants with WT are used. These overlay only differ in the resonance of one lysine. Thus, the difference of the WT and mutant spectra represents the contribution of intensity of the mutated lysine. In figure 3.22 such overlays of the K204R and K207R mutants with WT are shown. The difference in intensity in the central peak (the peak K204 and K207 resonances contribute to) is highlighted by the grey shading. Hence, the area of grey shading can be seen as a representation of the K204 and K207 intensities. In the peptide-bound state independent of pH and for both residues the difference is substantial. In comparison, the difference is much smaller in all overlays of the apo state. This suggests that the intensity of K204 and K207 peaks is considerably decreased in the apo compared to the peptide-bound state. Hence, indirect determinations of K204 and K207 intensities support the earlier conclusions of the apo state showing additional line broadening and being more dynamic on the microsecond-millisecond timescale than the peptide-bound state.

Summarising this section, linewidths indicates that pH changes, over the physiologically relevant range, do not affect the amount of conformational exchange exhibited by the C-terminus. However, the KDELR2 C-terminus appears to be highly flexible in the apo state and exists in an equilibrium between multiple conformational states. Peptide binding causes the C-terminus to adopt a more defined conformational state, thus shifts the position of the equilibrium.

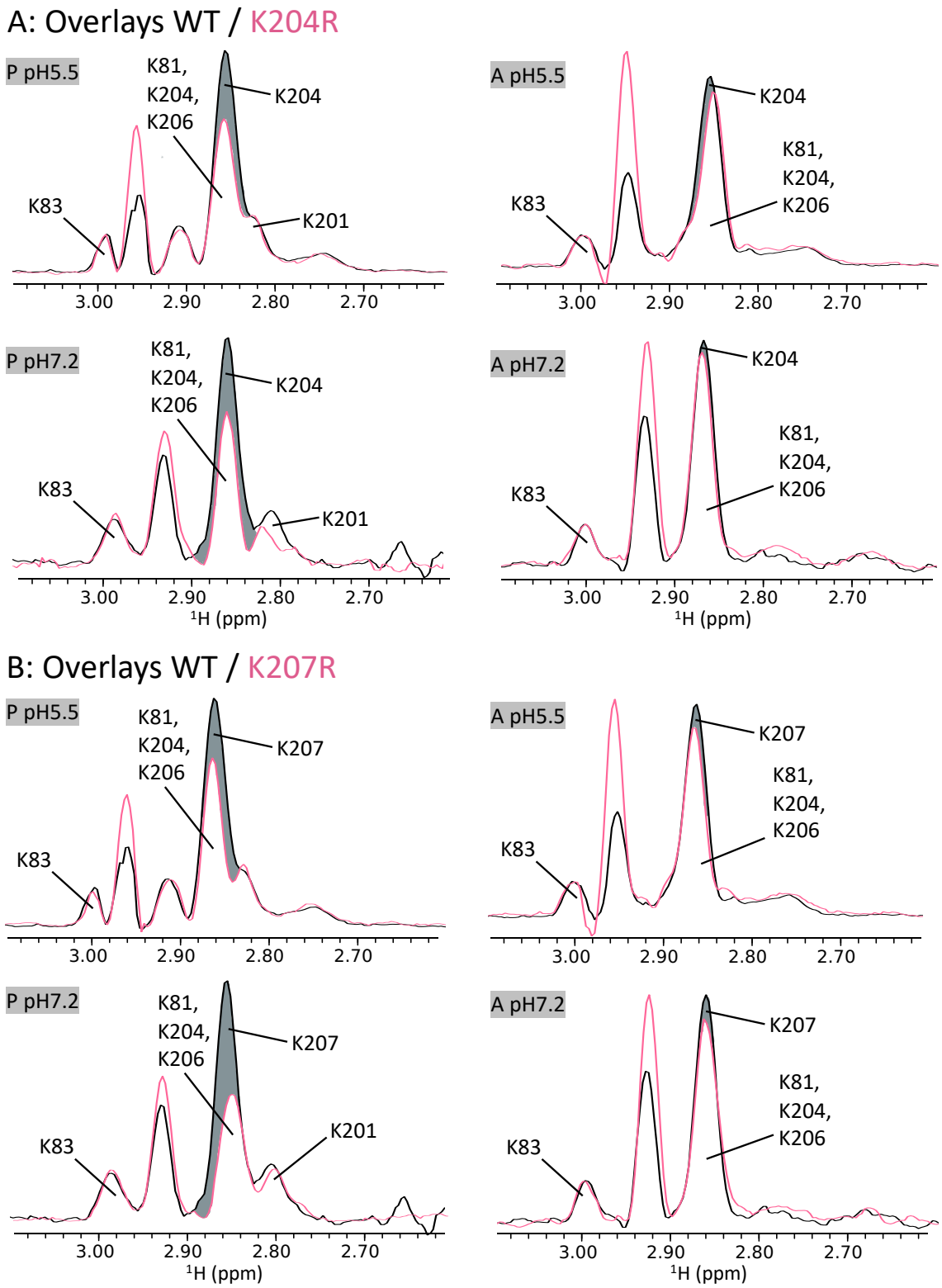

Figure 3.22: Overlays of 1D projections of (A) the K204R mutant (red) and WT (black) and (B) the K207R (red) mutant and WT (black). The difference between mutants and WT is highlighted in grey. Intensities of K83 were matched to scale the 1D projections. P: peptide-bound KDELR2, A: apo KDELR2. All spectra recorded on a 950 MHz spectrometer.

3.8 E143-K207 salt bridge

Crystal structures of KDELR2 in the peptide-bound state indicate a salt bridge between K207 and E143 (fig. 1.6). This salt bridge is speculated to stabilise the 'active' conformation of the C-terminus. E143 is strictly conserved and forms part of the COPII recognition motif. Thus, I hypothesise that this salt bridge may act as a 'switch' between the mutually exclusive COPII and the C-terminal COPI binding motifs. In order to test this hypothesis a KDELR2 E143A mutant was produced. The E143A mutation was predicted to destabilise the 'active' conformation of the C-terminus if the salt bridge can no longer form.

^{13}C SOFAST-HMQC spectra were collected of the mutant and overlays with WT are shown in figure 3.23. If the E143A mutation were to destabilise the 'active' conformation of the C-terminus, this would be reflected in line broadening of the C-terminal lysine peaks when peptide is bound, similar as to what was observed for WT KDELR2 in the apo state. However, the comparison of peptide-bound mutant and WT spectra shows that this does not happen. The linewidths/intensities as well as the chemical shifts of the C-terminal lysine peaks are almost identical. This data indicates that the E143A mutation does not influence the conformation of the C-terminus and suggests that the E143-K207 salt bridge is not required to stabilise the 'active' conformation of KDELR2.

Furthermore, methyl peaks of lysines involved in salt bridges have previously been observed significantly upfield in the ^{1}H dimension compared to other lysine methyls [56]. These typically have chemical shifts between 2.0 ppm and 2.2 ppm. The occurrence of the K207 peak at 2.86 ppm in the ^{1}H dimension, thus, suggests that we do not observe the E143-K207 salt bridge in solution.

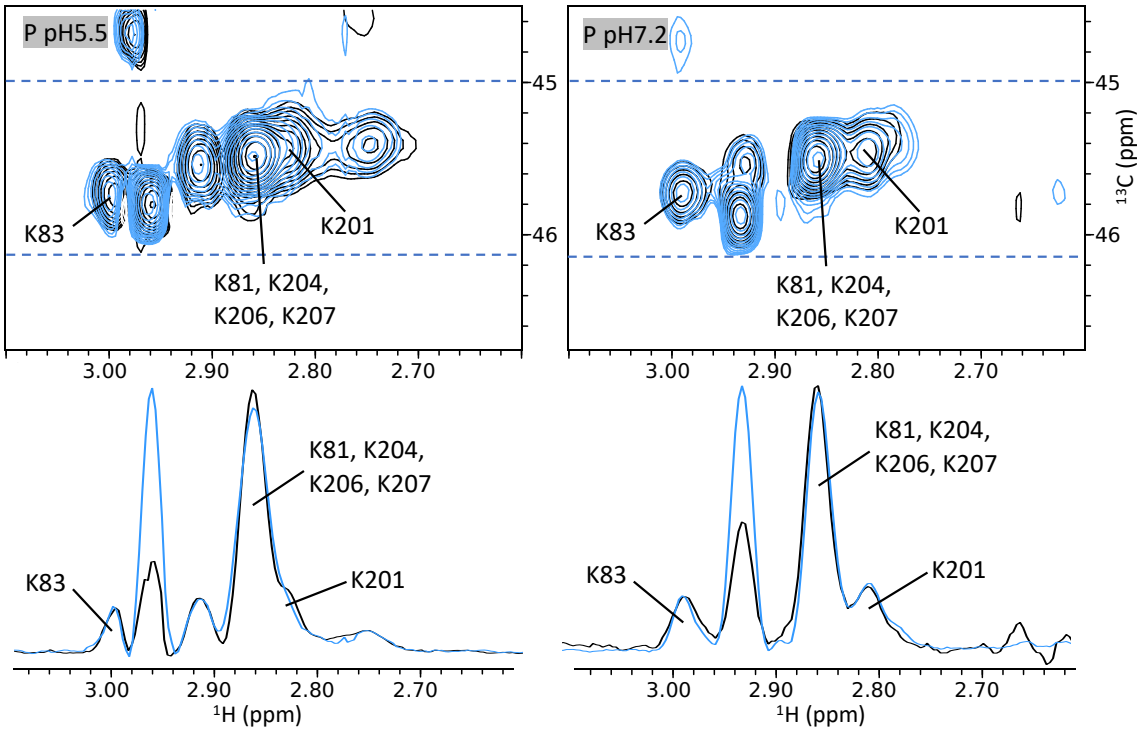

Figure 3.23: Role of the E143-K207 salt bridge. Overlay of ^{13}C SOFAST-HMQC spectra recorded of WT (black) and the E143A mutant (blue). The blue dotted lines indicate the area where of which the 1D projections were produced. Intensities of K83 were matched to scale the 1D projections. P: peptide-bound KDELR2, A: apo KDELR2. All data recorded on a 950 MHz spectrometer.

3.9 Sybody 37

The binding of sybody 37 (Syb37) to the luminal side of KDELR2 (fig. 1.7) leads to the redistribution of the receptor to the lysosome [17]. The crystal structure of the Syb37-KDELR2 complex was solved (fig. 1.7), however, the molecular basis of this behaviour was not revealed. Thus, this question was addressed with solution NMR.

Firstly, a sample of KDELR2 in complex with Syb37 had to be produced. The sybody was incubated for 1 h with apo KDELR2 at pH 6.6 to allow binding. As it was important to have samples with pure complex, the binding efficiency was assessed by analytical size-exclusion chromatography (fig. 3.24). The SEC elution profile shows 3 separated peaks. The composition of the three peaks was analysed by gel electrophoresis. Peak 1 mostly consists of KDELR2 and only very little sybody. This most likely corresponds

to a polymerisation state of the receptor which does not bind sybody. The second peak possesses a big shoulder as this is usually observed in the SEC elution profile of KDELR2. Both the main peak and the shoulder consist of approximately equal amounts of KDELR2 and sybody, which indicates the formation of the complex. The fractions of peak 2 were pooled and used to prepare the NMR sample. The third peak consists of excess sybody only.

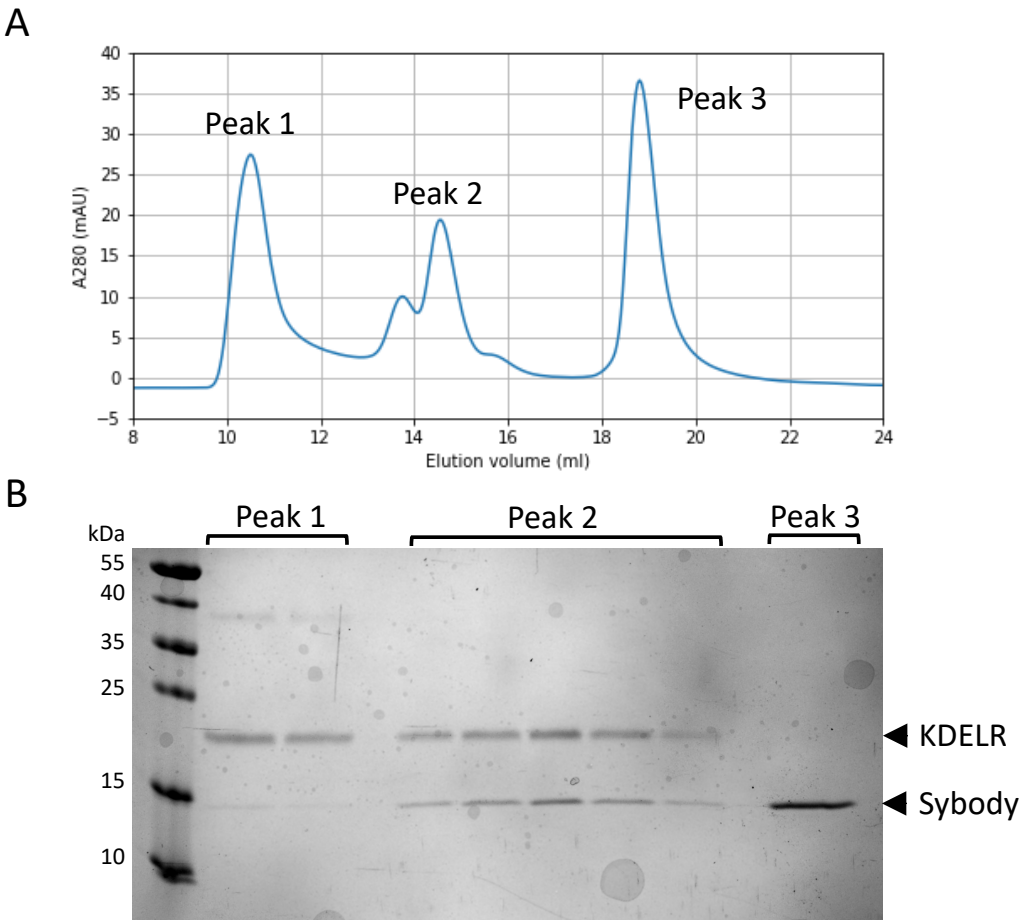

Figure 3.24: Analysis of sybody binding. (A) Elution profile of the sample run on SEC. (B) Polyacrylamide gel of the SEC fractions.

The spectra recorded of the Syb37-KDELR2 complex are overlaid with spectra of KDELR2 in the apo state (fig. 3.25). As usual the intensity of the K83 peak was matched to scale the 1D projections. It is important to mention that the concentration of the sybody samples was lower than the standard due to inefficiency of the complex formation. Consequently, the signal-to-noise is worse in the complex spectra which led

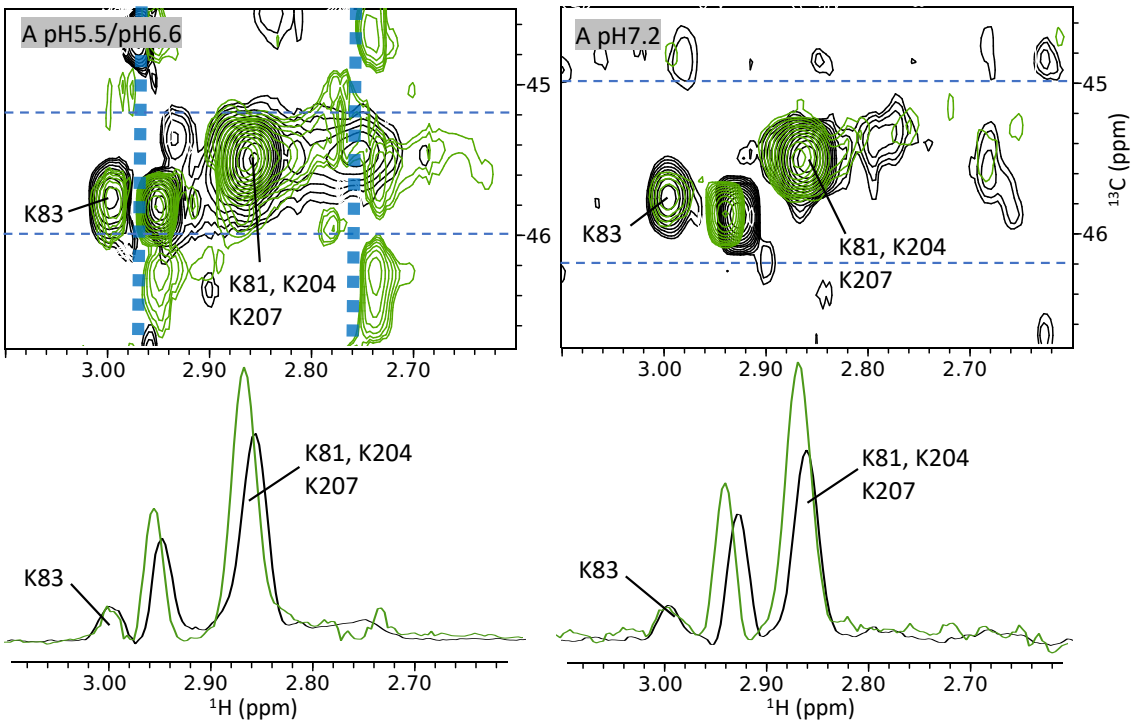

Figure 3.25: The impact of Syb37 binding on KDELR2. Overlay of ^{13}C SOFAST-HMQC spectra recorded of KDLER2 in its apo state (black) and the Syb37-KDELR2 complex (green). The horizontal blue dotted lines indicate the area where of which the 1D projections were produced. The vertical blue dotted line indicate regions of buffer interference. The spectrum of the complex at pH 6.6 is overlaid with the KDELR2 spectrum at pH 5.5 to reduce the buffer interference. As discussed in a previous section the chemical shifts of protein peaks at both pH values are identical. Intensities of K83 were matched to scale the 1D projections. A: apo KDELR2. KDELR2 spectra recorded on a 950 MHz spectrometer, the spectra of the KDELR2-Syb37 complex were recorded on a 750 MHz spectrometer.

to greater uncertainty in the scaling of the 1D projections.

The overlays show that sybody binding leads to an increase in intensity of the peak to which resonances of K204 and K207 contribute. This increase is substantial and appears to indicate a real change in this protein peak. As the two samples were labelled in the same way we can assume identical methylation efficiency. Thus, the increase in peak intensity compared to the apo state would suggest a decrease in peak broadening. This in turn would imply that Syb37 binding to the apo KDELR2 leads to the stabilisation of the conformation of the C-terminus.

Furthermore, a change in chemical shift of the K204/K207 peak supports the notion

that a change in the KDELR C-terminus is observed. The slight downfield shift of this peak in the complex spectrum suggest that the conformation stabilised by Syb37 is different to the state stabilised by the peptide. In the crystal structure, the C-terminus occupies the same conformation in the complex as in the apo state. Thus, I speculate that Syb37 stabilises the 'inactive' state of the C-terminus. The perturbation of chemical shifts is small, however, based on the crystal structures the C-terminal lysines are solvent exposed in both 'active' and 'inactive' states. Large changes in chemical shifts are not expected for this transition. The slight downfield shift of this peak would also be consistent with the deshielding of the lysines due to the C-terminus moving away from the negatively charged residues E143 and E145.

Taken together, the NMR spectra shown here of the Syb37-KDELR2 complex suggest that sybody binding to the luminal face of the receptor may lead to changes in conformation of the C-terminus on the cytosolic side. Nevertheless, we have to keep in mind that there might be slight inaccuracies in the scaling of 1D projections and be cautious when comparing peak intensities. A spectrum of the complex at higher resolution is required for more confidence in this finding. Furthermore, other lysines contribute to the peak of interest and we cannot be sure that the observed changes indeed originate from K204 or K207. Spectra of Syb37 in complex with the K204R and K207R mutants would provide more information as overlays of such spectra with WT would allow to evaluate the change in these two resonances.

4 Discussion

Here, I study the behaviour of the KDELR2 C-terminus to investigate the molecular mechanism by which the trafficking receptor signals across the membrane to initiate vesicle retrieval. Using NMR this project focussed on the dynamic behaviour of the receptor in solution and complements static information derived from X-ray crystallography.

4.1 pH regulates cargo binding only

The role of pH in the regulation of cargo binding and dissociation from KDELR has been characterised in detail [17, 21, 16]. By determining the protonation state of the pH sensor residue histidine 12, pH modulates the receptor's affinity for ERS. In this way, the low pH in the Golgi favours cargo binding and the neutral pH in the ER triggers release.

This study analysed the possible involvement of H12 protonation in KDELR signalling. Thus, I investigated if a change in pH influences the conformation of the receptor C-terminus. For this purpose, NMR spectra of KDELR at different pH were recorded. Neither chemical shifts nor linewidths provided evidence for a change in conformation at the C-terminus over the physiological range. As this would be reflected in at least one of the two observables (chemical shift and linewidth), the data suggests that pH does not influence the conformation of the KDELR C-terminus. The absence of a conformational rearrangement conclusively shows that the protonation state of H12 does not directly influence KDELR signalling. This suggests that regulation of cargo binding and KDELR signalling are two separate mechanisms. pH, through the protonation of H12, appears

to be solely involved in the first of these two.

This finding is consistent with cellular experiments. These showed that in the absence of ligand KDELR is mostly localised to the Golgi and not the ER, suggesting that protonation of H12 alone does not trigger KDELR signalling and initiate retrograde trafficking [17, 21].

4.2 The dynamic equilibrium of the KDELR C-terminus

Line shape analysis revealed that KDELR signalling is a highly dynamic process rather than a simple on/off transition between an 'active' and an 'inactive' state, as this is observed in the crystal structures (fig. 1.2). I hypothesis that the C-terminus exists in a conformational equilibrium between 'active' and 'inactive' states, that the position of this equilibrium is affected by peptide binding (but not pH), and that receptor signalling depends on the position of this equilibrium. The proposed model of KDELR signalling is summarised in figure 4.1.

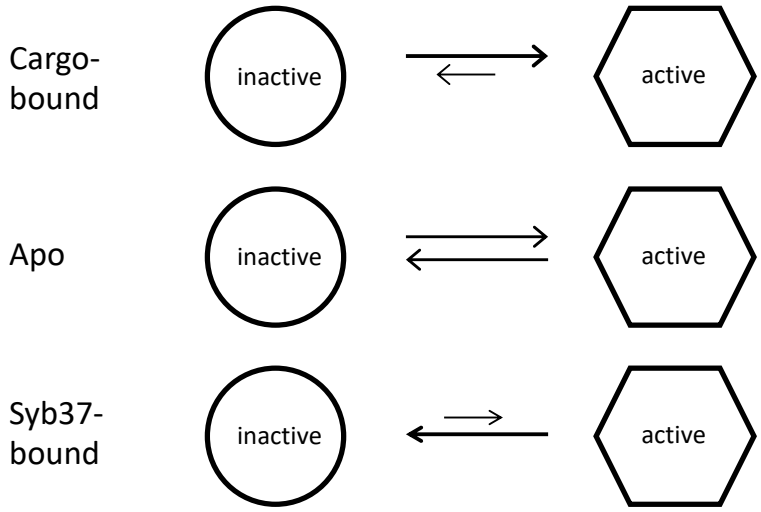

Figure 4.1: The dynamic equilibrium model of the KDELR2 signalling. 'Active' and 'inactive' refer to the conformations of the KDELR C-terminus as shown in figure 1.2.

In the apo state, severe broadening of C-terminal lysine peaks is observed. This finding suggests extensive conformational exchange and that the conformation of the C-terminus is not well defined. The C-terminus may exchange between 2-states, the

'inactive' and 'active' conformations as observed in the crystal structures (fig. 1.2). However, we cannot exclude the possibility that the C-terminus is sampling a larger number of active and inactive states in solution and crystal structures only provide a 'snapshot' of two such conformations. Most importantly, the data suggests that the C-terminus exists in an equilibrium between two or more conformations, wherein the 'active' state is a relatively small proportion of the sampled states in the absence of peptide.

Upon peptide binding, the NMR spectra become more disperse and have narrower linewidths. This indicates a more defined conformation and comparably less dynamics on the microsecond-millisecond timescale in the peptide-bound state, suggesting that the peptide stabilises one of the conformational states of the C-terminus. I speculate that the stabilised conformation is an 'active' state of the receptor, as captured by the crystal structures of the peptide-bound KDELR (fig. 1.2). As the peptide mimics cargo binding, it is highly likely that cargo shifts the conformational equilibrium towards the 'active' state in a similar fashion.

However, a low level of peak broadening remains in the peptide-bound state which indicates that the peptide is not able to fully stabilise the 'active' conformation of KDELR. A similar phenomenon was observed in the μ-opioid receptor [49]. Binding of extra cellular ligand alone did not lead to the full receptor activation and G-protein binding to the intracellular side was required in addition. KDELR may function by a similar principle and both binding of cargo and COPI could be required for complete stabilisation of the KDELR C-terminus in its active conformation. NMR spectra of KDELR in complex with peptide and COPI are required to confirm this hypothesis.

Contrary to expectations, the E143-K207 salt bridge is not involved in the stabilisation of the 'active' state of the receptor. Moreover, the NMR data suggests that we do not observe the salt bridge in solution. A comparison of the three crystal structures of peptide-bound KDELR (fig. 4.2) shows that there is disagreement over the formation of the salt bridge. The far C-terminus (residues from 207) differs in conformation across

the three structure indicating increased flexibility of these residues. As a result, the salt bridge is only observed in two of the structures. This suggests that in solution the far C-terminus may sample a number of conformations when peptide is bound to the receptor with the salt bridge only forming in a subset of those. The NMR data indicates that a conformation as shown by PDB 6I6H, where no salt bridge between E143 and K207 forms, may be more prevalent in solution.

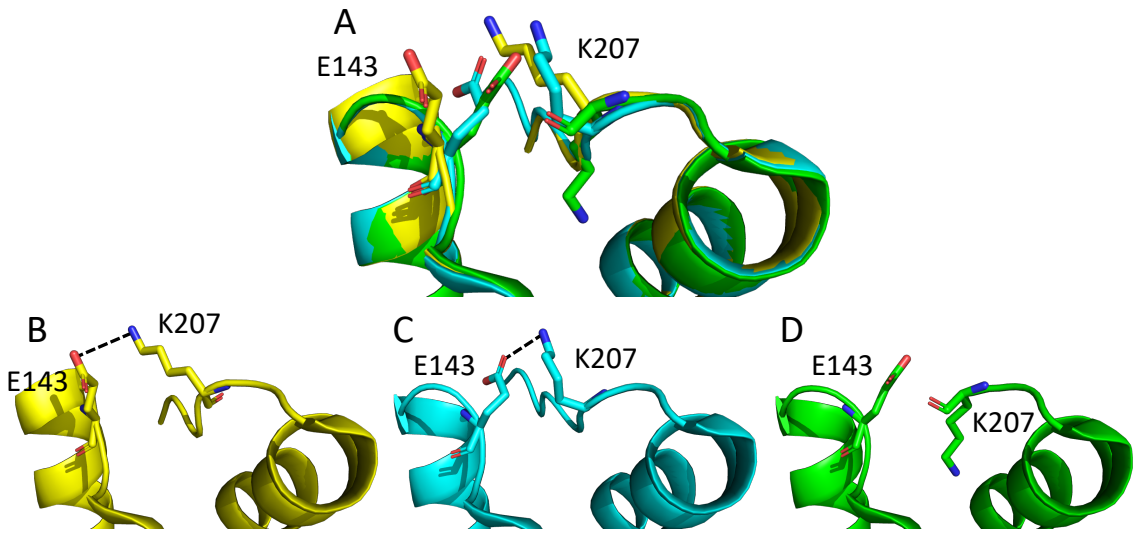

Figure 4.2: Conformation of the far C-terminus. (A) Overlay of the three crystal structures of peptide-bound KDELR2 at pH 6.0. (B) KDELR2 bound to HDEL peptide, PDB: 6Y7V. (C) KDELR2 bound to RDEL, PDB: 6ZXR. (D) KDELR2 bound to KDEL, PDB: 6I6H. In structures where the E143-K207 salt bridge is observed it is highlighted by a dashed black line. Residues E143 and K207 are shown in stick representation.

Lastly, I present some evidence that sybody 37 stabilises a conformation of the KDELR C-terminus which differs from the 'active' state stabilised by the peptide. In the crystal structures the sybody-bound and apo KDELR (fig. 1.7) occupy a highly similar conformation. An RMSD of 1.4 Å was calculated across the entire structure and an RMSD of 0.6 Å when only comparing the last part of TM7 and the C-terminus (residues 195-203). This conformation was describe as an 'inactive' state of the receptor. As established above, the crystal structure only depicts a 'snapshot' of the conformation of the apo receptor, which is highly flexible and samples both 'active' and 'inactive' states in solution. I speculate that the sybody shifts the conformational equilibrium to stabilise the 'inactive' state of the receptor as shown in the crystal structure. This finding

suggests that Syb37-bound and apo KDELR may not behave identically in solution and could explain why Syb37 leads to the redistribution of the receptor to the lysosome which is not observed for apo-KDELR. However, NMR spectra of the complex at higher resolution are required for more confidence in the data.

This study shows that KDELR2 signalling depends on a dynamic equilibrium of its conformational states, similar as this has been observed previously in several GPCRs, such as the the β_2-adrenergic receptor, the β_1-adrenergic receptor, the μ-opioid receptor and the adenosine A_{2A} receptor [44, 45, 46, 47, 48, 49, 50]. This finding suggests a mechanisms involving a conformational equilibrium that can be shifted in either direction by ligands could be shared by many classes of cellular receptors.

4.3 KDELR signalling in the cell

Based on findings in this study a model of KDELR signalling in the cell is proposed (fig. 4.3).

The low pH of the Golgi primes KDELR to stabilise cargo binding. However, on its own protonation of H12 does not induce KDELR signalling. The event of cargo binding is signalled across the membrane by stabilisation of the 'active' conformation of the C-terminus. In turn, this leads to rapid recruitment of COPI and the consequent retrograde trafficking to the ER. As cargo is typically present at much higher concentrations than KDELR [18, 20, 21, 22] this ensures the efficient trafficking of cargo and fast recycling of KDELR back to the Golgi.

In the apo state, the KDELR2 C-terminus exists in a conformational equilibrium of 'active' and 'inactive' states. I speculate that the transient adoption of the 'active' conformation leads to a low level of COPI recruitment. Thus, even in a cargo depleted environment KDELR is retrieved to the ER, though at a much slower rate. This prohibits that KDELR follows the bulk flow to the lysosome where it would get degraded and ensures that the receptor remains within the trafficking system.

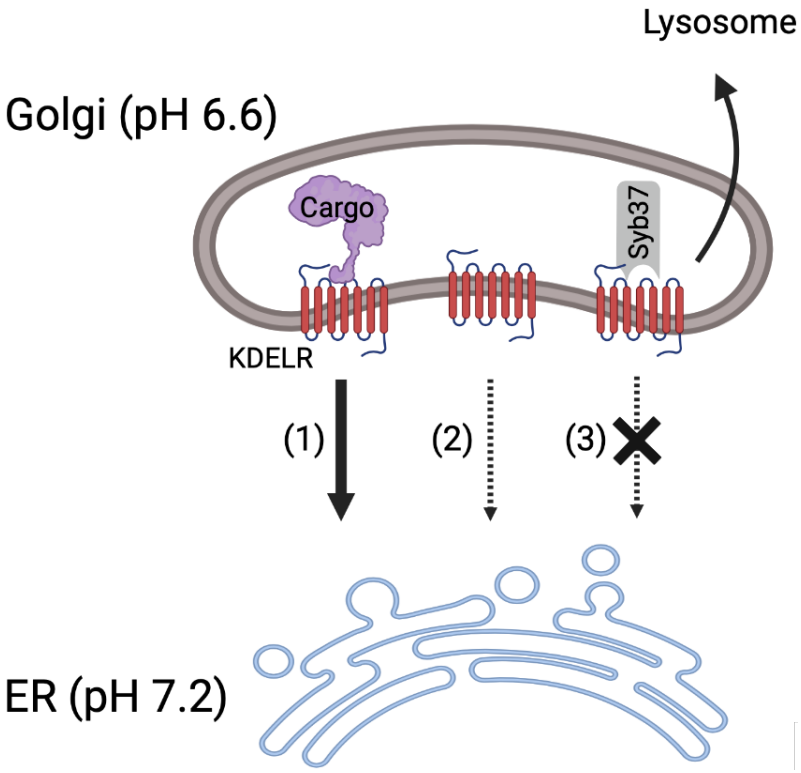

Figure 4.3: Model of KDELR signalling in the cell. (1) Cargo-bound KDELR is rapidly transported to the ER. (2) In the apo state, KDELR is retrieved at a lower rate to prevent it from following the bulk flow to the lysosome and getting degraded. (3) Syb37 binding inhibits KDELR signalling leading to its redistribution to the lysosome.

Binding of Syb37 inhibits KDELR signalling by stabilisation of an 'inactive' state. Thus, sybody-bound KDELR is not able to recruit COPI and is not retrieved to the ER. As a result the complex follows the bulk flow to the lysosome [17].

4.4 Limitations

Owing to substantial overlap of many protein peaks much of the analysis of KDELR dynamics is based on changes in peak intensity rather then linewidths. As previously explained peak broadening leads to a decrease in peak intensity [40]. However, in the used experimental set-up other factors may influence this observable. There is the possibly that differences in methylation efficiency of individual samples led to changes in peak intensity. NMR data shows that the decrease of peak intensity of apo-KDELR is independent of the state the sample was labelled in (fig. 3.20). This provides evidence

that we indeed observe line broadening in the spectra of KDELR in its apo state. However, I am not able to directly prove that the labelling efficiency is identical in both peptide-bound and apo samples. Labelling efficiency of individual lysine residues can be measured by a trypsin digestion followed by mass spectrometry [69]. If the labelling efficiency is identical then a decrease in intensity must occur through increased relaxation which causes peak broadening. Thus, I suggest determination of the labelling efficiency as an important further experiment to confirm the presence of peak broadening.

Furthermore, I have not carried out an exhaustive assignment of the lysines in this study. I only assigned 6 of a total of 11 lysine residues (K22, K25, K35, K64 & K140 were not assigned). Some of the unassigned lysines are clearly moving, either with pH and peptide. A full assignment would provide a better picture of the conformational changes in KDELR and would reveal what other parts of KDELR move with receptor activation.

4.5 Future directions

Lipids are important regulators of transmembrane proteins [80] and have recently been described to modulate transporters located in the Golgi [71, 81]. Thus, the involvement of lipids in the regulation of trafficking receptors seems likely [19]. It has been discovered that lipids with long hydrophobic tails inhibit KDELR signalling even if cargo is bound to the receptor. It was hypothesised that these lipids block movements of KDELR TM7 which inhibits the gain of structure of the C-terminal COPI binding motif. In a next step of this project, it is aimed to address the lipid regulation of KDELR2. For this purpose, it is planned to apply the NMR methods developed here to investigate the conformational dynamics of KDELR2 in lipid nanodiscs. If these experiments are successful, this would not only provide exciting new insight into the lipid regulation of cellular trafficking but also validate reductive methylation and ^{13}C NMR as a platform to study proteins in nanodiscs.

5 Conclusion

This work marks the first solution NMR study of a trafficking receptor and bridges the divide between static crystal structures and the behaviour of the receptor in solution. KDELR is an impressive example that a dynamic rather than a on/off model of activation provides a receptor with additional flexibility in its signalling mechanism. This flexibility helps the receptor to efficiently respond to a range of cellular conditions. The study further highlights that an appreciation of dynamic properties is required to fully understand the molecular basis of protein function. Structural biology is entering an exciting phase with new tools emerging that allow the detailed study of protein dynamics.

6 References

[1] N. Gomez-Navarro and E. Miller, "Protein sorting at the ER–Golgi interface," *Journal of Cell Biology*, vol. 215, pp. 769–778, dec 2016.

[2] L. Ellgaard and A. Helenius, "Quality control in the endoplasmic reticulum," *Nature Reviews Molecular Cell Biology*, vol. 4, pp. 181–191, mar 2003.

[3] E. Miller, B. Antonny, S. Hamamoto, and R. Schekman, "Cargo selection into COPII vesicles is driven by the Sec24p subunit," *The EMBO Journal*, vol. 21, pp. 6105–6113, nov 2002.

[4] E. A. Miller, T. H. Beilharz, P. N. Malkus, M. C. S. Lee, S. Hamamoto, L. Orci, and R. Schekman, "Multiple cargo binding sites on the COPII subunit Sec24p ensure capture of diverse membrane proteins into transport vesicles.," *Cell*, vol. 114, pp. 497–509, aug 2003.

[5] C. Howe, M. Garstka, M. Al-Balushi, E. Ghanem, A. N. Antoniou, S. Fritzsche, G. Jankevicius, N. Kontouli, C. Schneeweiss, A. Williams, T. Elliott, and S. Springer, "Calreticulin-dependent recycling in the early secretory pathway mediates optimal peptide loading of MHC class I molecules," *The EMBO Journal*, vol. 28, pp. 3730–3744, dec 2009.

[6] C. Hammond and A. Helenius, "Quality control in the secretory pathway: retention of a misfolded viral membrane glycoprotein involves cycling between the ER, intermediate compartment, and Golgi apparatus.," *Journal of Cell Biology*, vol. 126, pp. 41–52, jul 1994.

[7] S. Munro and H. R. Pelham, "A C-terminal signal prevents secretion of luminal ER proteins," *Cell*, vol. 48, pp. 899–907, mar 1987.

[8] H. R. Pelham, K. G. Hardwick, and M. J. Lewis, "Sorting of soluble ER proteins in yeast.," *The EMBO Journal*, vol. 7, pp. 1757–1762, jun 1988.

[9] G. Griffiths, M. Ericsson, J. Krijnse-Locker, T. Nilsson, B. Goud, H. D. Söling, B. L. Tang, S. H. Wong, and W. Hong, "Localization of the Lys, Asp, Glu, Leu tetrapeptide receptor to the Golgi complex and the intermediate compartment in mammalian cells.," *Journal of Cell Biology*, vol. 127, pp. 1557–1574, dec 1994.

[10] J. C. Semenza, K. G. Hardwick, N. Dean, and H. R. Pelham, "ERD2, a yeast gene required for the receptor-mediated retrieval of luminal ER proteins from the secretory pathway," *Cell*, vol. 61, pp. 1349–1357, jun 1990.

[11] I. Majoul, M. Straub, S. W. Hell, R. Duden, and H.-D. Soeling, "KDEL-Cargo Regulates Interactions between Proteins Involved in COPI Vesicle Traffic: Measurements in Living Cells Using FRET," *Developmental Cell*, vol. 1, pp. 139–153, jul 2001.

[12] N. Gomez-Navarro and E. A. Miller, "COP-coated vesicles," jan 2016.

[13] N. Dean and H. R. Pelham, "Recycling of proteins from the Golgi compartment to the ER in yeast.," *Journal of Cell Biology*, vol. 111, pp. 369–377, aug 1990.

[14] M. J. Lewis and H. B. Pelham, "Ligand-Induced Redistribution of a Human KDEL Receptor from the Golgi Complex to the Endoplasmic Reticulum," *Cell*, vol. 66, pp. 353–364, 1992.

[15] A. Deschamps, A. S. Colinet, O. Zimmermannova, H. Sychrova, and P. Morsomme, "A new pH sensor localized in the Golgi apparatus of Saccharomyces cerevisiae reveals unexpected roles of Vph1p and Stv1p isoforms," *Scientific Reports*, vol. 10, no. 1, pp. 1–11, 2020.

[16] Z. Wu, S. Newstead, and P. C. Biggin, "The KDEL trafficking receptor exploits pH to tune the strength of an unusual short hydrogen bond," *Scientific Reports*, vol. 10, no. 1, pp. 1–12, 2020.

[17] P. Bräuer, J. L. Parker, A. Gerondopoulos, I. Zimmermann, M. A. Seeger, F. A. Barr, and S. Newstead, "Structural basis for pH-dependent retrieval of ER proteins from the Golgi by the KDEL receptor," *Science*, vol. 363, no. 6431, pp. 1103–1107, 2019.

[18] D. Wilson, M. Lewis, and H. Pelham, "pH-dependent binding of KDEL to its receptor in vitro.," *Journal of Biological Chemistry*, vol. 268, pp. 7465–7468, apr 1993.

[19] S. Newstead and F. Barr, "Molecular basis for KDEL-mediated retrieval of escaped ER-resident proteins - SWEET talking the COPs.," *Journal of cell science*, vol. 133, oct 2020.

[20] A. A. Scheel and H. R. Pelham, "Identification of amino acids in the binding pocket of the human KDEL receptor.," *The Journal of biological chemistry*, vol. 273, pp. 2467–72, jan 1998.

[21] A. Gerondopoulos, P. Bräuer, T. Sobajima, Z. Wu, J. L. Parker, P. C. Biggin, F. A. Barr, and S. Newstead, "A signal capture and proofreading mechanism for the KDEL-receptor explains selectivity and dynamic range in ER retrieval," *eLife*, vol. 10, pp. 1–29, 2021.

[22] D. N. Itzhak, S. Tyanova, J. Cox, and G. H. Borner, "Global, quantitative and dynamic mapping of protein subcellular localization," *eLife*, vol. 5, p. e16950, jun 2016.

[23] A. Pidoux and J. Armstrong, "Analysis of the BiP gene and identification of an ER retention signal in Schizosaccharomyces pombe.," *The EMBO Journal*, vol. 11, pp. 1583–1591, apr 1992.

[24] J. C. Semenza and H. R. Pelham, "Changing the specificity of the sorting receptor for luminal endoplasmic reticulum proteins," *Journal of Molecular Biology*, vol. 224, pp. 1–5, mar 1992.

[25] I. Raykhel, H. Alanen, K. Salo, J. Jurvansuu, V. D. Nguyen, M. Latva-Ranta, and L. Ruddock, "A molecular specificity code for the three mammalian KDEL receptors," *Journal of Cell Biology*, vol. 179, pp. 1193–1204, dec 2007.

[26] K. A. Trychta, S. Bäck, M. J. Henderson, and B. K. Harvey, "KDEL Receptors Are Differentially Regulated to Maintain the ER Proteome under Calcium Deficiency.," *Cell reports*, vol. 25, pp. 1829–1840, nov 2018.

[27] V. Saudek, "Cystinosin, MPDU1, SWEETs and KDELR Belong to a Well-Defined Protein Family with Putative Function of Cargo Receptors Involved in Vesicle Trafficking," *PLoS ONE*, vol. 7, p. e30876, feb 2012.

[28] L.-Q. Chen, B.-H. Hou, S. Lalonde, H. Takanaga, M. L. Hartung, X.-Q. Qu, W.-J. Guo, J.-G. Kim, W. Underwood, B. Chaudhuri, D. Chermak, G. Antony, F. F. White, S. C. Somerville, M. B. Mudgett, and W. B. Frommer, "Sugar transporters for intercellular exchange and nutrition of pathogens," *Nature*, vol. 468, pp. 527–532, nov 2010.

[29] V. Kalatzis, N. Nevo, S. Cherqui, B. Gasnier, and C. Antignac, "Molecular pathogenesis of cystinosis: effect of CTNS mutations on the transport activity and subcellular localization of cystinosin," *Human Molecular Genetics*, vol. 13, pp. 1361–1371, may 2004.

[30] A. Jézégou, E. Llinares, C. Anne, S. Kieffer-Jaquinod, S. O'Regan, J. Aupetit, A. Chabli, C. Sagné, C. Debacker, B. Chadefaux-Vekemans, A. Journet, B. André, and B. Gasnier, "Heptahelical protein PQLC2 is a lysosomal cationic amino acid exporter underlying the action of cysteamine in cystinosis therapy.," *Proceedings*

of the National Academy of Sciences of the United States of America, vol. 109, pp. e3434–43, dec 2012.

[31] C. Barlowe, "Signals for COPII-dependent export from the ER: what's the ticket out?," *Trends in cell biology*, vol. 13, pp. 295–300, jun 2003.

[32] F. Townsley, D. Wilson, and H. Pelham, "Mutational analysis of the human KDEL receptor: distinct structural requirements for Golgi retention, ligand binding and retrograde transport.," *The EMBO Journal*, vol. 12, pp. 2821–2829, jul 1993.

[33] F. Letourneur, E. C. Gaynor, S. Hennecke, C. Démollière, R. Duden, S. D. Emr, H. Riezman, and P. Cosson, "Coatomer is essential for retrieval of dilysine-tagged proteins to the endoplasmic reticulum," *Cell*, vol. 79, pp. 1199–1207, dec 1994.

[34] L. Jackson, M. Lewis, H. Kent, M. Edeling, P. Evans, R. Duden, and D. Owen, "Molecular Basis for Recognition of Dilysine Trafficking Motifs by COPI," *Developmental Cell*, vol. 23, pp. 1255–1262, dec 2012.

[35] M. Karplus and J. Kuriyan, "Molecular dynamics and protein function," *Proceedings of the National Academy of Sciences*, vol. 102, pp. 6679–6685, may 2005.

[36] K. Henzler-Wildman and D. Kern, "Dynamic personalities of proteins," *Nature*, vol. 450, pp. 964–972, dec 2007.

[37] A. J. Baldwin and L. E. Kay, "NMR spectroscopy brings invisible protein states into focus," *Nature Chemical Biology*, vol. 5, pp. 808–814, nov 2009.

[38] D. Kern, E. Z. Eisenmesser, and M. Wolf-Watz, "Enzyme Dynamics During Catalysis Measured by NMR Spectroscopy," *Methods in Enzymology*, vol. 394, pp. 507–524, jan 2005.

[39] H. M. McConnell, "Reaction Rates by Nuclear Magnetic Resonance," *The Journal of Chemical Physics*, vol. 28, pp. 430–431, mar 1958.

[40] I. R. Kleckner and M. P. Foster, "An introduction to NMR-based approaches for measuring protein dynamics," *Biochimica et Biophysica Acta (BBA) - Proteins and Proteomics*, vol. 1814, pp. 942–968, aug 2011.

[41] A. G. Palmer, C. D. Kroenke, and J. P. Loria, "Nuclear magnetic resonance methods for quantifying microsecond-to-millisecond motions in biological macromolecules.," *Methods in enzymology*, vol. 339, pp. 204–38, 2001.

[42] N. R. Latorraca, A. J. Venkatakrishnan, and R. O. Dror, "GPCR Dynamics: Structures in Motion," *Chemical Reviews*, vol. 117, pp. 139–155, jan 2017.

[43] M. Casiraghi, E. Point, A. Pozza, K. Moncoq, J.-L. Banères, and L. J. Catoire, "NMR analysis of GPCR conformational landscapes and dynamics," *Molecular and Cellular Endocrinology*, vol. 484, pp. 69–77, mar 2019.

[44] R. Nygaard, Y. Zou, R. O. Dror, T. J. Mildorf, D. H. Arlow, A. Manglik, A. C. Pan, C. W. Liu, J. J. Fung, M. P. Bokoch, F. S. Thian, T. S. Kobilka, D. E. Shaw, L. Mueller, R. S. Prosser, and B. K. Kobilka, "The dynamic process of β2-adrenergic receptor activation," *Cell*, vol. 152, no. 3, pp. 532–542, 2013.

[45] A. Manglik, T. H. Kim, M. Masureel, C. Altenbach, Z. Yang, D. Hilger, M. T. Lerch, T. S. Kobilka, F. S. Thian, W. L. Hubbell, R. S. Prosser, and B. K. Kobilka, "Structural Insights into the Dynamic Process of β 2 -Adrenergic Receptor Signaling," *Cell*, vol. 161, pp. 1101–1111, may 2015.

[46] R. O. Dror, D. H. Arlow, P. Maragakis, T. J. Mildorf, A. C. Pan, H. Xu, D. W. Borhani, and D. E. Shaw, "Activation mechanism of the 2-adrenergic receptor," *Proceedings of the National Academy of Sciences*, vol. 108, pp. 18684–18689, nov 2011.

[47] K. J. Kohlhoff, D. Shukla, M. Lawrenz, G. R. Bowman, D. E. Konerding, D. Belov, R. B. Altman, and V. S. Pande, "Cloud-based simulations on Google Exacycle

reveal ligand modulation of GPCR activation pathways," *Nature Chemistry*, vol. 6, pp. 15–21, jan 2014.

[48] S. Isogai, X. Deupi, C. Opitz, F. M. Heydenreich, C.-J. Tsai, F. Brueckner, G. F. X. Schertler, D. B. Veprintsev, and S. Grzesiek, "Backbone NMR reveals allosteric signal transduction networks in the β1-adrenergic receptor," *Nature*, vol. 530, pp. 237–241, feb 2016.

[49] R. Sounier, C. Mas, J. Steyaert, T. Laeremans, A. Manglik, W. Huang, B. K. Kobilka, H. Déméné, and S. Granier, "Propagation of conformational changes during μ-opioid receptor activation," *Nature*, vol. 524, pp. 375–378, aug 2015.

[50] L. Ye, N. Van Eps, M. Zimmer, O. P. Ernst, and R. Scott Prosser, "Activation of the A2A adenosine G-protein-coupled receptor by conformational selection," *Nature*, vol. 533, pp. 265–268, may 2016.

[51] S. Ye, E. Zaitseva, G. Caltabiano, G. F. X. Schertler, T. P. Sakmar, X. Deupi, and R. Vogel, "Tracking G-protein-coupled receptor activation using genetically encoded infrared probes," *Nature*, vol. 464, pp. 1386–1389, apr 2010.

[52] C. Altenbach, A. K. Kusnetzow, O. P. Ernst, K. P. Hofmann, and W. L. Hubbell, "High-resolution distance mapping in rhodopsin reveals the pattern of helix movement due to activation," *Proceedings of the National Academy of Sciences*, vol. 105, pp. 7439–7444, may 2008.

[53] N. Leioatts, T. D. Romo, S. A. Danial, and A. Grossfield, "Retinal Conformation Changes Rhodopsin's Dynamic Ensemble," *Biophysical Journal*, vol. 109, pp. 608–617, aug 2015.

[54] A. Manglik and B. Kobilka, "The role of protein dynamics in GPCR function: insights from the β2AR and rhodopsin," *Current Opinion in Cell Biology*, vol. 27, pp. 136–143, apr 2014.

[55] J. D. Violin, A. L. Crombie, D. G. Soergel, and M. W. Lark, "Biased ligands at G-protein-coupled receptors: promise and progress," *Trends in Pharmacological Sciences*, vol. 35, pp. 308–316, jul 2014.

[56] M. P. Bokoch, Y. Zou, S. G. F. Rasmussen, C. W. Liu, R. Nygaard, D. M. Rosenbaum, J. J. Fung, H.-J. Choi, F. S. Thian, T. S. Kobilka, J. D. Puglisi, W. I. Weis, L. Pardo, R. S. Prosser, L. Mueller, and B. K. Kobilka, "Ligand-specific regulation of the extracellular surface of a G-protein-coupled receptor," *Nature*, vol. 463, pp. 108–112, jan 2010.

[57] J. Jentoft, T. Gerken, N. Jentoft, and D. Dearborn, "13C Methylated ribonuclease A. 13C NMR studies of the interaction of lysine 41 with active site ligands.," *Journal of Biological Chemistry*, vol. 256, pp. 231–236, jan 1981.

[58] G. R. Moore, M. C. Cox, D. Crowe, M. J. Osborne, F. I. Rosell, J. Bujons, P. D. Barker, M. R. Mauk, and A. G. Mauk, "N epsilon,N epsilon-dimethyl-lysine cytochrome c as an NMR probe for lysine involvement in protein-protein complex formation.," *The Biochemical Journal*, vol. 332, pp. 439–49, jun 1998.

[59] L. R. Dick, A. D. Sherryll, M. M. Newkirki, D. M. Gray, H. Hines, and B. Dallas, "Reductive methylation and 13C NMR studies of the lysyl residues of fd gene 5 protein. Lysines 24, 46, and 69 may be involved in nucleic acid binding.," *The Journal of Biological Chemistry*, vol. 263, no. 35, p. 5323, 1988.

[60] N. Jentoft and D. G. Dearborn, "Labeling of Proteins by Reductive Methylation Using Sodium Cyanoborohydride," *The Journal of Biological Chemistry*, vol. 254, no. 11, pp. 4359–4365, 1979.

[61] J. Jentoft, N. Jentoft, Gerken TA, D. Dearborn, - Journal of Biological, and undefined 1979, "13C NMR studies of ribonuclease A mentholated with [12C] Formaldehyde.," *The Journal of Biological Chemistry*, vol. 254, no. 11, pp. 4366–4370, 1979.

[62] G. E. Means and R. E. Feeney, "Reductive alkylation of amino groups in proteins," *Biochemistry*, vol. 7, pp. 2192–2201, jun 1968.

[63] G. E. Means, "Reductive alkylation of amino groups," *Methods in enzymology*, vol. 47, pp. 469–478, 1977.

[64] W. R. Rypniewski, H. M. Holden, and I. Rayment, "Structural consequences of reductive methylation of lysine residues in hen egg white lysozyme: an X-ray analysis at 1.8-A resolution.," *Biochemistry*, vol. 32, pp. 9851–8, sep 1993.

[65] V. Tugarinov, P. M. Hwang, J. E. Ollerenshaw, and L. E. Kay, "Cross-Correlated Relaxation Enhanced 1 H-13 C NMR Spectroscopy of Methyl Groups in Very High Molecular Weight Proteins and Protein Complexes," *Journal of the American Chemical Society*, vol. 125, pp. 10420–10428, aug 2003.

[66] I. Pritišanac, M. T. Degiacomi, T. R. Alderson, M. G. Carneiro, E. AB, G. Siegal, and A. J. Baldwin, "Automatic Assignment of Methyl-NMR Spectra of Supramolecular Machines Using Graph Theory," *Journal of the American Chemical Society*, vol. 139, pp. 9523–9533, jul 2017.

[67] F. M. Poulsen, J. C. Hoch, and C. M. Dobson, "Structural study of the hydrophobic box region of lysozyme in solution using nuclear Overhauser effects," *Biochemistry*, vol. 19, pp. 2597–2607, jun 1980.

[68] C. Amero, M. Asunción Durá, M. Noirclerc-Savoye, A. Perollier, B. Gallet, M. J. Plevin, T. Vernet, B. Franzetti, and J. Boisbouvier, "A systematic mutagenesis-driven strategy for site-resolved NMR studies of supramolecular assemblies," *Journal of Biomolecular NMR*, vol. 50, pp. 229–236, jul 2011.

[69] K. J. Roberson, P. N. Brady, M. M. Sweeney, and M. A. Macnaughtan, "Methods to identify the NMR resonances of the 13C-dimethyl N-terminal amine on reductively methylated proteins.," *Journal of visualized experiments : JoVE*, no. 82, pp. 1–9, 2013.

[70] J. L. Parker and S. Newstead, "Method to increase the yield of eukaryotic membrane protein expression in saccharomyces cerevisiae for structural and functional studies," *Protein Science*, vol. 23, pp. 1309–1314, sep 2014.

[71] J. L. Parker and S. Newstead, "Structural basis of nucleotide sugar transport across the Golgi membrane," *Nature*, vol. 551, pp. 521–524, nov 2017.

[72] D. Drew, S. Newstead, Y. Sonoda, H. Kim, G. von Heijne, and S. Iwata, "GFP-based optimization scheme for the overexpression and purification of eukaryotic membrane proteins in Saccharomyces cerevisiae," *Nature Protocols*, vol. 3, pp. 784–798, apr 2008.

[73] P. Schanda and B. Brutscher, "Very fast two-dimensional NMR spectroscopy for real-time investigation of dynamic events in proteins on the time scale of seconds," *Journal of the American Chemical Society*, vol. 127, pp. 8014–8015, jun 2005.

[74] F. Delaglio, S. Grzesiek, G. W. Vuister, G. Zhu, J. Pfeifer, and A. Bax, "NMRPipe: A multidimensional spectral processing system based on UNIX pipes," *Journal of Biomolecular NMR*, vol. 6, p. 293, 1995.

[75] R. L. J. Keller, *The Computer Aided Resonance Assignment Tutorial*. Goldau: Cantina Verlag, 1st ed., nov 2004.

[76] S. T. Larda, M. P. Bokoch, F. Evanics, and R. Scott Prosser, "Lysine methylation strategies for characterizing protein conformations by NMR," *Journal of Biomolecular NMR*, no. 54, pp. 199–209, 2012.

[77] J. Keeler, *Understanding NMR Spectroscopy*. Chichester UK: John Wiley and Sons, 2nd ed., 2010.

[78] I. D. Campbell, "Nuclear magnetic resonance," in *Biophysical Techniques*, ch. 6.1, pp. 210–242, 2012.

[79] C. A. Waudby, M. Ouvry, B. Davis, and J. Christodoulou, "Two-dimensional NMR lineshape analysis of single, multiple, zero and double quantum correlation experiments," *Journal of Biomolecular NMR*, vol. 74, no. 1, pp. 95–109, 2020.

[80] J. A. Lundbæk, S. A. Collingwood, H. I. Ingólfsson, R. Kapoor, and O. S. Andersen, "Lipid bilayer regulation of membrane protein function: gramicidin channels as molecular force probes," *Journal of The Royal Society Interface*, vol. 7, pp. 373–395, mar 2010.

[81] J. L. Parker, R. A. Corey, P. J. Stansfeld, and S. Newstead, "Structural basis for substrate specificity and regulation of nucleotide sugar transporters in the lipid bilayer," *Nature Communications*, vol. 10, p. 4657, dec 2019.